RADIO EMISSION

Associated with Cosmic Ray Air Showers

A Thesis presented for the degree of

Doctor of Philosophy

by

DONALD MALCOLM McDONALD

Physics Department

University of Adelaide

November, 1980.

FRONTISPIECE General View of Buckland Park.

CONTENTS

SUMMARY

Early work on the properties of the radio emission associated with Cosmic Ray Air Showers led to the expectation that the distribution in frequency and space of the pool of radiation on the ground contained information about the shower development and hence, indirectly, about the composition of the primary cosmic ray particles themselves. The present thesis describes work carried out in conjunction with the Buckland Park Air Shower Array, to investigate the frequency spectra of the radio emission produced by showers of sea level size greater than 10^5 particles. An estimate of the normalised field strength of the observed pulses was made in order to throw light on the discrepancies between the measurements made by other groups working in the northern hemisphere. A simple model of shower decay was used to yield an estimate of the shower elongation rate. The value obtained, albeit with large uncertainty, is significantly in excess of other values in the same energy range obtained through non-radio methods. Limitations and uncertainties in the radio approach are discussed.

Finally, in an appendix, the development of a preliminary experiment set up to study temporal aspects of the energy flow of particles within 50m of the air shower core is described.

This Thesis contains neither material which has been accepted for the award of any other degree or diploma, nor, to the best of the author's knowledge and belief, any material previously published or written by any other person, except where due reference is made.

D.M. McDONALD

ACKNOWLEDGEMENTS

I wish to thank my supervisor, Professor John Prescott, for his advice and encouragement through the years.

Thanks are due to all the members of the Physics Department at Adelaide, and in particular, the members of the Cosmic Ray Group, past and present, for their friendship and co-operation.

Thanks are due especially to B. Smith for financial advice!

CHAPTER 1

INTRODUCTION

1.1 Astrophysical Aspects of Cosmic Ray Studies.

The composition of primary cosmic ray particles can be measured directly at low energies (below 10^{15}eV) through balloon, rocket and satellite borne detectors. At 10^{12}eV the primaries are mainly protons, with some 15% helium and only 2% heavier nuclei; however at higher energies the proportion of protons may fall (Hillas, 1975). At still higher energies, the rapidly falling flux does not allow direct measurements. The composition must be inferred from the characteristics of the extensive air showers produced as a result of the interactions of the primary particle with nuclei in the atmosphere. At the highest energies, the questions of composition, origin and energy spectrum are interlinked.

1.1.1 Primary Energy Spectrum and Anisotropies.

The energy spectrum can be described as a power law, with a knee at 5×10^{15}eV, and an ankle at 10^{19}eV (fig 1.1). Regions of changes in slope are of particular interest; they may reflect changes in origin of the primaries, and thus, possibly, changes in composition and anisotropy. The apparent continuation of the spectrum above 10^{19}eV is of particular interest, since the 3^{o}K black body radiation imposes constraints on the primary particles. (Greisen, 1966).

At cosmic ray energies the 3^{o} radiation is Doppler shifted above the pion photoproduction threshold for protons, and photodisintegration for nuclei and should produce a cutoff in the spectrum for a uniform extragalactic origin. For protons, this cutoff should occur about

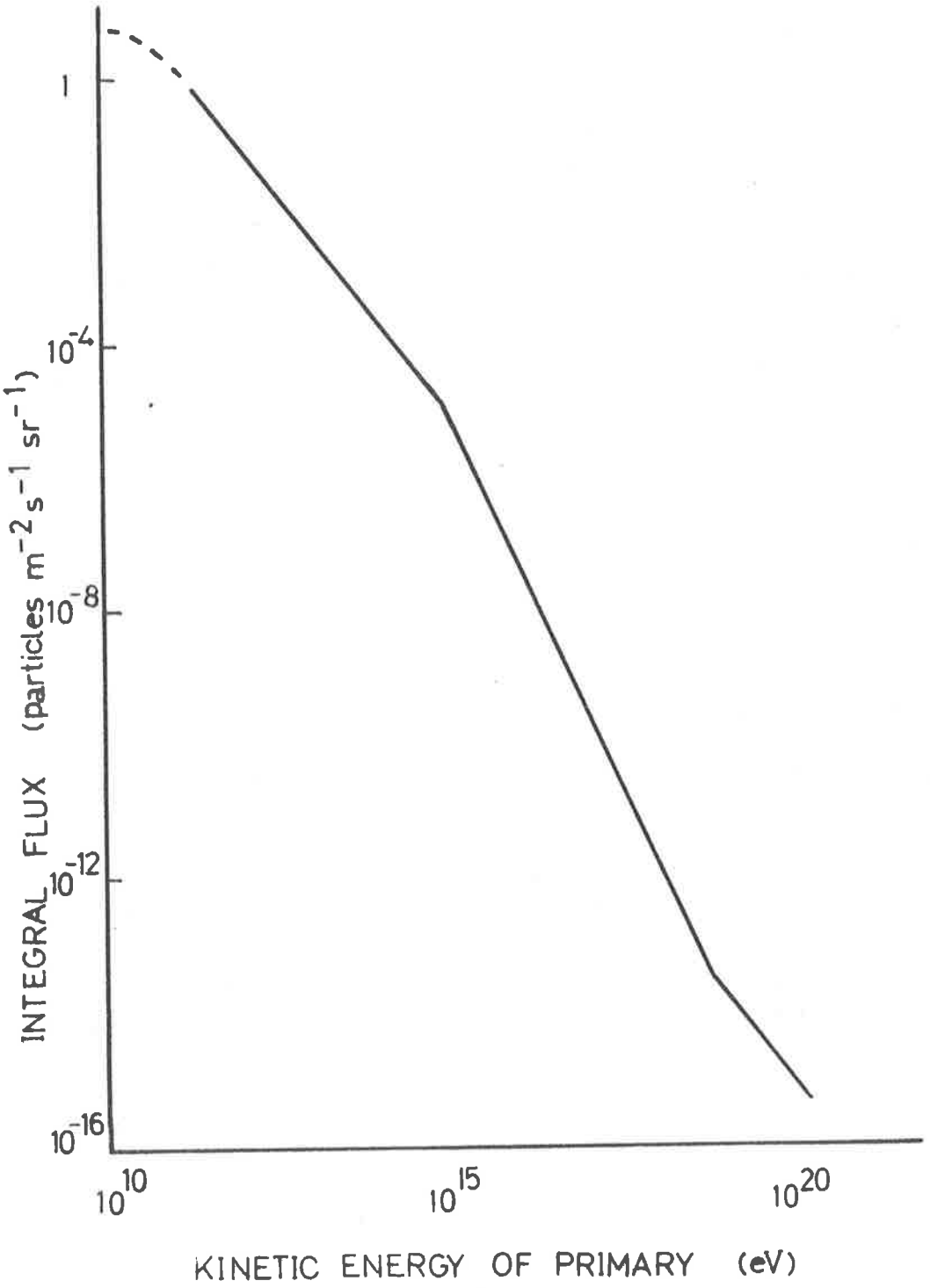

Fig 1.1 Integral Primary Energy Spectrum.

5×10^{19}eV, with a corresponding characteristic lifetime of 10^{8}yrs (at 2×10^{20}eV), while for iron nuclei the cutoff energy is around 10^{20}eV. If the energies of the largest recorded showers are accepted, then this would suggest a relatively local origin for the particles, within, say, the local (Virgo) supercluster, the centre of which is close enough (60×10^{6}yrs) that losses should not appear until above 10^{20}eV for protons (Hillas, 1975). If recent scaling model calculations by Hillas (1979) are correct, they would reduce air shower energies somewhat, easing these restrictions.

If the particles originate in the galaxy (or halo), anisotropies should be significant. For protons the radius at 10^{20}eV is 10^{21}m (for a 3×10^{-10}T magnetic field), larger than the thickness of the galactic disc (10^{19}m). The radius is reduced for a heavy nuclei, by the atomic number. The arrival directions of the particles should therefore be weighted in the direction of origin, which, for a galactic origin, would be expected to be in the galactic plane.

Recent observations have, in fact, revealed anisotropies: at Haverah Park, an anisotropy has been observed at 10^{17}eV, but is less marked at 10^{18}eV, perhaps reflecting a change in composition, or in origin.

At still higher energies, an increase in the average galactic latitude of the anisotropy has been observed near 10^{19}eV where the spectrum changes slope. At these energies, galactic protons can, according to our present knowledge, be ruled out, but galactic heavy nuclei remain a possibility. The weight of informed opinion would, however, consider the local supercluster (with a greater than average density of galaxies) as the likely region of interest (Lapikens et al, 1979a, Krasilnikov, 1979, Wdowczyk and Wolfendale, 1979).

1.2 Extensive Air Showers.

Details of the primary particles must be inferred from ground-based observations on extensive air showers. Our interpretation of measurements relies on the continuing development and refinement of self-consistent models of the details of high energy interactions. Since the energies involved are far beyond those available with accelerators, details such as multiplicity and inelasticity must be extrapolated over many orders of magnitude. It is consequently difficult to extract the 'right' answers from a wealth of possibilities. Consequently considerable effort has been expended on the search for shower parameters that are sensitive to particular features of the primary particles or their interactions, but relatively insensitive to others.

1.2.1 The Nuclear Cascade.

When the primary cosmic ray particle collides with a nitrogen or oxygen nucleus in the atmosphere, a number of secondaries are produced which interact further to produce a nuclear cascade. A heavy nucleus breaks up into its constituent nucleons so that a large number of superimposed cascades develops. At higher energies, the growth of the cascade can be sustained further, so the maximum development of the nuclear cascade is reached deeper in the atmosphere. The interaction length of the proton is about 80g cm^{-2}. There is thus a finite probability of no interaction occurring until several interaction lengths deep in the atmosphere (a 10% chance of no interactions until 200g cm^{-2}, for example). For a heavy nucleus, the interaction length is greatly reduced. Thus, comparing protons and iron nuclei of the same energy, the position of the shower maximum will be higher in the atmosphere, and subject to fewer fluctuations for the iron nuclei.(e.g. Dixon et al, 1974, Dixon and Turver, 1974.)

1.2.2 The Muon Component.

The nuclear particles remain within a few metres of the axis. The pions produced in the nuclear interactions give rise to the muon and electro-magnetic components. Charged pions may either interact further in the atmosphere or decay into muons. Since these muons have a very long interaction length, the number of muons seen at sea level is essentially an integral over the shower development, and thus provides a good indicator of the relative shower energy.

1.2.3 The Electromagnetic Component.

Neutral pions decay with a half life of 10^{-16} seconds into two gamma-rays, each of which initiates an electromagnetic cascade. Gamma rays produce electron-positron pairs by pair-production, and an electron produces a gamma ray by bremsstrahlung. These processes continue until the energy falls below 100MeV where other energy loss processes (ionisation for electrons and Compton scattering for photons) become increasingly important. Some 90% of the particles observed at maximum are in the electromagnetic component, (e.g. Hillas, 1975). Thus as the shower develops, electromagnetic cascades are continually initiated by neutral pions so that at any stage, a number of cascades overlap. An electromagnetic cascade typically reaches a maximum after $\sim$200g cm^{-2} and then dies away with an attenuation length of $\sim$60g cm^{-2}. The attenuation length of the total electromagnetic component, (approximately 200g cm^{-2}) is dependent largely on the decay of the nuclear cascade.

The lateral dimension of the shower is determined by scattering. As lower energy electrons are scattered through greater angles, the mean energy of the particles decreases as the core distance increases. The mean energy of electrons decreases as the cascade develops, so that the

electron energy distribution depends on the combination of the state of shower development, atmospheric pressure and core distance.

The scattering also leads to a lag of particles behind the shower front, again in an energy-dependent manner. The resulting longitudinal thickness of the shower thus increases (from a few meters) as the core distance increases, as will be discussed further in the appendix.

The total number of particles at shower maximum is proportional to the primary energy. Although many experiments attempt to measure the height of maximum development, the maximum itself is rather broad, typically 200g cm^{-2} between the 90% levels (e.g. Aguirre et al, 1979a).

1.2.4 The Primary Composition.

There are two basic approaches to the determination of the primary mass at extensive air shower energies. One is to measure average shower characteristics, using model calculations to estimate the effects produced by different primary masses. For example, since the multiple scattering of muons is small, their lateral distributions are closely related to their height of production (and to details of high energy interactions). The properties of the muon component can, in principle, be used to investigate primary mass (Orford and Turver, 1968).

The central electron density for a given shower size should also depend on primary mass. The mean value (and also the fluctuations) in the density are smaller for heavy primaries than for protons. The Sydney and Kiel groups obtained contradictory results at $3x10^{15}$-10^{17}eV, the former group finding an apparent increase in the fraction of heavy particles in the beam, and the latter suggesting a pure proton (or possibly mixed) beam (McCusker et al, 1969, Samorski et al, 1971).

Properties of the hadron component are also sensitive to primary mass. In particular, the energy spectrum cuts off more steeply for heavy primaries. A summary of the available data by Grieder (1977) suggests that any major change in the primary mass composition (from mainly protons) is excluded up to 10^{15}-10^{16}eV.

Some measurable properties of air showers are somewhat model sensitive. Consequently fluctuations in a number of shower parameters, expected to be greater for protons than for heavy primaries, have been studied.

1.2.5 Fluctuation Studies.

The simplest model for the showers produced by a heavy nucleus of mass number A and energy E is that they are made up of a superposition of 'A' smaller proton-initiated showers of energy E/A. This corresponds to the total fragmentation of the nucleus before entry into the atmosphere, and is an approximation to total disintegration in the first interaction. In a more realistic model, the heavy nucleus only partially fragments in its first interaction, the shower develops deeper and thus more closely resembles a proton-initiated shower of the same energy (Dixon et al, 1973).

In addition to the fluctuations in shower development resulting from variability of the depth of first interaction, as mentioned above, there may be contributions from the inelasticity (the fraction of the energy lost to secondary particles in interactions) and the details of the distribution in energy and number of the secondaries in each interaction.

As mentioned above, air showers are detected at most arrays when they are past maximum development and are decaying. As a result, fluctuations in the depth of maximum development will produce significant fluctuations in electron numbers at sea level. The standard deviation

of the fluctuations in the depth of maximum development is of the order of 100g cm^{-2} for a 10^{16}eV proton primary, which produces a fluctuation in electron numbers at sea level of about 3. The reduction for iron nuclei is about a factor of 2. For a mixed composition, the distribution of average depths of maximum development for showers produced by different nuclei will lead to a further contribution to the observed fluctuations.

Thus, studies of shower fluctuations should lead to some indication of the primary mass. The choice of suitable ground parameters, one related to shower energy and another related to shower development, is important. Studies of muon to electron ratio fluctuations appear to exclude heavy primaries at 10^{15}-10^{16}eV (Dzibowski et al, 1977). Recent studies have concentrated on investigating individual showers. Suitable pairs of parameters have been considered by Dixon and Turver (1974). Smith and Turver (1973) considered this approach with optical Cerenkov pulses. Several groups have developed the Cerenkov technique; in particular the dependence of Cerenkov pulse width on the height of maximum development has been used by the Adelaide group (e.g. Thornton and Clay, 1979). Allan (1971b,c) investigated the properties of the radio emission, in particular the lateral distribution, as an indicator of the depth of maximum development, as will be discussed in the next chapter.

Techniques are being developed to study individual shower development curves, for comparison with shower energy. The Cerenkov pulse shape itself can be used for this purpose; in fact, an array of Cerenkov detectors can be used to reconstruct the development curve (in Cerenkov light) of individual showers, including the arrival directions, without any particle information (Orford and Turver, 1976). The 'Fly's Eye' experiment at Utah, designed to detect the atmospheric fluorescence emission from very large showers, may also be used to

trace shower development (Elbert et al, 1979). Such techniques, in suitable observing conditions, are, in principle, highly suited to the study of primary composition.

CHAPTER 2

RADIO EMISSION

2.1 Introduction.

Visible Cerenkov light emitted by highly relativistic cosmic ray particles was first detected in 1952 (Galbraith and Jelley, 1953). Operational limitations imposed by the need for low background light led Jelley (1958b) to consider the use of microwave frequencies. The $\nu\, d\nu$ spectrum of Cerenkov radiation would lead to a low signal to noise ratio at such frequencies. However, because the wavelengths become comparable with the distances between particles in the shower, coherence would be expected with a considerable enhancement of signal. Nevertheless, for a shower with equal numbers of positive and negative particles, the emission would be effectively cancelled out at wavelengths greater than a few centimetres.

2.1.1 Charge excess mechanism.

In 1962 Askar'yan pointed out that positron annihilation in flight and also the production of Compton and secondary ionisation electrons (δ rays) lead to a net negative charge excess in the shower, which he calculated to be as much as 10% of the total number of particles at maximum development (Askar'yan 1962, 1965). This leads to greatly enhanced field strengths, since for N emitting particles, and a charge excess E, the intensity is proportional to $(EN)^2$ rather than N, as for incoherent emission. For $N=10^7$, E=0.1, this increase is of the order of 10^5.

More recent work has shown the charge excess to be a decreasing function of shower particle energy, with the main contribution being from the Compton process. For the model of Fujii and Nishimura (1970),

the excess varies from 20% at 2 MeV to 1% at 100MeV.

2.1.2 Geomagnetic mechanism.

Askaryan (1962) also drew attention to a suggestion by Goldanski of the possible contribution to the coherent emission by a shower dipole moment set up by charge separation in the earth's magnetic field. Following the detection of radio emission at Jodrell Bank by Jelley et al (1965), the influence of this field was considered by Kahn and Lerche (1966). They found, for a simple model, that this mechanism could be the dominant one. The field exerts a force on the moving particles:

$$\underline{F} = q\,\underline{v} \times \underline{B}$$

The deflection of positive and negative particles to opposite sides thus sets up a dipole moving through the atmosphere. Coupled with the continuous production of electron positron pairs, this leads to a transverse current in the shower. In fact, it is this transverse current which they found to be the dominant source of emission, followed by the charge excess (or 'enhanced Cerenkov' mechanism), with a suggestion that the electric dipole may be significant at higher frequencies. The first successful demonstration of an asymmetry related to the geomagnetic field was reported at the Calgary conference in 1967 by Prescott et al (1968).

2.1.3 Atmospheric Electric Field.

The possible contribution of the earth's electric field to the generation of radio pulses was first considered by Wilson (1957) and later by Charman in 1967. In fine weather the field is vertical, with a typical gradient of the order of $100 Vm^{-1}$, falling steadily with altitude

to 0.1 Vm^{-1}, at about 20km height. The field may however reach values of 50 kVm^{-1} below thunderclouds, and even higher values within the clouds themselves. There may be significant variation in direction as well (Chalmers, 1957, Mason 1971).

Charman considered three possible mechanisms; transverse charge separation for showers at large zenith angles, longitudinal separation for vertical showers, and radiation produced by the movement of low energy ionisation electrons. (Charman 1967, 1968, Charman and Jelley, 1968).

It is expected that transverse charge separation will rival the geomagnetic field as a mechanism when $E_T \sim B_T c$, which for the earth's magnetic field of about 50 μT would require electric field strengths of some kVm^{-1} for a comparable pulse. For a mainly vertical electric field, showers from large zenith angles will be more likely to produce radiation from this mechanism, although the variation in direction of the field during disturbed atmospheric conditions probably does not allow the directions of individual showers yielding 'suspicious' pulses to be examined too closely.

The longitudinal charge separation was found to be insignificant in comparison with the charge excess mechanism. However, this is not so with the movement of slow electrons before their capture in times ranging from tens of ns at sea level to hundreds of ns at 20km altitude. Charman's calculation suggested that for horizontal showers this mechanism may be more significant than the charge excess mechanism at frequencies below 10MHz. Sivaprasad (1978) made use of the results obtained by Crompton (1974) for the drift of electron swarms in dry air, and found that the resulting field strengths were only a tenth of those due to the geomagnetic, with the spectrum continuing to lower frequencies.

Anomalous pulses associated with thunderstorm activity have been found by the groups at Mt. Chacaltaya, Bologna, Haverah Park, MSU and ourselves. (Hazen, Hendel 1971, Mandolesi et al, 1974, Allan et al, 1975, Atrashkevich et al, 1975). The proportion of such pules varies from

array to array, being about 10% at MSU, but only 1% at Haverah Park. For work involved with primary composition, contamination by such a variable mechanism must be considered in experimental design.

2.1.4 Other mechanisms.

A number of other mechanisms which might produce radio emission have been suggested. However none has been found which compares with the geomagnetic, geoelectric or charge excess mechanisms. A summary of such mechanisms has been made by Jelley (1965). Owing to the low conversion efficiency of shower energy into radio emission, the possibility of a significant contribution to the emission from some other, as yet unidentified, mechanism, cannot be ruled out. In this context, the question of the large and varying field strengths at low frequencies is yet to be resolved (Crouch, 1979).

2.2 Radio Pulse Calculations.

There are several avenues of approach to the calculations of the radio emission. Maxwell's equations may be applied to the shower as a whole, using suitable simplifying assumptions and approximations to reduce the mathematical complexity, or one can consider the radiation mechanisms in turn, calculate the yield from a single particle and then integrate the result over the whole shower taking account of coherence conditions, phase shifts and so on. A particular example of the latter approach is Allan's adoption of the Feynman treatment for radiation from a charged particle.

2.2.1 The Macroscopic Approach.

The first calculations adopted the 'macroscopic' approach,

applying Maxwell's equations to simplified models of the air shower. Kahn and Lerche (1965) regarded the shower structure as a disc travelling vertically down, neglecting curvature and shower development, changes in atmospheric density and the effect of Coulomb scattering (Lerche, 1967).

Fujii and Nishimura (1970) and Castagnoli et al (1969) extended these calculations. Fujii and Nishimura applied both one dimensional and three dimensional cascade theory, and included the effects of altitude variation, the shape of the shower front and the lateral distribution of the transverse current in the shower. Castagnoli et al used a 3-D Monte Carlo calculation of the electron cascade development, and included Coulomb scattering.

There was general agreement among these authors for the relative importance of charge excess and geomagnetic mechanisms. The transverse current set up in the shower disc was found to be dominant in the tens of MHz range of frequencies, with charge excess becoming significant at higher frequencies. These calculations all assumed an infinitely thin shower disc, introducing the effects of finite shower thickness as a convolution. As will be described later, this leads to a discrepancy with more recent work which concludes that charge excess might be more significant at lower frequencies (Shutie 1973).

Approaches to the calcuations using Maxwell's equations tend to be time-consuming and complicated, and the nature of the results to be expected is not intuitively obvious at the start of the calculation. It was not until Allan's application of Feynman's formulation for the radiation from a relativistic particle that the problem became easier to visualise.

2.2.2 The Feynman Treatment.

In 1967, Allan proposed a completely different approach to the

problem of calculating the radiation, based on the formulation of electrodynamics due to Feynman (1963), viz.

$$\varepsilon = \frac{-q}{4\pi\,\varepsilon_0}\left[\frac{\underset{\sim}{e}_r}{r^2} + \frac{r}{c}\frac{d}{dt}\left(\frac{\underset{\sim}{e}_r}{r^2}\right) + \frac{1}{c^2}\frac{d^2\underset{\sim}{e}_r}{dt^2}\right]$$

where, $\underset{\sim}{e}_r$ is the vector in the direction of the charge, and r its distance, both measured at the retarded time.

For a relativistic particle, only the third term is significant. The radiation is thus given by the product of the charge and the apparent angular acceleration as seen by the observer (i.e. at the retarded time), viz

$$\varepsilon = \frac{q}{4\pi\,\varepsilon_0 c^2}\,\ddot{\theta}$$

Since the application of the formula is limited to highly energetic particles, low frequency calculations obtained by its use should be treated with caution. The Feynman treatment includes both the 'near field' and 'far field' components of more conventional approaches.

The formula is applicable, in principle, to all the possible mechanisms of emission. Thus, simplified models of shower development and particle motions may be used to allow the visualisation of the main features of the emission far more easily than the approaches using Maxwell's equations. The radiation is calculated by considering the accelerations of the shower particles responsible for the emission, namely the electrons and positrons. The calculation proceeds as follows. The total angular deflection of the soft component as a function of the observed time is obtained. Double differentiation of this θ-t curve produces the shape of the radio pulse. The frequency spectrum follows by performing a Fourier Transform on this pulse.

The general shape of the θ-t curve is determined by geometrical path differences and the refractive index of the atmosphere. At large

radial distances, the emission from the early stages of the shower development arrive in sequence close together, while that from later stages is more spread out. Even without considering the effects of individual mechanisms, this produces a θ-t curve with an initial sharp rise followed by a slower increase as emission from the later stages of the shower strikes the antenna. Double differentiation produces a sharp pulse followed by a long overswing, the areas under the pulse being equal. This yields a frequency spectrum which is flat in the tens of MHz range, falling off on both sides (see fig 2.1).

Near the shower core, the effect of the refractive index, itself depending on atmospheric density, becomes important. By slowing down radiation from the early stages of shower development, the temporal order of arrival of the emission at the antenna is reversed for small core distances. For a radially symmetric mechanism such as charge excess, the signal on axis will be zero.

The Feynman treatment does not specifically include the Cerenkov angle. In fact, there is no sharp change in the character of the radiation as the particle energy drops below the Cerenkov threshold (Allan, 1971a). The simple treatment by Colgate (1967) refers to this latter case, where diffraction effects play a dominant role.

2.2.3 Shower thickness.

The discrepancy between the calculations of Fujii and Nishimura (1970, 1971) and those obtained using the approach pioneered by Allan (1967, 1971) can be attributed to the effect of shower thickness. The longitudinal distribution of particles in the shower depends on their energy, and in particular, the higher energy particles are concentrated closer to the leading edge of the shower than are lower energy particles. This implies that the upper frequency limit to the radiation is not necessarily limited

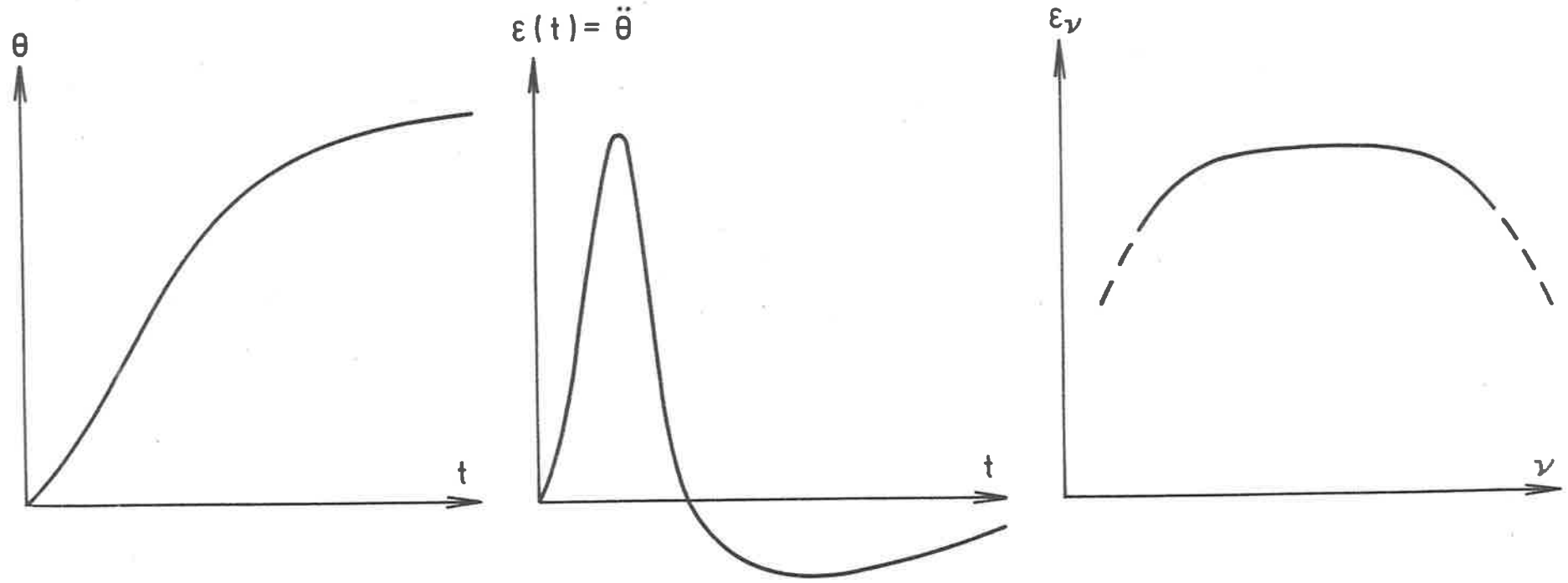

Fig 2.1 Relation between θ-t curve and frequency spectrum (schematic)

by the shower front thickness. Fujii and Nishimura assumed that the effect of the longitudinal shower structure could be taken into account as a convolution with the radiation calculated for an infinitesimally thin shower. In other words, the spectrum of the calculated radiation could be multiplied by the Fourier Transform of the longitudinal shower structure function to yield the 'true' spectrum. (This appears in large part to be responsible for the steeply falling ($\nu^{-\frac{1}{2}}$) spectrum presented by these authors in 1969). Since the charge excess is largely associated with lower energy electrons whose deflections, because of longitudinal lag, will be observed later than those of higher energy electrons, the radiation will be associated with lower frequencies than would be the case for a 'thin' disc. The longitudinal shower structure thus plays a vital role in determining the relative significance of the different mechanisms as a function of frequency.

2.2.4 The Kharkov Work.

The calculations by the Kharkov group consider the explicit expressions in the frequency domain for the radiation produced by individual particles, for particular mechanisms and then integrate over the whole shower, taking account of Coulomb scattering and coherence conditions. Their approach perhaps lacked the elegance of the Feynman treatment, and the results were somewhat different in nature from those derived with the latter technique. They considered the magnetic bremsstrahlung (synchrotron) mechanism (Kaminsky et al, 1977) and later, charge excess as well (Volovik et al, 1976). The lateral distributions thus obtained show a dip which is more pronounced for early developing showers, and becomes larger and moves closer to the axis as the frequency increases (150m at 30MHz to 75m at 100MHz). The shape of the spectrum is largely determined by interference conditions. Comparisons of two measured spectra with fitted curves suffered from an apparent lack of directional information for their data, thus allowing an extra variable for curve fitting (in

addition to the height of maximum development).

The synchrotron mechanism, briefly considered by Jelley (1965) is a special case of the geomagnetic mechanism, and is therefore, in principle, included naturally in the treatment by Allan and colleagues.

2.2.5 Development of the Feynman Treatment.

Allan's approach has been adopted by several authors. Clay (1972), Hough (1973) and Shutie (1973), used more sophisticated models of shower development.

Hough used Monte Carlo calculations to obtain an energy by height matrix of neutral pions, whose decay initiates the development of electromagnetic cascades. The resulting electron distribution was stored as a matrix with dimensions of atmospheric height, radial distance and energy. The lateral displacements and delays due to geomagnetic deflections of the electrons were estimated, after Allan (1971a) as:

$$Dg = \frac{.32D}{P}, \quad Lg = \frac{.05L}{P}$$

where D and L are the known lateral displacements and delays (due to Coulomb scattering) and P is the pressure in atmospheres.

The calculation was performed for an observer on the E-W axis, for a horizontal N-S geomagnetic field, and particles lying on the E-W plane. This restriction leads to a slight steepening of the calculated lateral distributions.

Shutie considered further physical processes (bremsstrahlung, ionisation loss, Compton scattering). He calculated the magnetic deflection by following individual electron tracks, splitting them into segments and calculating from the radius of curvature in the geomagnetic field, the deviation due to the field, together with (random) scatter.

The results of this approach differ in details only as the calculations are made more sophisticated, and the general outline remains unchanged. In particular, the lateral distributions depend mainly on the height of shower maximum, although not as strongly as first appeared to be the case (Allan, 1971b). The intuitive expectation was that the pool of radiation would contract as the shower develops later in the atmosphere. The most recent results, those of Shutie (1973) suggest that beyond 150m, the field falls off exponentially, with a similar exponent for all showers. The field strengths at these distances decrease for late developing showers. Since emission from later stages of shower development arrives much later than that from earlier stages it is the high frequency components that are mainly affected by emission from early stages of shower development. However, near the axis, the reversal in the relative times of arrival make this region more sensitive to changes lower in the atmosphere. There is a region, between 50 and 100m from the axis, where the field strengths are relatively independent of shower development, although not so usefully independent as first appeared from the work of Allan (1971b) and Hough (1973).

Analogous to the effects on the lateral distribution of different shower developments are those on the frequency spectra. It was expected that the shape of the frequency spectra should depend strongly on shower development. At large core distances, diffraction effects might be expected to result in a loss of high frequencies for late development; however, at such distances, greater than 200m from the core, extraction of the signal from noise is becoming increasingly difficult. At lesser core distances the main effect of later developments is to reduce the field strengths with little change in spectral shape. Below about 20MHz, the charge excess mechanism appears to become more significant, as previously mentioned.

Diagrams of the effect of changing the height of maximum development

on the lateral distributions and frequency spectra are presented in fig. 2.2. These diagrams, extracted from the thesis of Shutie (1973) refer to the same shower development function, shifted up or down in the atmosphere. It is possible to obtain unusual development curves which may not have a clearly defined height of maximum (Shutie, 1973, Dixon and Turver, 1974). There is little change in the radio distribution for inclined showers; the significant parameter is the depth of atmosphere through which the shower has developed to reach its maximum.

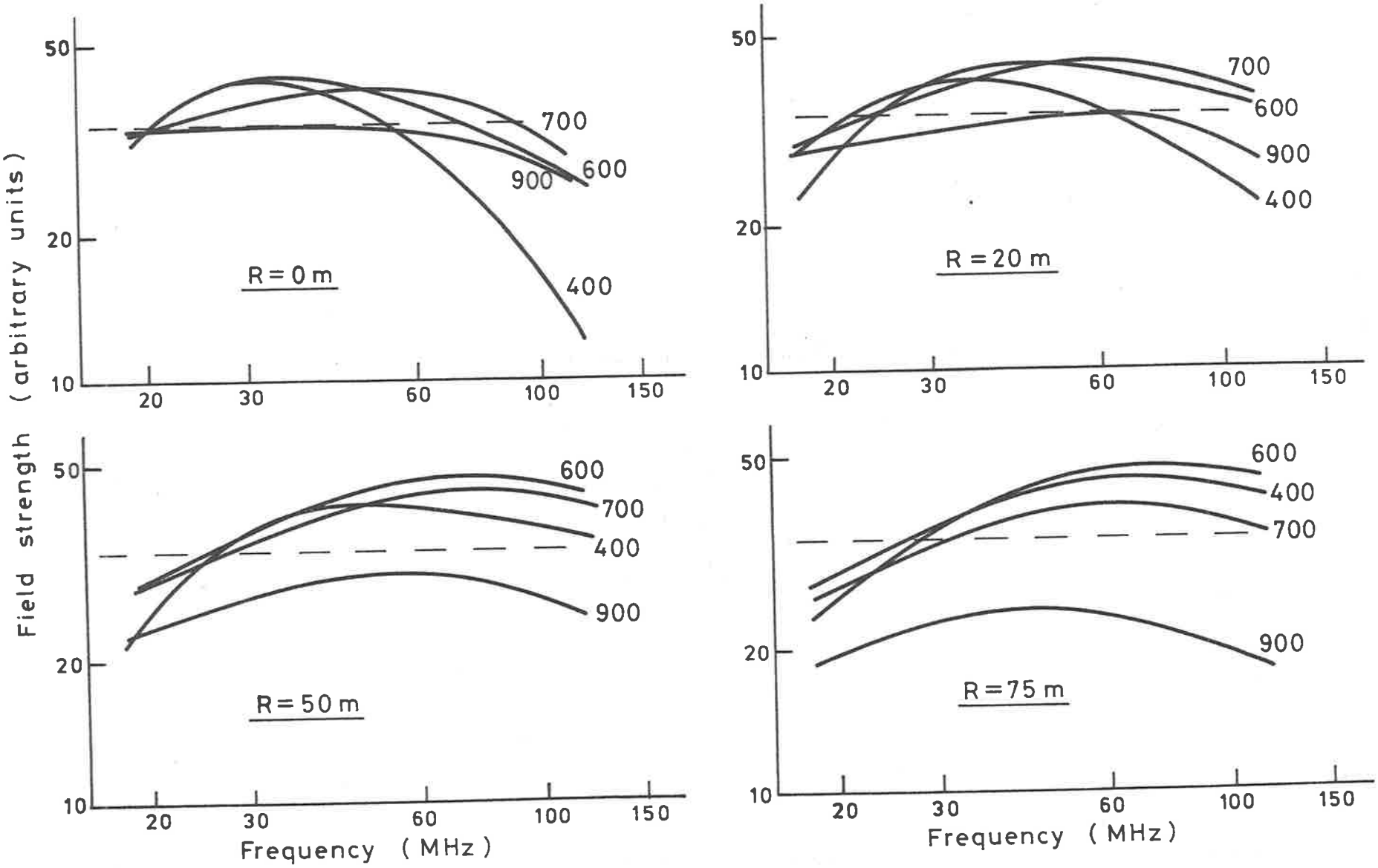

Fig 2.2 Frequency spectra for different core distances and nominal depths of shower maximum.

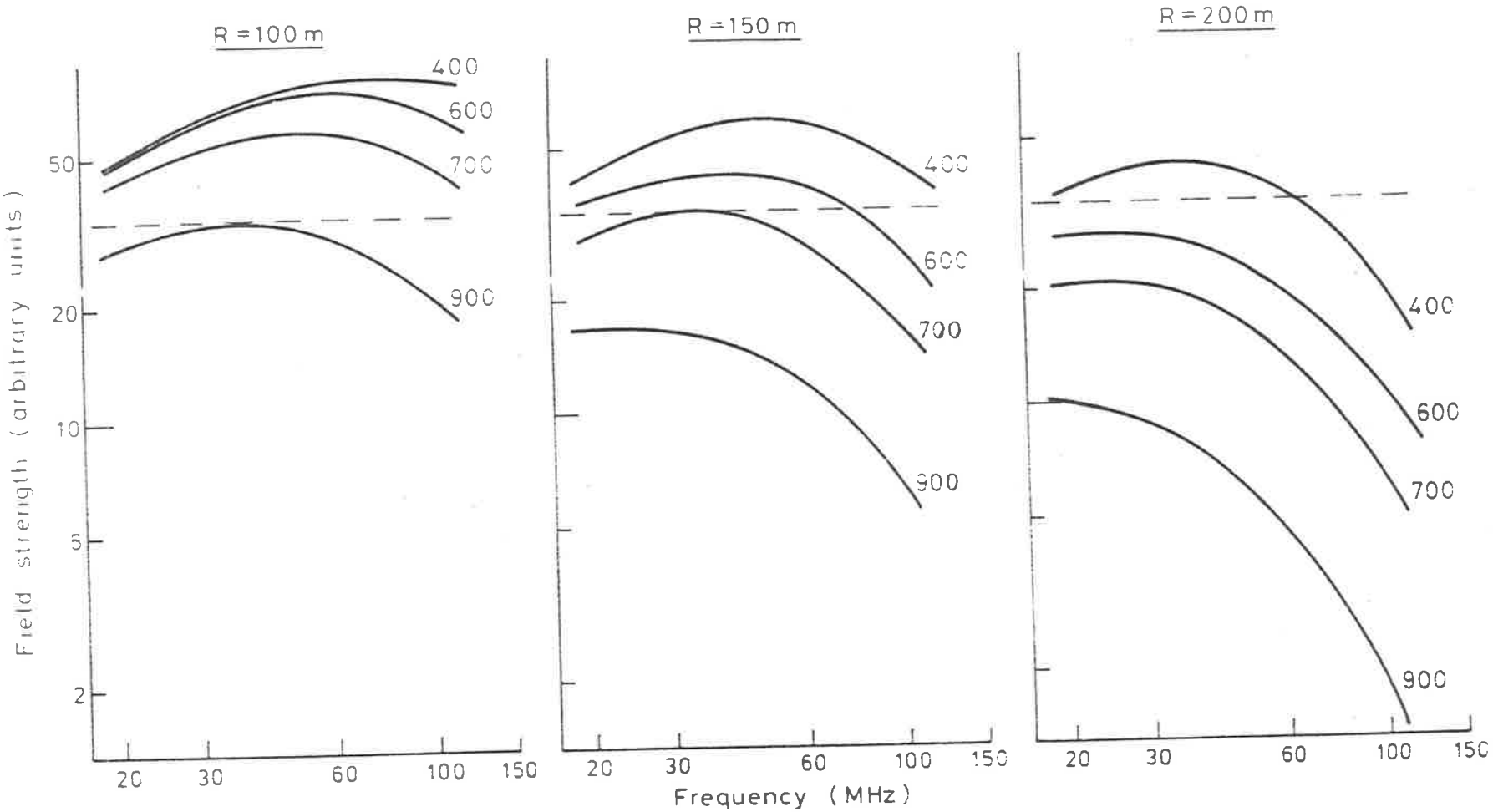

Fig 2.2 · Continued.

CHAPTER 3

EXPERIMENTAL WORK ON RADIO EMISSION

Following the detection of the radio emission (Jelley et al, 1965), experimental work was concentrated in several areas. Firstly, the emission was studied for its own sake, to establish the mechanisms involved. Secondly, there were hopes that radio detection would enable the construction of efficient air shower detectors at much lower cost than conventional particle detectors (scintillators and water Cerenkov detectors). Thirdly, particular features of the emission were studied, not only for their intrinsic interest, but also in an effort to establish the nature of the primary particle flux.

3.1. Purely Radio Detection.

Several groups have investigated the possibility of dispensing with particle detectors, relying solely on radio data for analysis. Early hopes that the economic detection of very large air showers might be made possible with relatively few widely spaced detectors have not been fulfilled.

The Michigan group, working at Mt. Chacaltaya, found that with several antennas they could obtain shower directions in satisfactory agreement with those obtained from particle detectors. However, correlations between pulse heights and size and core distances were poor. They were not able to dispense with a particle detector for triggering and timing reference pulses. (Hazen et al, 1970).

At Mt. Chacaltaya, 5200 m.a.s.l., radio emission comes mainly from the very early stages of shower development, resulting in fluctuations in pulse heights, even though most of the showers observed at this altitude are fairly near maximum development where the particle numbers are changing relatively slowly. This is in contrast to an array at sea level,

where it is the electron size which fluctuates most significantly.

Several groups have considered detecting showers at large zenith angles with long baselines to reduce interference. Radiation from such showers is expected to have a greater lateral spread than that from small zenith angles. For a given electron size at sea level, the total shower energy increases with zenith angle (e.g. Charman, 1967, Fegan et al, 1968, Colgate, 1971).

These approaches have proved unsuccessful, and attempts to detect showers solely by their radio emission have been abandoned. More recently, the detection of very large showers from their atmospheric fluorescence emission has been considered. The 'Fly's Eye' experiment at Utah was designed to permit investigation of the spectrum, composition and anisotropies of showers at energies 10^{16}-10^{21}eV (Bergeson et al, 1975a,b). Preliminary results obtained with a prototype at Volcano Ranch demonstrated encouraging agreement between the shower analysis obtained by the two detectors (Cassidy et al, 1977). Although the collecting area of the instrument may have been overestimated initially, recent reports show promise of its usefulness in tackling problems of shower development and hence composition (Elbert et al, 1979).

3.2.1. Mechanisms.

Much of the study of mechanisms has been aimed at distinguishing between the two most favoured mechanisms, the geomagnetic and the charge excess. There are two commonly applied tests. The simplest is to record the directions from which showers come, compared with an unbiased collection of showers. At the latitude of Haverah Park, Calgary and Moscow, showers from the south will be more nearly parallel to the geomagnetic field than those from the north, and the geomagnetic mechanism will be less effective. For a given observed field strength, there should

be more radio showers from the north than from the south. This then is the so-called 'N-S asymmetry' test for the geomagnetic mechanism.

(At a low latitude array, such as Mt. Chacaltaya, with a field directed north-south, more radio showers would be expected from the east and west than from the north and south).

This test has lent support to the geomagnetic machanism at a number of arrays over a range of 20-60MHz. (e.g. Prescott et al, 1968, Allan et al 1969, Abrosimov et al 1970, Bray 1969).

A further test is the measurement of the polarisation of individual radio pulses, compared with that expected for different mechanisms, (linear polarisation normal to the geomagnetic field, radial polarisation (for charge excess), vertical polarisation (for the electric field mechanism). The test has been done with two antennas with planes of polarisation normal to each other. Tabulated results indicate that only a few showers are incompatible with a geomagnetic mechanism. (Allan et al, 1971a, Khristiansen et al, 1971a,b, Atrashkevich, 1975). The errors associated with field strength measurements make such conclusions difficult to quantify.

The dependence of the measured and calculated polarisation on the sine of the angle between the geomagnetic field and the shower axis has been studied further. The MSU group found that the relatively few pulses incompatible with the geomagnetic mechanism came mainly from small angles to the field, whereas no such systematic effect was observed for either the charge excess or geoelectric mechanisms (Vernov et al, 1970). This was confirmed by the Calgary group, which found that the data were consistent with an in phase admixture of radial polarisation (e.g. charge excess) (Hough et al, 1970).

A more convincing result was the Calgary group's demonstration of a linear dependence of the field strength at 22MHz on $\underline{V}x\underline{B}$, with a

contribution from other mechanisms amounting to about 15% of the maximum geomagnetic contribution (Prescott, et al 1968, 1971, Hough et al, 1970).

The coherence of the emission may be checked by investigating the dependence of radio pulse heights on shower size. In the simplest approximation the radio pulse amplitude will vary as N or $N^{\frac{1}{2}}$ for a coherent or incoherent process respectively. With good statistics and care to minimize noise contamination, a linear dependence at sea level has been found (Allan et al 1970, Vernov et al 1969), although the Calgary group found a kink in the spectrum which they suggested might be due to a change in composition from iron to proton nuclei at 10^{16}-10^{17}eV (Clay et al, 1971).

Experimental evidence for a geoelectric contamination of the emission was discussed in section 2.3. There is general agreement that the geomagnetic mechanism is dominant in the tens of MHz range, with a contaminating contribution from the geoelectric mechanism dependent on atmospheric conditions.

3.3 Lateral Distributions.

Early work produced lateral distributions by sampling different showers at different core distances, and gradually building up a distribution. More recently the use of a number of antennas has allowed the lateral distributions of individual showers to be determined, particularly with a view to investigating details of the shower development. This work will be discussed below.

3.4.1 Spectra

There is little point deriving spectra from a comparison of different experiments. Different detecting systems may operate at different

energies, with different collecting areas, particle detectors, methods of analysis and radio shower parameters such as radial distance and antenna characteristics. Such comparisons by Fegan (1972) and Felgate and Stubbs (1972) could be fitted by power law spectra even steeper than the $\nu^{-\frac{1}{2}}$ dependence calculated by Fujii and Nishimura (1970), for their over-simplified model. The first measurements at one site were made by Spencer (1969) with zenith pointed antennas placed near the centre of a simple scintillator array. Measurements were made on different samples of showers, with different bandwidths, beamwidths and system noise backgrounds. The normalised spectrum (44,105,239 and 408MHz) followed an inverse power law.

At Mt. Chacaltaya, a single log periodic dipole antenna pointed off zenith was used to check signal strengths simultaneously at 57, 85 and 177MHz. For a limited sample of fifteen showers, with a variety of core distances, the signal fell with frequency in the ratio 6:3:2 (Hazen et al, 1971).

The Kharkov group too used a system comprising a spiral antenna with seven narrow band channels between 30 and 160MHz (Volovik et al, 1973). The spectra of five individual showers published showed a rapid decrease from 30-50MHz (near the lower end of the antenna's working range) and a smooth and slow change at higher frequencies. (Volovik et al, 1974). They did not measure shower arrival directions. Comparison of the spectra with calculations has been discussed in section 2.2.

The group most directly comparable with the Adelaide group is that at Bologna. The group used 'boxing ring' antennas at three frequencies, thus giving them a means of checking the polarisation of individual events, (Mandolesi et al, 1976). Their results, averaged, are consistent with a flat spectrum, but with sufficient uncertainty to accommodate the spectral shape suggested by the calculations of Hough (1973) and Shutie (1973), referred to in the previous section.

The Haverah Park and MSU groups have also recorded pulses at more than one frequency simultaneously, but with separate antennas and recording systems. Signals recorded at Haverah Park were twice as large at 60MHz as at 30MHz (Allan et al, 1971a), as reported at the Hobart conference. Since then, their reported field strengths have decreased; this is attributed to improved rejection of out of band signals owing to the addition of rejection filters (Allan et al, 1975). This serves to emphasise the uncertainties associated with field strength comparisons with independent systems. The comparison of 32 and 58MHz signals at MSU revealed considerable fluctuations from shower to shower. The "spectrum" was almost flat over the range of core distances 50-200m (Atrashkevich et al, 1971, 1973, 1975).

3.4.2 Other Frequencies.

Much of the work at higher and lower frequencies has been summarised elsewhere (Allan, 1971a). At lower frequencies measurements have been made down to 100kHz. The Calgary group detected emission at 22MHz and 3.6MHz but could not detect 10MHz pulses above the noise background (Prescott et al, 1970, Hough et al, 1971). The discovery of very large field strengths at 2MHz (Allan et al, 1970, Stubbs, 1971), 3.6MHz and 100kHz (Gregory et al, 1973), required a mechanism orders of magnitude more effective than the geomagnetic (Allan, 1972). Although the charge excess mechanism is expected to become more effective than the geomagnetic below 20MHz (Shutie, 1973), it falls far short of explaining these high field strengths. Polarisation studies at 6MHz support an appreciable non-geomagnetic origin of the radiation (Felgate and Stubbs, 1972), although subsequent analysis has reduced the significance of this conclusion (private communication).

However, such high values have not been found in more recent work at 2MHz at Yakutsk, Haverah Park and Adelaide (Khristiansen et al, 1972, Atrashkevich et al, 1973, Allan et al, 1973, Clay et al, 1973b). The earlier values were obtained from measurements on pulses submerged in noise; the quoted values (of the order of $1mVm^{-1}$ MHz^{-1}) are therefore order-of-magnitude estimates only. Indeed, the repetition (with improvements) of Stubbs' 2MHz experiment yielded an upper limit only, no pulses above noise being observed at all (Clay et al, 1975, Crouch, 1979).

At 100kHz, emission with both diurnal and longer period time variations was found, which defied explanations in terms of spurious experimental contamination. This suggests the possibility of some kind of time-varying contribution to the measurements at higher frequencies also. At times of high field strength the energy in the radio pulse is a significant fraction of the initial air shower energy. In fact, an extrapolation to about 30kHz would require an energy equal to that of the initial primary particle (Clay et al, 1973b). Interactions with the geoelectric field have been considered, (Sivaprasad, 1978), but the calculated contribution is too small to explain the emission. This behaviour thus remains an unsolved problem.

At higher frequencies radio pulses have been detected by the Harwell and Dublin groups up to 550MHz using both scintillator and Cerenkov triggers, the latter being less core selective because of the flatter lateral distribution. A summary by Fegan (1972) suggested an inverse square dependence of field strength on frequency, using selected data. This spectrum extended down to frequencies where more recent work, with the benefit of full shower analysis for individual events, suggest a flattening of the spectrum.

3.5.1 Radio Investigation of the Primary Mass.

Allan's investigation of the characteristics of the radio emission has shown it to be highly dependent on the shower development. Since the transfer of energy to the electromagnetic pulse is more efficient at higher altitudes, the energy in the radio pulse will be greater for a heavy nucleon than for a proton primary, while the shower size at sea level will be less, except for the highest energy primaries.

The influence of the position of maximum development on the lateral distribution has received the most attention. It appears that in the region 50-100m from the shower core, the lateral distribution, as previously mentioned, is relatively independent of the details of shower development, except for showers reaching maximum development near the array. The differences between showers with different depths of shower maximum show up at greater lateral distances, where the distribution falls off approximately exponentially. Calculations by Shutie on individual cascades also indicated that the effect of the zenith angle on individual showers could be explained largely by the extra depth of atmosphere between shower maximum and the antenna (Shutie, 1973).

Work was conducted at Haverah Park and also MSU, two air shower installations which can provide a thorough shower analysis for individual events, including arrival direction, core location and a good estimate of primary energy. Early work at Haverah Park appeared to support a proton component of the radiation (Shutie, 1973), but later analysis on a larger sample indicated that no clear conclusion could be drawn (Allan et al, 1975). There was as much scatter in the region where calculations suggest little dependence on shower development as at greater distances. The problem is compounded by the reduced collecting rate of pulses at such distances as a result of the falling lateral distribution. There may,

as well, be contributions to the fluctuations in emission from the geoelectric mechanism. In consequence, the Haverah Park group has now discontinued the radio work.

The MSU group, working at 32 and 58MHz, were largely concerned with the mechanism of the emission. However they did find the form of the lateral distribution to be correlated with the zenith angle, the muon to electron ratio and the age parameter S; in other words a dependence on the position of shower maximum. The lateral distribution as expected, was found to become narrower as the shower maximum approached sea level. The large fluctuations in the form of the lateral distributions recorded, suggested the presence of a proton component in the primary flux. However, the group did not commit itself to a more quantitative conclusion. (Atrashkevich et al 1971, 1973, 1975, Khristiansen et al, 1971a). The MSU group has now also terminated its radio work. The conclusions regarding primary composition from the radio lateral distribution may be summarised as follows; at Haverah Park, an early indication of a proton component, later reconsidered, and at MSU, a tentative suggestion of a proton component.

3.5.2 Dependence of Frequency Spectra on Shower Development.

The frequency spectrum of individual showers should also lead to an indication of primary mass. It was hoped that the shape of the spectrum would reflect the height of maximum shower development, but calculations suggest that in this range of frequencies the shape of the spectrum is not a sensitive parameter, but that the relative values of the spectra differ for different developments. This poor sensitivity coupled with the significant change in the shape of the spectrum for different lateral distances makes this a less attractive approach than

that of studying lateral distributions at a fixed frequency. That these lateral distributions change only slowly with frequency is clear both from calculations and from experiment. (Shutie 1973, Atrashkevich et al, 1975).

3.5.3 Experimental Work.

The two groups which have recorded spectra for individual showers have been described previously; the groups at Bologna and Kharkov, neither of which have drawn any conclusions about the primary composition on the basis of the spectra.

However, the principle of the determination of heights of maximum development relies on the measurement of two parameters, one a good indicator of shower size and the other sensitive to shower development. For an array with particle detectors comprising scintillators, which yield the electron size at sea level, the method of approach can be reversed. The field strength of the emission in the range 50-100m is the better estimator of the shower size at maximum development, while fluctuations in the sea level shower size reflect fluctuations in shower development.

The Bologna group has applied this technique, studying fluctuations in the electron shower size, and the electron density at different distances from the axis, with the radio field strengths as the independent parameter. Their measurements were claimed to be consistent with a proton component of the primary flux, on the basis that the fluctuations observed were larger than those expected for a pure heavy composition (Mandolesi et al, 1976, Baggio et al, 1977).

All groups working in the field have found it necessary to ignore a certain fraction of events which are (usually) attributed to the geoelectric mechanism. The possibility of such a contribution to the scatter

in field strengths, even in fine weather conditions, cannot be ruled out. Fluctuations in parameters would tend to be over-estimated and hence favour a proton component. It is perhaps significant that the only analysis with a 'control' group of data, namely that by the Haverah Park group, did not find residual fluctuations attributable to shower development (Allan et al, 1975a).

CHAPTER 4

4.1.1 The Buckland Park Extensive Air Shower Array.

A plan of the Buckland Park Air Shower Array is shown in fig 4.1; a detailed description of its design and operation may be found in the thesis of P.C. Crouch, and it was briefly described at the Plovdiv conference (Crouch 1979, Crouch et al, 1977). At the time that the present experiment was begun, the array comprised eight NE102 plastic scintillator detectors, each of area $1m^2$ and thickness 5cm. Five of the detectors (the 'fast' array, A,B,C,D,E) were used with Philips XP1040 photomultipliers to estimate the shower direction, from fast timing measurements. Two of these (A,D) and the other three (F,G,H) comprised the 'slow' array. These detectors also use RCA8055 photomultipliers to record particle densities at the different sites from which shower size and core location are calculated.

The array was subsequently extended northwards by the addition of three sites (I,J,K), increasing the area enclosed by the array from $8x10^3 m^2$ to $3x10^4 m^2$. These sites are used to record particle densities; in addition particle densities are now measured in the remaining sites (B,C,E) previously used only for timing measurements. Thus the array in its present form gives an improved analysis of showers falling near the 'fast' array, as well as an increased collecting area for larger showers north of the original array. A block diagram of the array operation is presented in fig. 4.2.

The triggering conditions of the array in its original form required a coincidence of three of the four outer 'slow' detectors at the three particle level, in addition to an output from the 'fast' array. Using detectors for both triggering and particle density

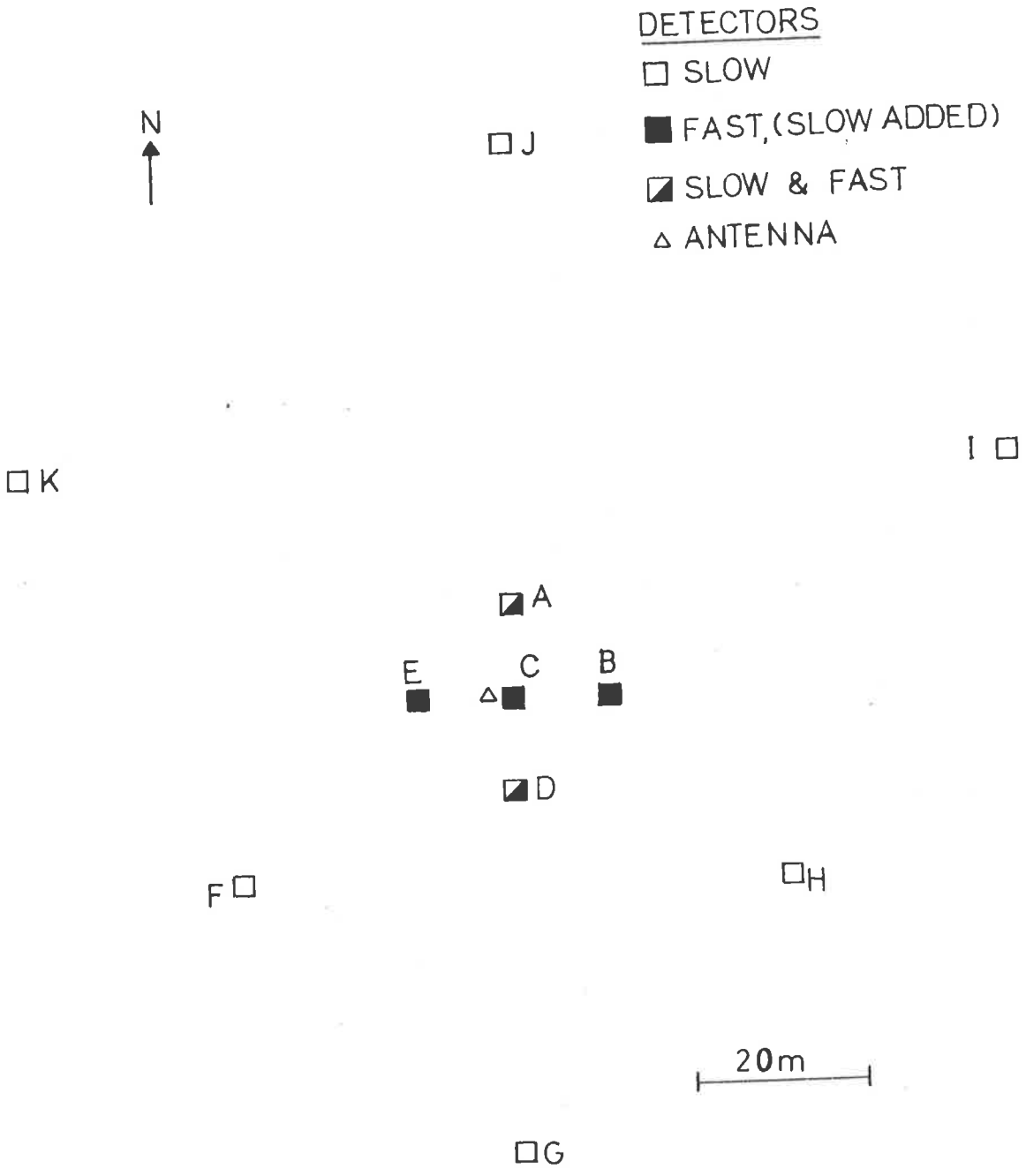

Fig 4.1 Plan of the Buckland Park Air Shower Array.

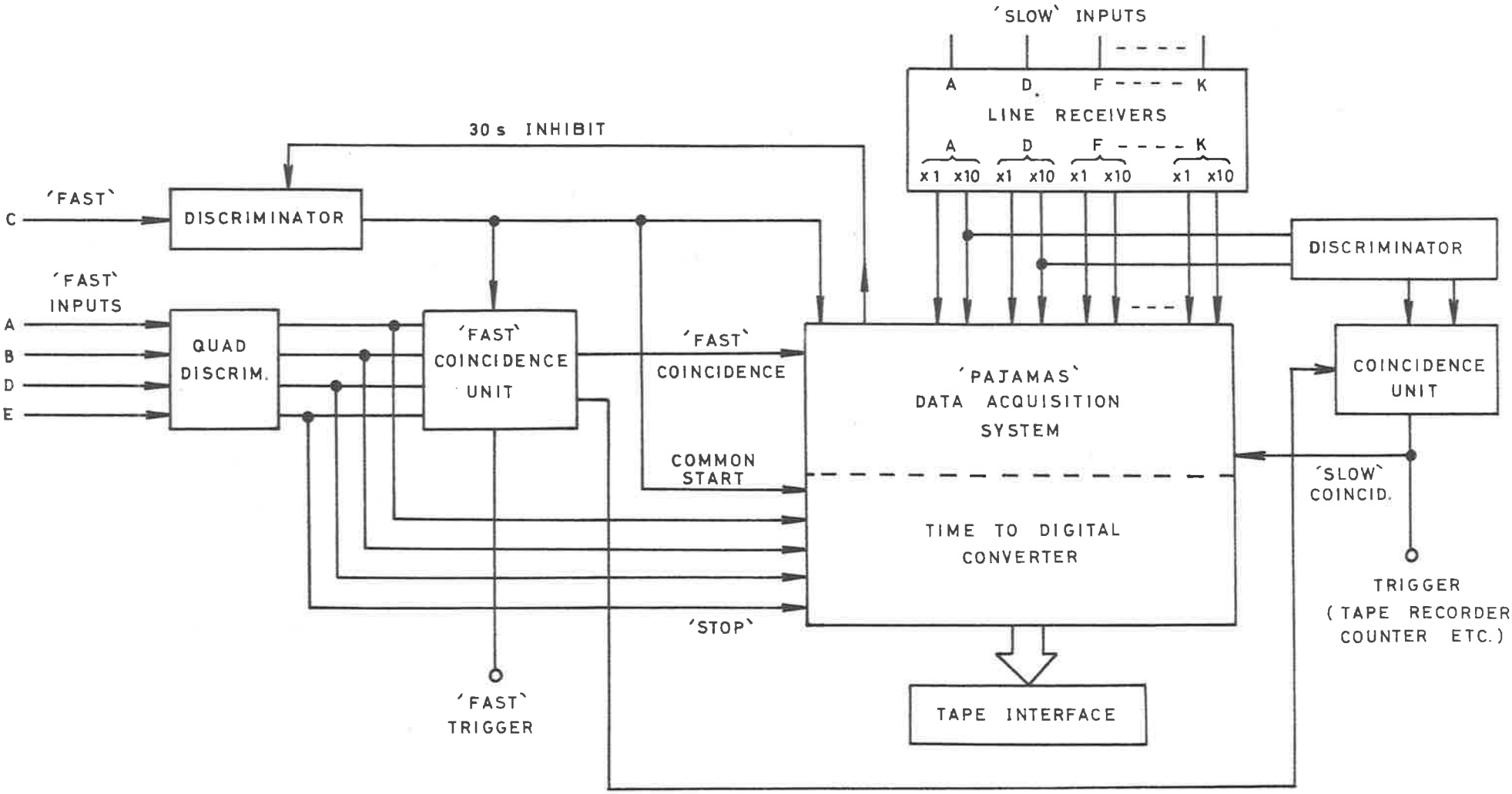

Fig 4.2 Simplified Schematic of the Array Operation.

measurement does lead to a problem with small showers. Since upwardly fluctuated densities are more likely to exceed the triggering thresholds, there is a tendency for systematic overestimation of shower size. For the expanded array, a change in triggering conditions was made. The requirement is now a coincidence between sites A and D, at the six and eight particle levels respectively (Crouch, 1979). This has a further advantage of reducing jitter in the time at which the array output trigger is produced relative to the passage of the air shower.

4.2 Shower Analysis.

4.2.1 Timing Measurements.

The times at which the shower front strikes the four 'fast' sites A,B,D,E, compared with hut 'C', allow the calculation of the zenith and azimuth angles of individual events. An estimate of the goodness of fit of a plane wavefront to the times is then given by the parameter 'σ' which is given by:

$$\sigma^2 = \sum_{i=1,4} \frac{(\text{time measured} - \text{time calculated})^2}{N - 2}$$

where N is the number of huts triggered by the shower. Although the array triggering conditions required all fast detectors to produce a signal exceeding their respective discrimination levels, the coincidence time interval is long enough that occasional signals arrive outside the possible range of acceptable times as determined by the detector spacing ($\sim\pm$70ns referred to 'C' detector). These events thus have less redundancy in the determination of directions. Events with two such times, or with inconsistent times (large σ), were not used further in the analysis in this thesis.

The accuracy of the measurement of arrival direction for average

values of $\sigma \sim 4.5$ is $2.5 \sec\theta$ (degrees) in zenith angle and $1.3 \operatorname{cosec}\theta$ (degrees) in azimuth.

4.2.2 Shower size and core location.

The calculated shower direction and the measured particle densities are used to calculate shower size and core location. A lateral distribution function of the form

$$f(R) = A/R \quad \exp(-R/R_0)$$

is fitted to the densities, where R is the perpendicular distance from the detector to the shower axis, and R_0 is set at 60m in the (initial) analysis. A least squares minimisation routine is applied to find the optimum core location and size for the shower.

The accuracy of the analysis has been investigated by P.C. Crouch (1979). It varies across the array and with size and direction. Typical errors in core location for showers of 2×10^6 particles are as much as 15m in parts of the extended array, but are less than 5m within the 'fast' array. A parameter " χ^2 " is used as an indicator of goodness of fit.

The analysis program has no automatic provision for dealing with events which saturate one or more detectors. It is, in fact, the recording electronics which saturate first; the linearity of the photomultiplier-scintillator combination has been found to be maintained up to this level (P. Gerhardy, private communication). Individual detectors also exhibited variations in response from time to time which led to the assignment of anomalous densities (in particular detectors B and J).

These events, characterised by very large χ^2 values, can be re-analysed individually, using a program developed for this application. The 'Cosmic Ray Analysis Program' (C.R.A.P., Liebing 1978) recalculates

core location and size. It allows the deletion of selected detectors, as required, and also allows a change in the scale parameter used in the lateral distribution chosen for the particle density distribution. This reanalysis was done for all the showers used in the radio analysis. It was clear that the particle density distribution used in the analysis, tended to be too steep at larger core distances. Reanalysis of events falling near the edge of the array were best fitted with the value of Ro increased by up to a factor of 2.5. Although the values of χ^2 were sensitive to this scale parameter, the actual resultant calculated shower sizes were relatively insensitive for events falling within the array.

In general, it is desirable not to use events which fall near the edge, or outside, the array. Fluctuations can lead to spurious results. For example, there are more small events which can be fluctuated upwards than large events fluctuated downwards. Consequently, the resultant energy spectrum tends to overestimate the rate of such large events. Where points on the density lateral distribution curve are obtained only on one side of the core, errors in the assigned size (and especially core location) are much greater. Of the events analysed, two which were given large χ^2 by the initial analysis, proved to have small density gradients across the array, suggesting large showers which fell far outside the array. A number of events fell near the edge of the array; these were retained in the further analysis, but with reservations.

Errors on the shower size and core location were estimated from maps of χ^2 calculated in a grid centred on the 'optimum' core location calculated by the analysis program. The core location ellipse is largely determined by the position of the nearest detectors. Except for shower cores falling close to individual detectors, changes in core location have comparatively little effect on the estimated shower size.

4.3 Antenna Location and Design.

Much of the recent work in detecting radio emission from air showers has employed the so-called "boxing ring" configuration of dipole antennas, comprising two pairs of dipoles mounted on the sides of a square, a quarter wavelength above ground. This arrangement allows the measurement of two perpendicular components of the emission (apart from relative signs, if a detector is used). From the shower direction, as measured by the array, and making an appropriate assumption about the relative signs of the two components measured by the antennas, the total field strength of signals emitted in the direction of the shower axis can be calculated. The relative signs of the two components depends on the nature of the polarisation of the emission, which in turn depends on the mechanism. For a particular mechanism (and hence polarisation), only one component need be measured in order to derive the total field.

In the present experiment, the initial aim of using one wideband-width channel (40-150MHz) effectively precluded the use of a boxing ring configuration (although in the modified form of the experiment finally adopted the use of such an arrangement of antennas in near proximity was an option). The final choice was a log periodic dipole antenna, which comprises a series of dipole elements arranged so that the length and separation of the successive elements are related by a constant factor. Thus, apart from the largest and smallest elements the structure can be described essentially in terms of angles. The phase of the transmission line is reversed between successive dipole elements, and the antenna is fed from the apex end, resulting in end fire radiation from the apex. The properties of such an antenna in free space are log periodic in the frequency domain, apart from some deterioration near the extremes of the working range of the antenna. The polar diagram is given, in simple terms,

by the product of a "dipole-like" response (for the individual elements) and an "array-like" response.

Polar diagrams for log periodic antennas have been measured and calculated by a number of authors for different geometrical factors and apex angles (e.g. Isbell, 1960, Carrel, 1961). The polar diagram has been shown to be relatively constant across the band, pattern break-up occurring only at the extremes of the working range.

The impedance of such an antenna is constant across the bandwidth only within certain limits, and this impedance variation must be taken into account in deriving the spectra for individual showers.

In the event, a commercial log-periodic dipole antenna was used (Antenna Engineering Aust. Pty. Ltd., Model 502). This is a 19 element antenna, with the last three elements being the same physical length, but helically wound to preserve the appropriate effective electrical length. The ratio of successive element lengths is .85, and the apex angle 62^{o}. The specified gain is 6dB (referred to a half wave dipole). The antenna was mounted on a pole over a ground plane near hut C, before the array extensions were contemplated. Its location at that time was chosen so as to obtain events over a wide range of core distances. A diagram of the antenna is shown in fig 4.3, and its location in fig. 4.1.

4.3.1 Impulse Response.

It is important to note that such a multiband antenna is 'wideband' in the sense of maintaining a wide frequency response, but does not preserve phase relations across the total bandwidth. In simple terms, the working point of the antenna moves down the antenna as the wavelength increases. This also applies to other wideband antennas such as the spiral antennas used by the Kharkov and Dublin groups.

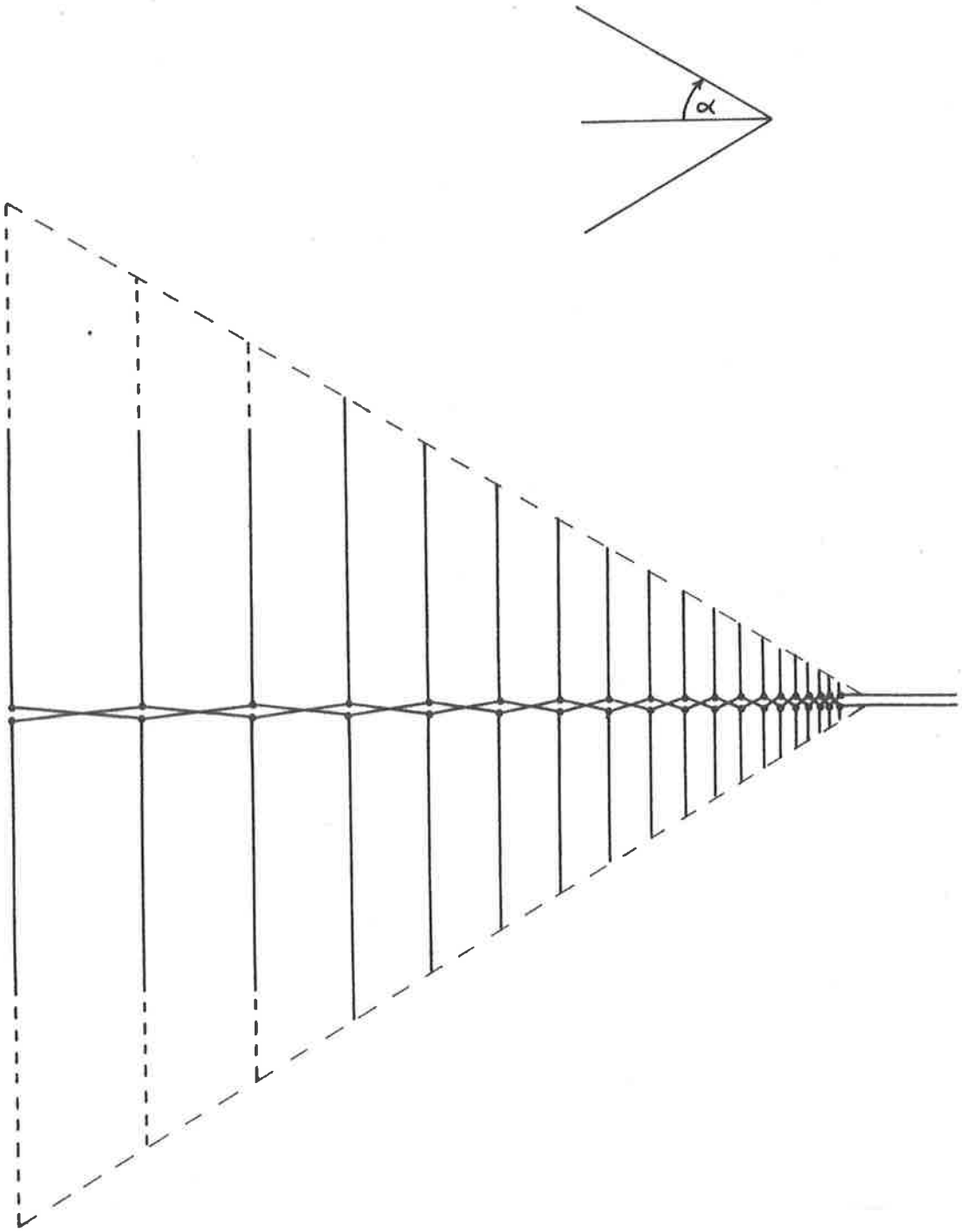

Fig 4.3 Log-Periodic Dipole Antenna.

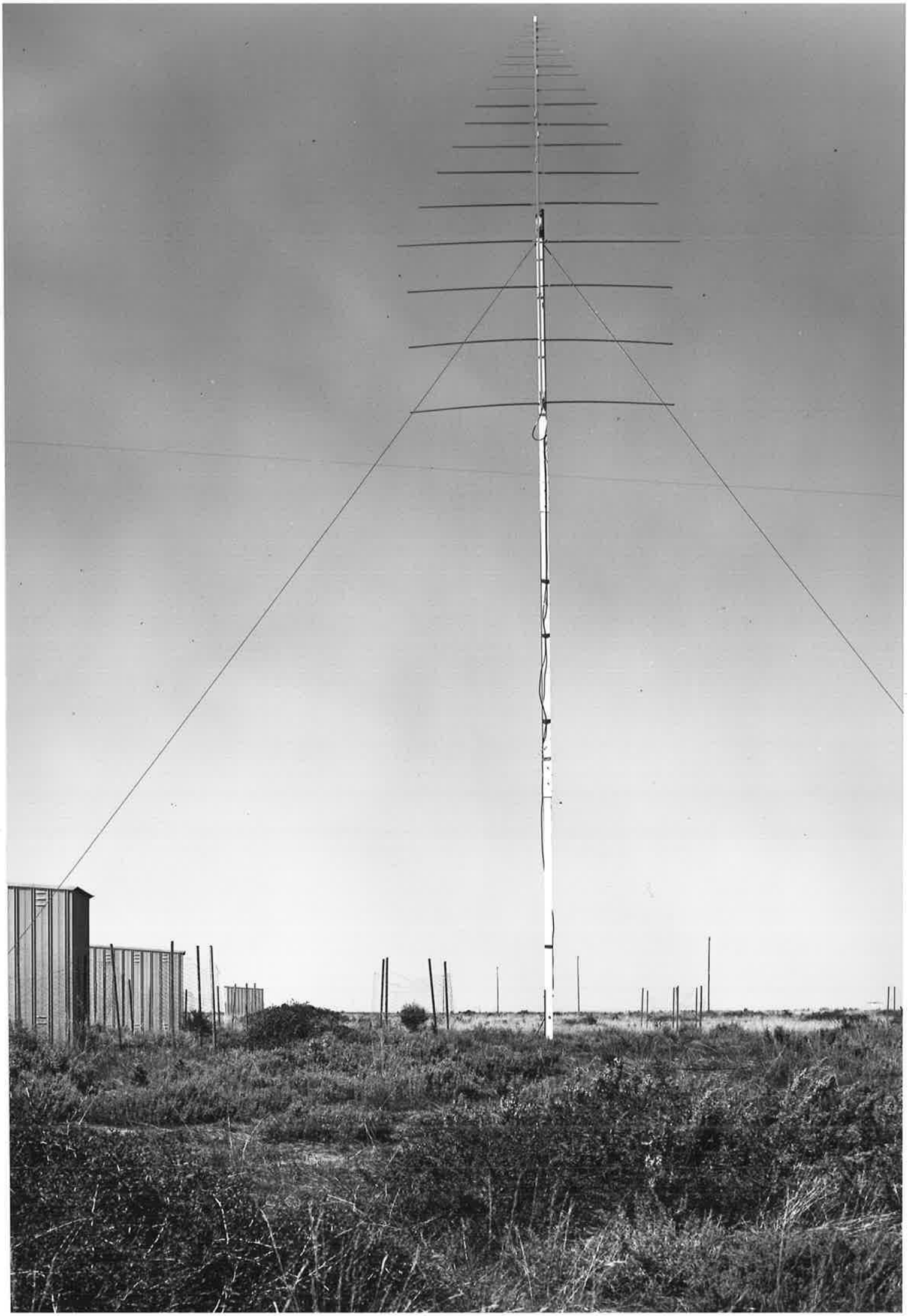

The transient behaviour of log periodic dipole antennas has been studied by several authors (see for example, Langenberg, 1979). According to the simplified calculation of Knop (1970), who assumed a model in which only the half-wavelength dipole radiates, the impulse response takes the form of an oscillation rapidly decaying in frequency, the instantaneous frequency depending on the apex angle 2α, and time t, viz

$$f = \frac{1}{4 \tan \alpha \, t}$$

The envelope of the response reaches its maximum at some time t',

$$t' = \frac{1}{4 \tan \alpha \, f_p}$$

where fp is a frequency in the pass band of the antenna. For the antenna used at Buckland Park, this suggests an impulse response of the order of 15ns in length. Fig 4.4 presents a sample calculation of the response for a vertically incident impulse and for a somewhat idealised antenna admittance dependence on frequency. A more sophisticated calculation with a more realistic antenna model would be needed for use in deconvolving required signals. Construction of another 'identical' antenna (or a scaled down pair of antennas) to allow transmission from one to the other would allow an experimental response to be measured. (Such a procedure has been used to obtain the "double" impulse response of a pair of spiral antennas (Pulfer, 1961).) The response will depend on the arrival direction of the received pulse, owing to phase differences between successive elements. For use with relatively narrow band receivers (such as are used in the multiplexed system to be described below), the antenna dispersion is not large enough to be significant.

4.4.1 Preliminary Work and Pilot Studies.

The first program for determining the spectrum of the radio emission

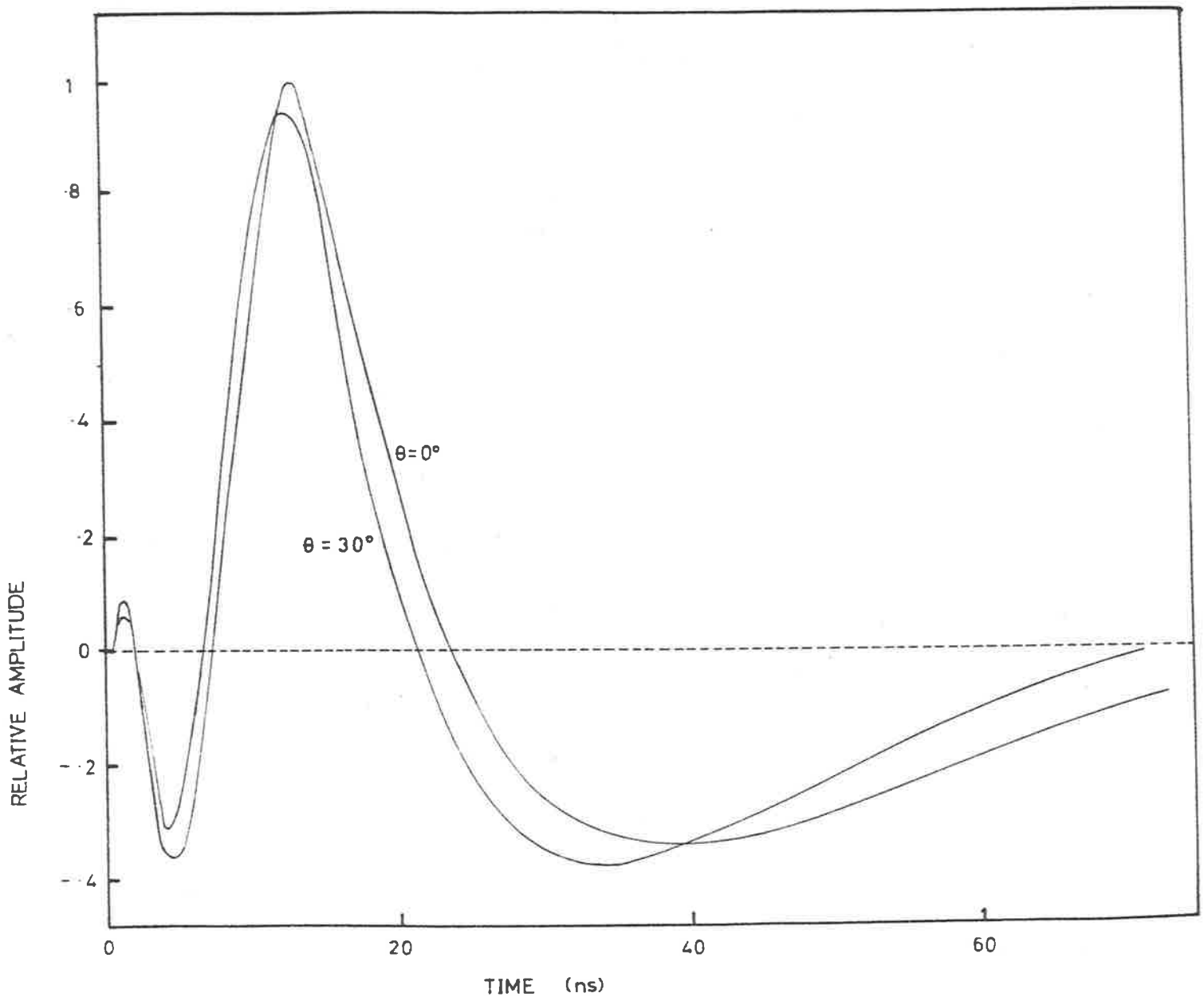

Fig 4.4 Impulse Response of Antenna.

at Buckland Park, a relatively quiet site (Clay et al, 1973), comprised the log periodic antenna feeding, via a bandpass filter, into a wideband (40-180MHz) amplifying system with a total gain of 60 dB. The system was run during early morning hours when television transmissions were off, and the undetected output was displayed directly on a Tektronix 7904 oscilloscope, running on 20ns/division. For several reasons, no measurable radio pulses standing out above noise were observed.

The factors contributing to this were as follows: firstly the level of interference proved to be larger (by a factor of about three) than values for the natural background ($\sim 1 \mu V m^{-1} MHz^{-1}$, e.g. David and Voge, 1969). The running time for data collection was thus increased by a factor of about eight from the initial estimate of 1-2 pulses per fortnight. A spectrum analyser was used to investigate the sources of background noise; a number of transmissions in the band were located, and the effective contribution to increasing the background level calculated, the sources are shown in fig 4.5.

In addition to the background level, the task of identifying radio pulses was complicated by the non-uniform phase characteristic in the impulse response of the antenna, as discussed above.

A further shortcoming of the system was the triggering arrangement. The oscilloscope was triggered directly by the particle array 'fast' trigger, rather than the 'slow' trigger, since the delay required in the radio signal would have both limited the bandwidth and also produced excess jitter in the position of the radio pulse on the screen. However, even with a 'fast' trigger, jitter in the position of the pulse on the screen simply from array geometrical conditions amounted to 50ns for showers with zenith angles less than 45 degrees.

This experiment was abandoned in the form described above, after observing no pulses standing out above noise at all in a period of ten

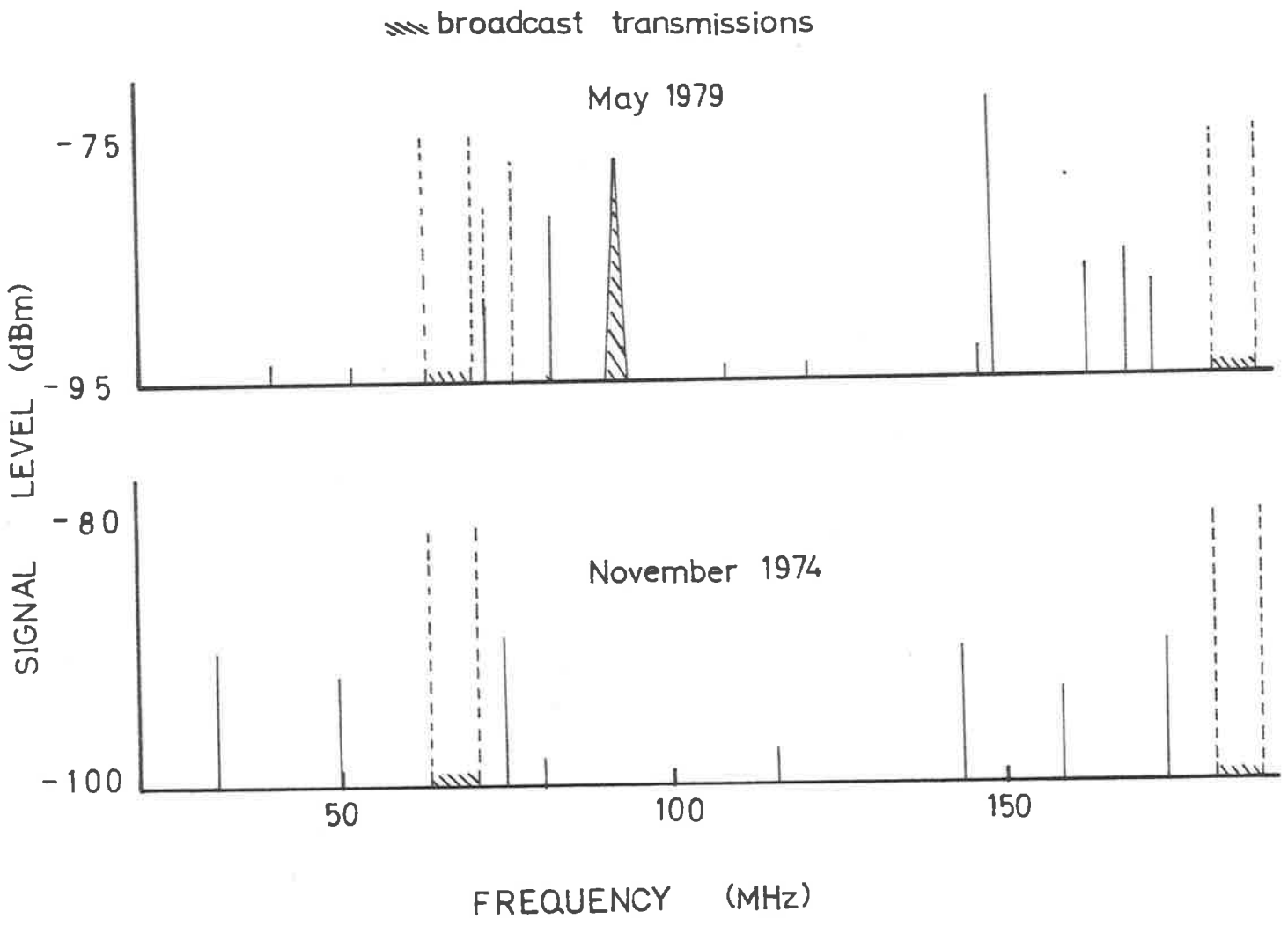

Fig 4.5 Background Transmissions.

months. Checks were then made to detect pulses at spot frequencies. A 50MHz receiver with a bandwidth of ~7MHz was used in place of the wide-band amplifiers. The traces were analysed in the now traditional way of measuring the largest amplitude in each of several time intervals, one of which includes the expected arrival time of a shower-coincident pulse. The deflections are squared (for a linear detector) and added, for each interval. The average for the "noise" bins is then subtracted from the "signal plus noise" bin to yield, in principle, the square of the signal field strength.

The results of these investigations were as follows: operating the 50MHz receiver (RHG model EVT50BB63) from the 'fast' trigger (i.e a coincidence between the detectors in the inner 30m array), 280 events satisfying noise criteria were observed. The traces were divided into 10 channels, each of 200 ns length, with the signal expected to be confined to one channel. The plot of the means of the ten channels is presented in fig 4.6, a significant excess is present in the eighth (and to some extent) the seventh channels. However this time is inconsistent with that expected for emission associated with the showers themselves; the expected column for excess is marked on the plot and is not significantly higher than the other noise channels. The presence of this interference, occurring some 750ns after the expected arrival time of shower associated pulses, was also observed when a 120MHz receiver (RHG model EVT12020RFI) was used in the same arrangement in place of the 50MHz receiver.

The source of this interference may be a combination of several factors. The signal from the antenna passed through a length of cable to the receiver, and a further length of cable (for delay) fed the signal to the oscilloscope. On setting up the system, some interference was observed in the eighth and ninth channels; this was tracked down to pick

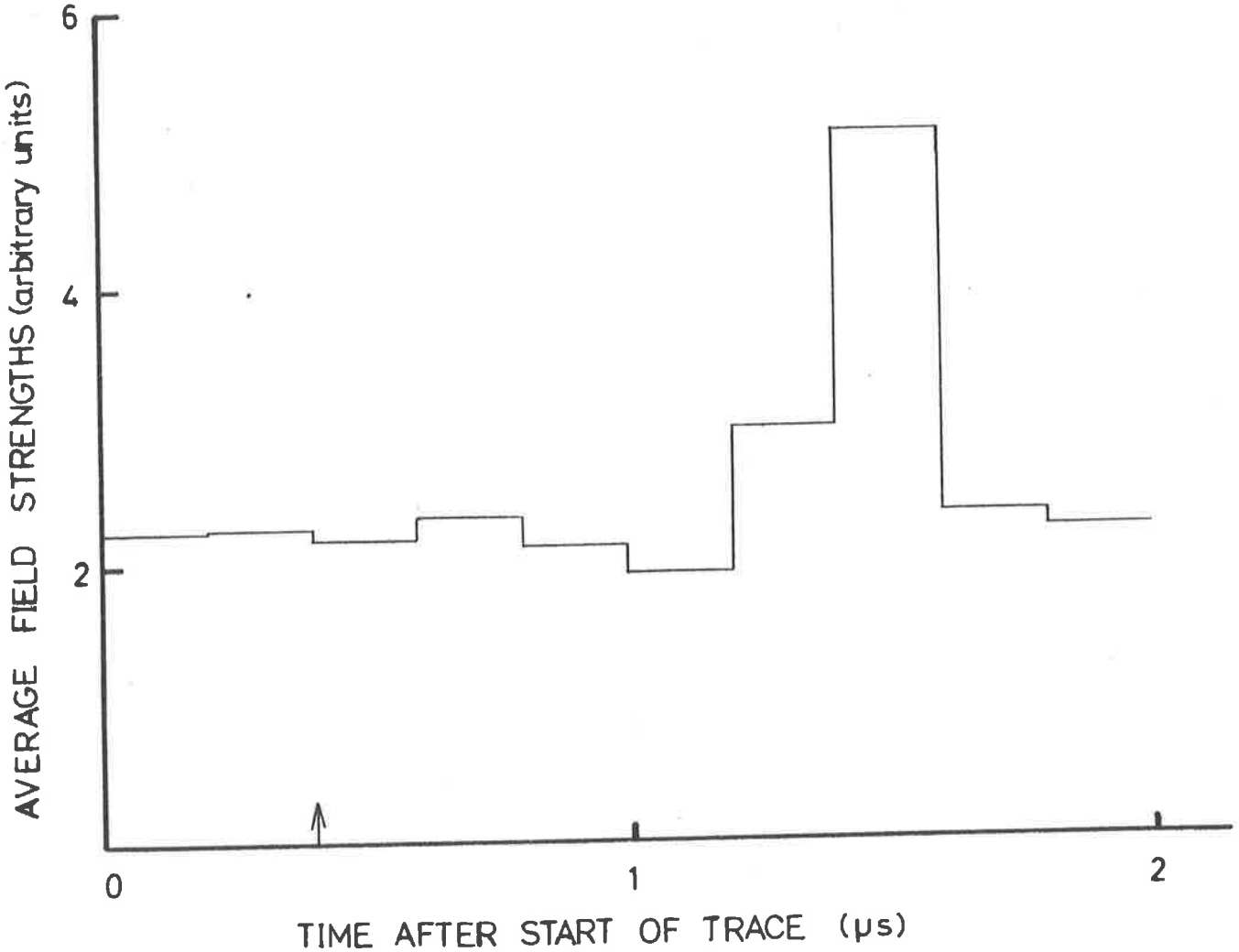

Fig 4.6 50 MHz signal amplitudes (triggered from 'fast' system) (The arrow marks the expected pulse position).

up between the cables carrying particle information from the detectors and the cable carrying the very low level radio signals. Rerouting the radio cable reduced the level of this interference. (Similar interference pulses at other times were present on some traces, consistent with particles travelling through detectors at other times). It would appear, however, that the problem was not entirely cured.

The system was modified, using the same 50MHz receiver but with the standard 'slow' trigger, reducing the rate of triggers by a factor of about six. The receiver was placed in a box mounted at the base of the antenna pole, and operated with greater gain. The signal cable was arranged to cross the particle array cable at right angles. The data were analysed in a way similar to the above; traces were divided into blocks and the largest excursion in each block measured and recorded.

A block of 229 events recorded in July and August, 1976 was treated in this way, and divided into 9 channels. The expected position of the radio signal being in the second channel. A significant excess was observed in this channel and was used to estimate the normalised field strength. Shower sizes and directions were known for individual events. The plot of mean field strengths appears in fig. 4.7. The conditions of operation were such that the receiver operated in the linear section of its characteristic (fig 4.8). The normalised field strength of the excess signal is of the order of $10\mu Vm^{-1}\ MHz^{-1}$.

A block of 327 events, of smaller average shower size, recorded subsequently to the above was analysed by splitting traces into only five bins. An intermittent source of interference appearing later in the trace contaminated about half the events. This was produced while another experiment was being conducted on some nights, and was caused by radiation as a result of the earthing arrangements associated with the array and ancillary experiment electronics being spread between two caravans with separate

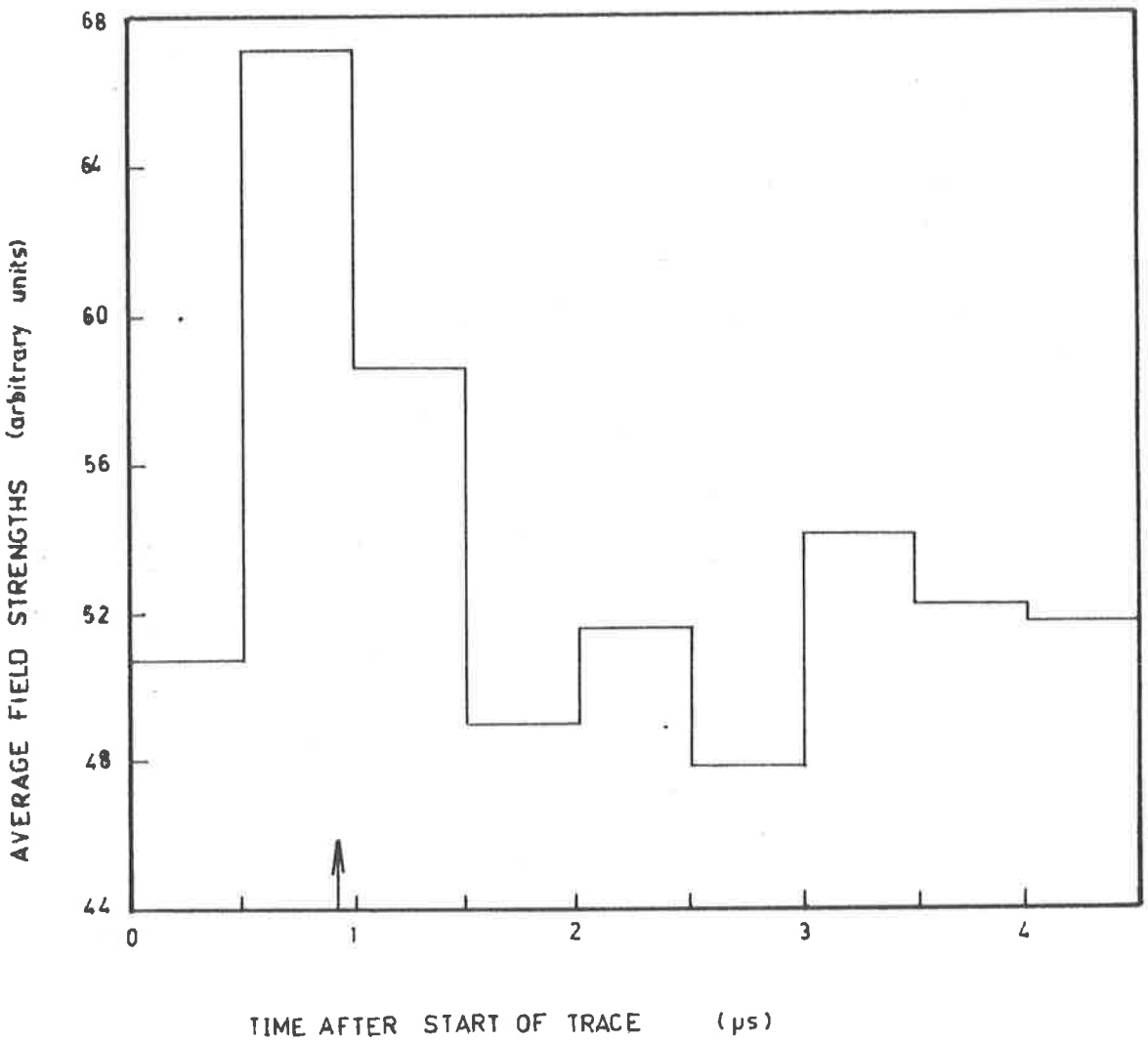

Fig 4.7 50 MHz signal amplitudes (triggered from 'slow' system) (The arrow marks the expected pulse position).

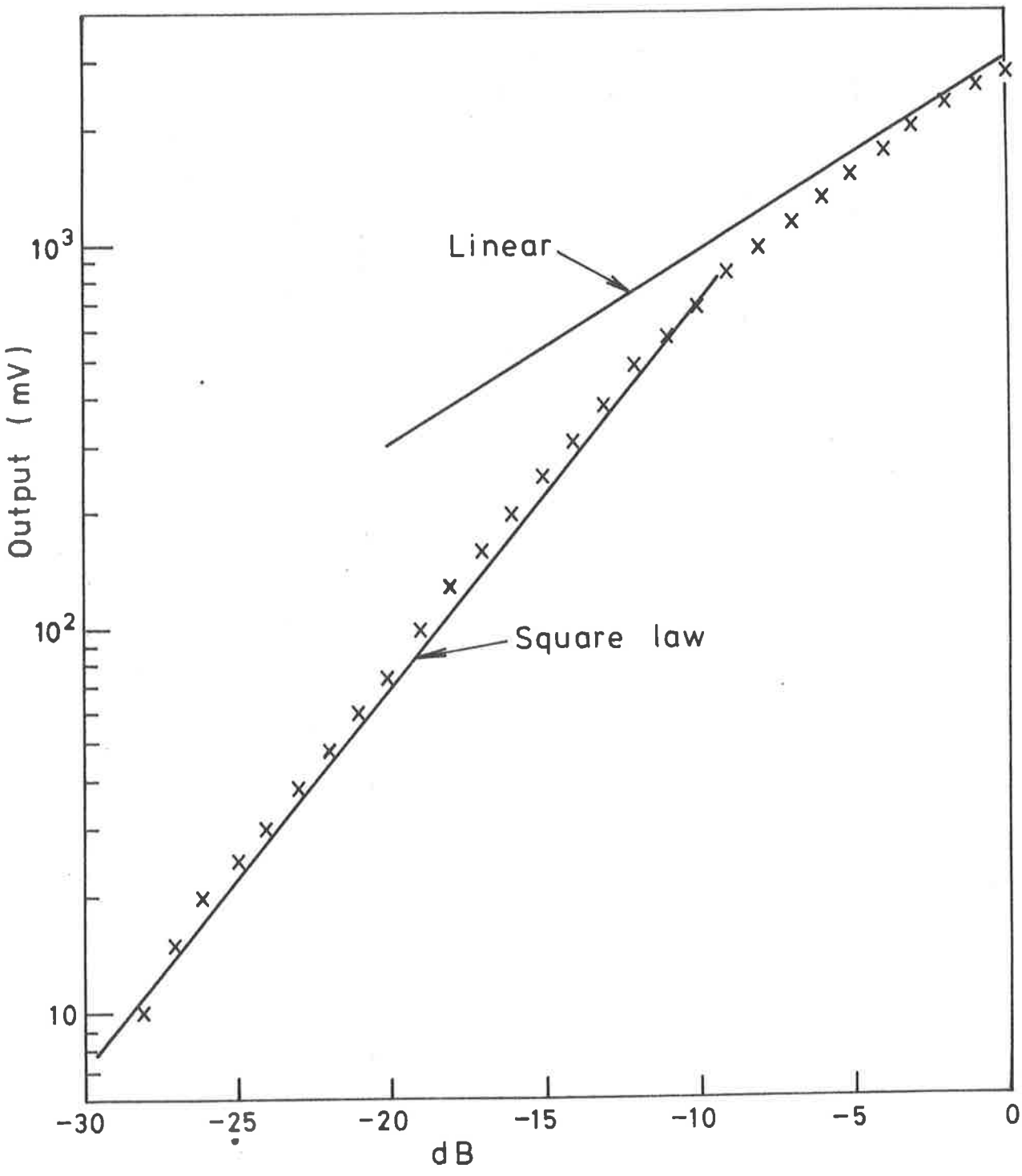

Fig 4.8a Amplitude characteristics of the 50 MHz Receiver.

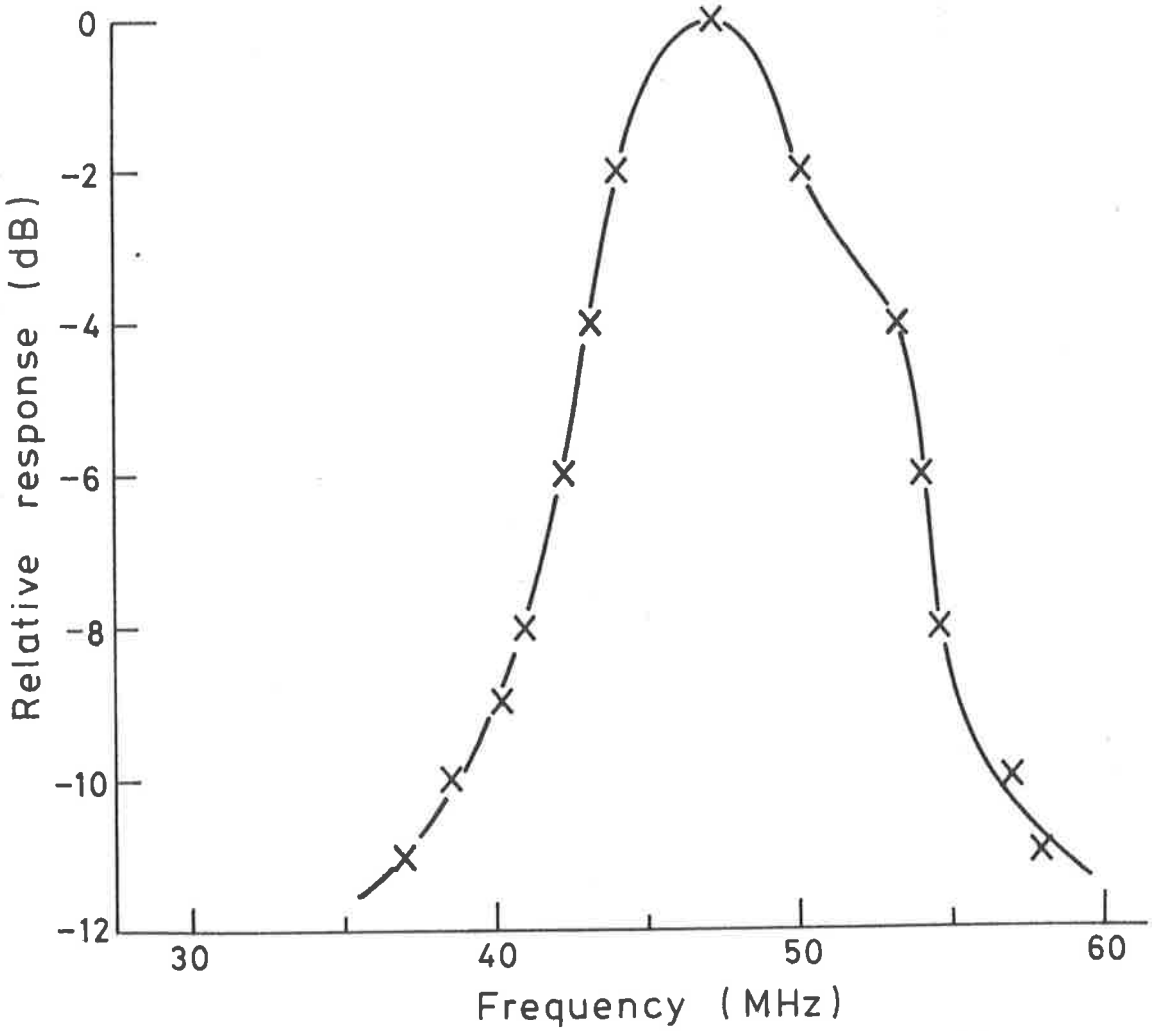

Fig 4.8b Frequency Response of the 50 MHz Receiver.

mains supplies. The plot from this data, omitting the obviously contaminated events, had no significant excess in the expected channel (fig 4.9a). From this block, 41 events larger than $5x10^5$ particles at sea level were considered, but also did not yield an excess (fig 4.9b); however with the number involved, the statistics were poor.

The net effect of these 50MHz observations was to establish an approximate value for the radio field strengths, and to define some of the operational problems, particularly with regard to local interference.

4.4.2 Test transmissions.

Test transmissions at two frequencies 50 and 120MHz were made as a check on antenna operation, and in particular on delays. A square-wave modulated signal was transmitted via a simple folded-dipole antenna in each case. The time of detection of the received signal was measured as a function of test antenna-to LPD antenna distance. The result (fig 4.9) is consistent with a short internal delay in the antenna.

4.5 Modified Recording System.

On the basis of the experience gained with the wideband system, a modified recording system was set up, with the following design characteristics in mind: firstly, the desirability of as wide a bandwidth as possible; secondly, the use of varicap-tuned modules to facilitate tuning adjustment; thirdly, triggering arranged so as to reduce jitter in the expected position of the pulse on the trace to a minimum; fourthly, signal multiplexing in order to display all channels on the one trace; finally, careful attention to cable layout and routing. This system will be described briefly below.

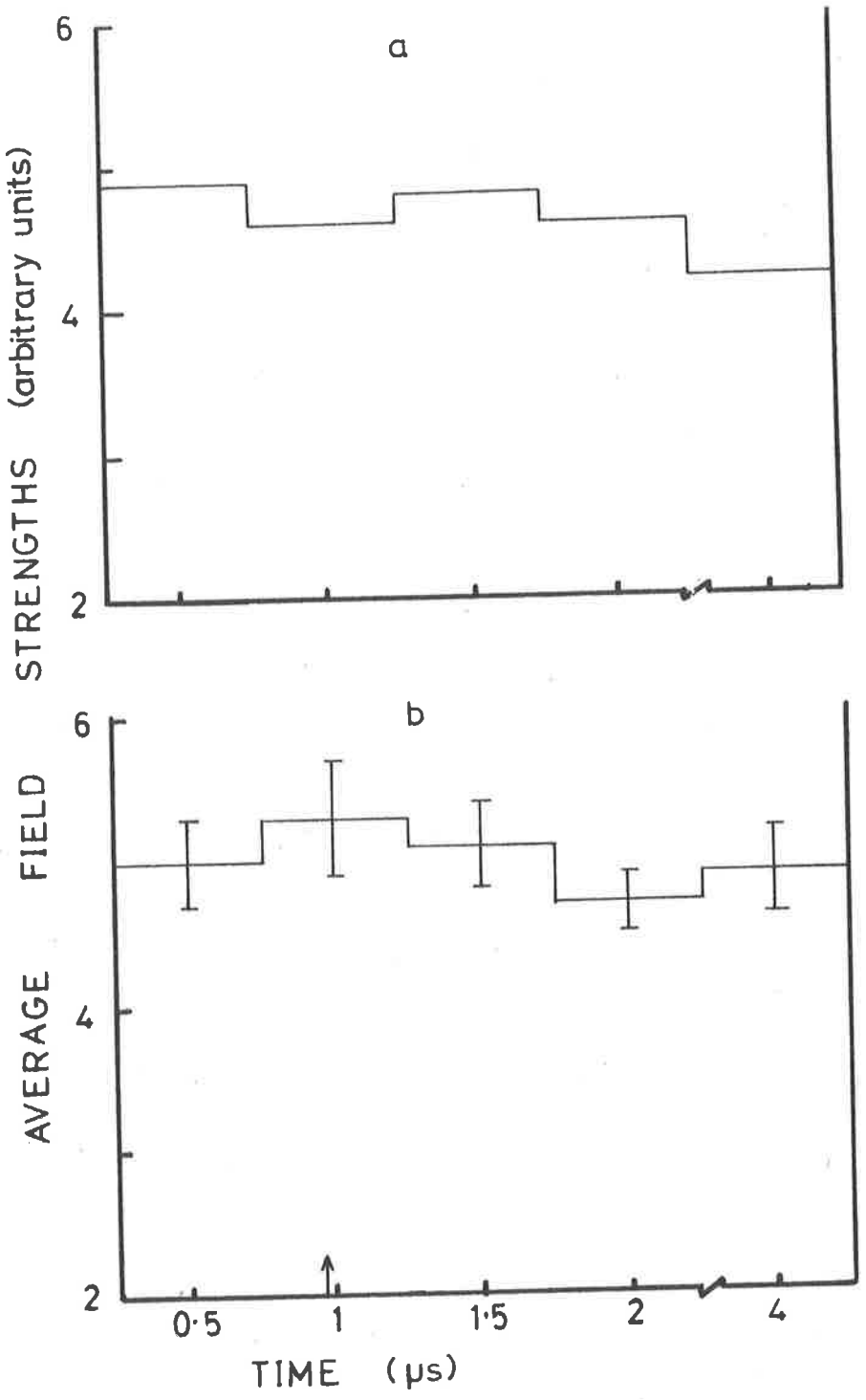

Fig 4.9a 50 MHz signal amplitudes (triggered from 'slow' system)

b 50 MHz largest showers. (The arrow marks the expected pulse position).

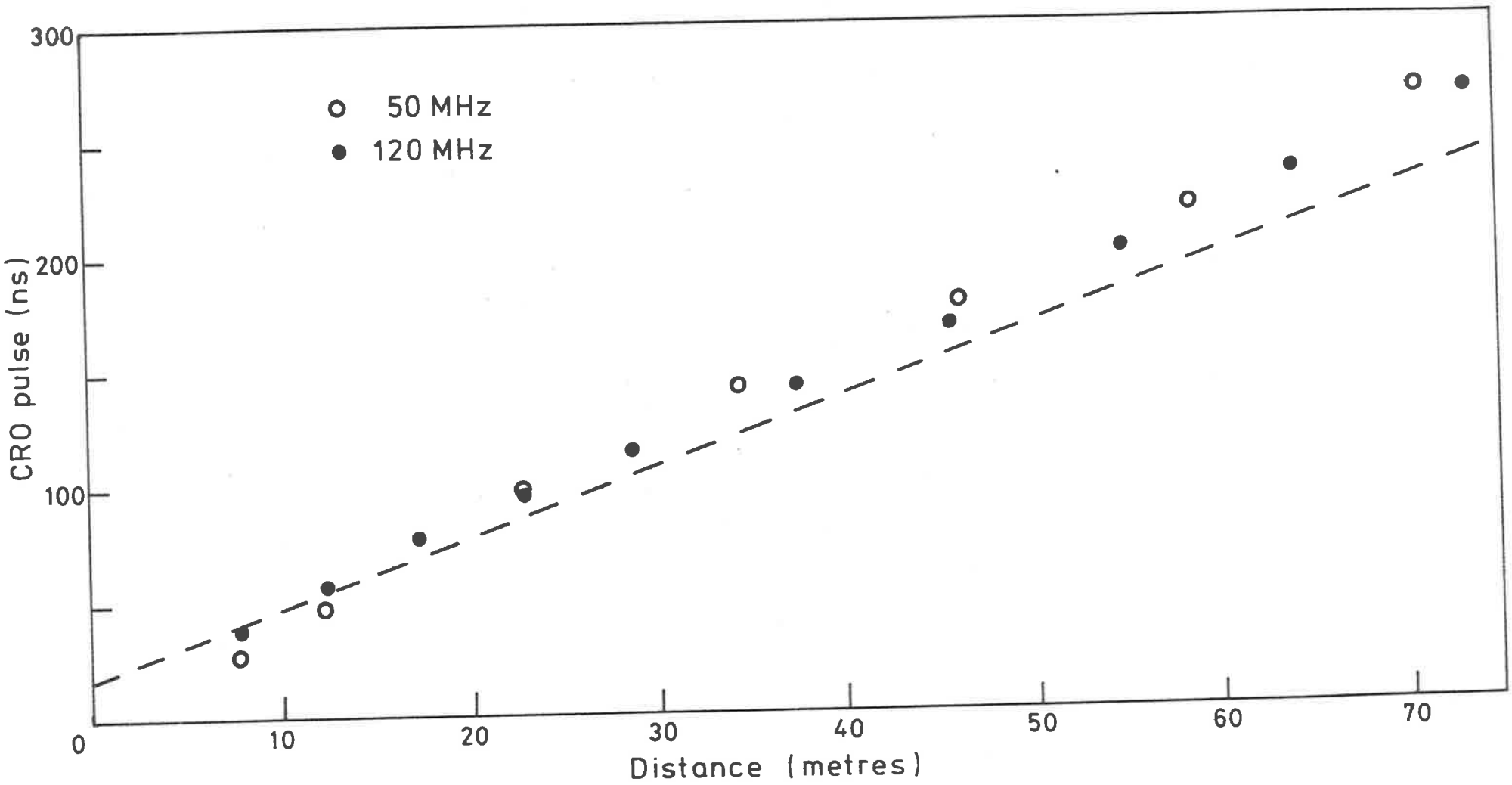

Fig 4.9 Delay in received signal as a function of the distance of the transmitting antenna from the log periodic antenna. (The slope of the dashed line represents the expected dependence).

4.5.1 Multiplexing System.

The radio detection system in its present form comprises several sections. The log periodic dipole antenna is connected to a wideband low-noise preamplifier (the design from CSIRO Division of Radiophysics, and noise figure less than 2dB). The preamplifier is mounted at the base of the antenna mast (see Fig. 4.10). To avoid preamplifier saturation a filter was added between the antenna and preamplifier to reject f.m. radio transmissions at (92.1 MHz). Television interference (63-70MHz and 181MHz upwards) was avoided by restricting hours of operation to between midnight and 6-30 a.m. The impedance of the filter varies significantly across the band, and was taken into account in the calibrations as described in section 4.5.2. A T.V. rejection notch filter was also constructed, but the matching was poor and its use was not adopted.

The signal from the preamplifier is then fed through 40 metres of cable to the recording van, to another preamplifier before the signal is split to feed four television-type detectors. The second preamplifier was necessary because the noise figures of the television tuners, specified at spot frequencies, proved to be too large at higher frequencies. The four detectors are based on Philips modules, each channel comprising a varicap tuner feeding an IF strip and then the detector stage (Philips modules U200, U210, U230). Front panel screwdriver controls allow the individual adjustment of the gains of the tuner and IF modules, and the frequency of the tuner. The outputs of the detectors pass through delay cables to a multiplexing unit, which switches in the channels at the appropriate time.

The multiplexer unit accepts two inputs from the array electronics.

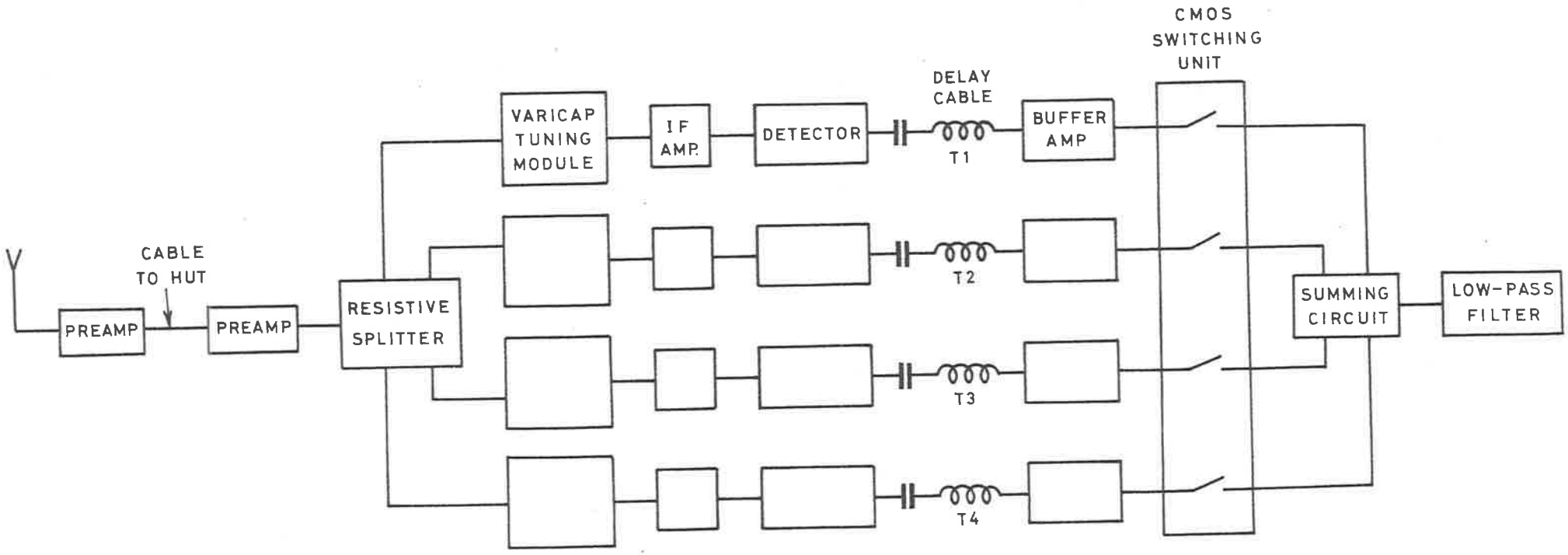

Fig 4.10 Block Diagram of 4-channel system.

To reduce jitter in the position of the trace on the screen to a minimum, the timing sequence is controlled by a pulse from the discriminator connected to the detector nearest the antenna ('C' fast). With the array coincidence requirements, this implies that a pulse is obtained whenever the array records an air shower. A coincidence circuit in the multiplexer triggers the oscilloscope only when a trigger pulse from 'C fast' is followed by the array output trigger pulse. The output from the multiplexer is displayed as a single trace on a Tektronix 7904 oscilloscope, viewed by a Beattie Coleman 35mm camera from which the shutter has been removed. The camera is advanced by the array output trigger. The event time (which is recorded on the analysed array output) appears on four pulsed 7-segment LED displays for each event for identification. The transistor and relay electronics driving the camera was a source of some interference and spurious triggering, and was later replaced by CMOS logic and a solid state relay (i.e. an optocoupled triac) with greatly improved reliability. A block diagram of the multiplexer is shown in fig 4.11.

As a check on possible gain fluctuations in the signal amplifiers, a tunnel diode "impulse" generator was used. This provided a pulse with FWHM of ~5 ns which was switched in the input to the splitter at predetermined intervals of 20 minutes. From the risetime (1·2ns) and falltime (·8ns) of the impulse (as measured by the Tektronix 7904 oscilloscope with specified risetime of ·8ns) the spectrum of the pulse was calculated to be flat over the frequency range used, and was consistent with calibrations. The circuit and pulse shape are shown in figs. 4.12 and 4.13.

The main source of variation in gain was found on testing, to be the detector module. This was largely controlled by using a

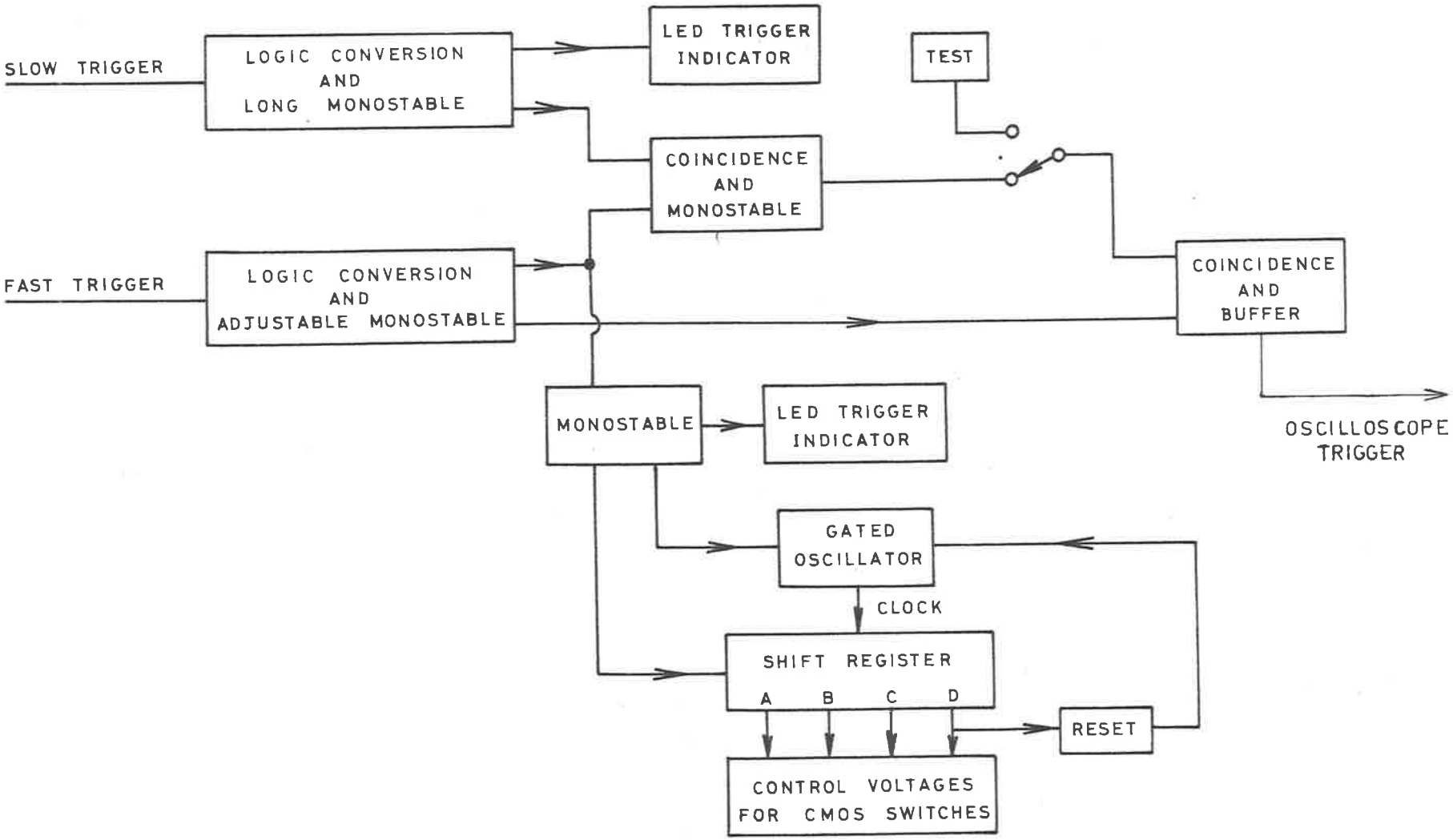

Fig 4.11 Block Diagram of Multiplexer.

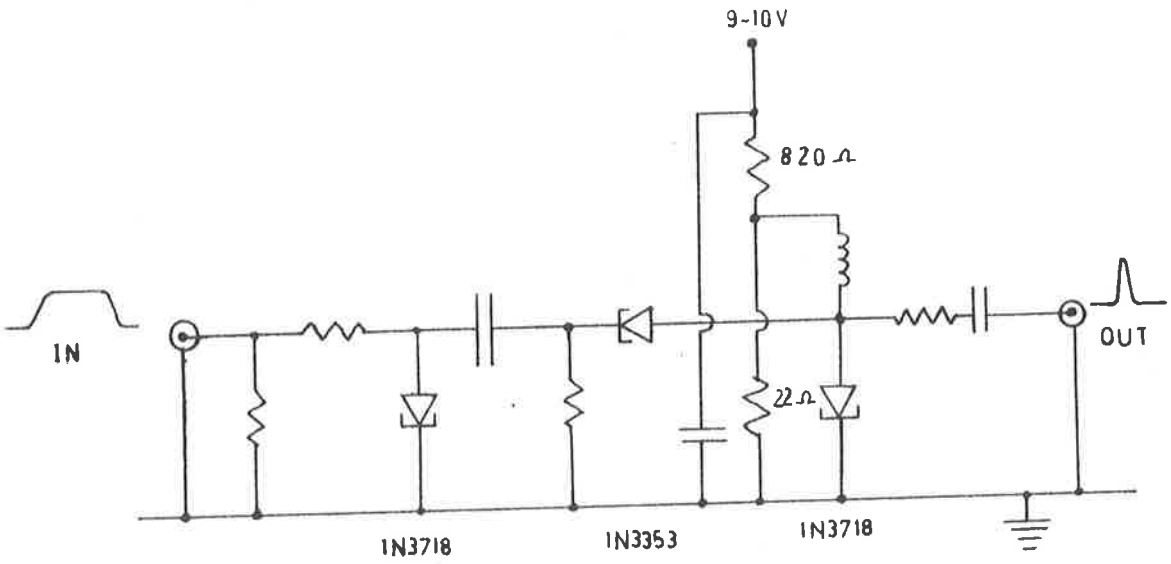

Fig 4.12 Circuit of Impulse Generator.

(modified from RCA Tech. Man TD-30, 1963)

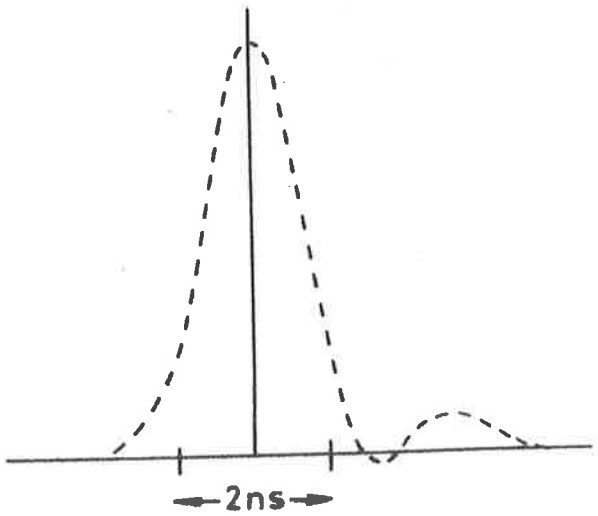

Fig 4.13 Pulse Shape of Impulse.

thermistor in the gain-control line to the IF stage. Testing with a hairdryer indicated negligible thermal dependence in the performance of the preamplifiers.

The frequencies chosen for the four-channel experiment were determined largely by background noise considerations. Although a logarithmic increase in frequency was considered desirable, within a range 45-160MHz, it turned out that the frequencies were more or less evenly spaced, from 45MHz to 135MHz. The selection was made by adjusting the tuning voltage in each module so as to obtain minimum noise on the oscilloscope screen, at a time when television transmissions were off. The background was later checked with a spectrum analyser, which confirmed that three channels lay in gaps between manmade transmissions, but there was an intermittent transmission in the fourth (75MHz centre frequency). Although the bandpass characteristics of the tuners changed somewhat over the tuning range, especially at the lower end, the response in individual channels could be tweaked with trimming capacitors in the tuner and IF module. The bandwidths of the channels were the same to within a few percent (see fig. 4.14). Sources of interference across the band, with filters in circuit, are shown in fig. 4.5.

4.5.2 Calibrations.

In addition to the systematic impulse check on the gain of the system, regular calibrations were carried out. The cable from the antenna to the first preamplifier was replaced by a cable from a signal generator. From the measured values of the impedances of the antenna, filter, and cable (measured from the same point), a correction can be made to relate signals from the antenna to signals from the generator.

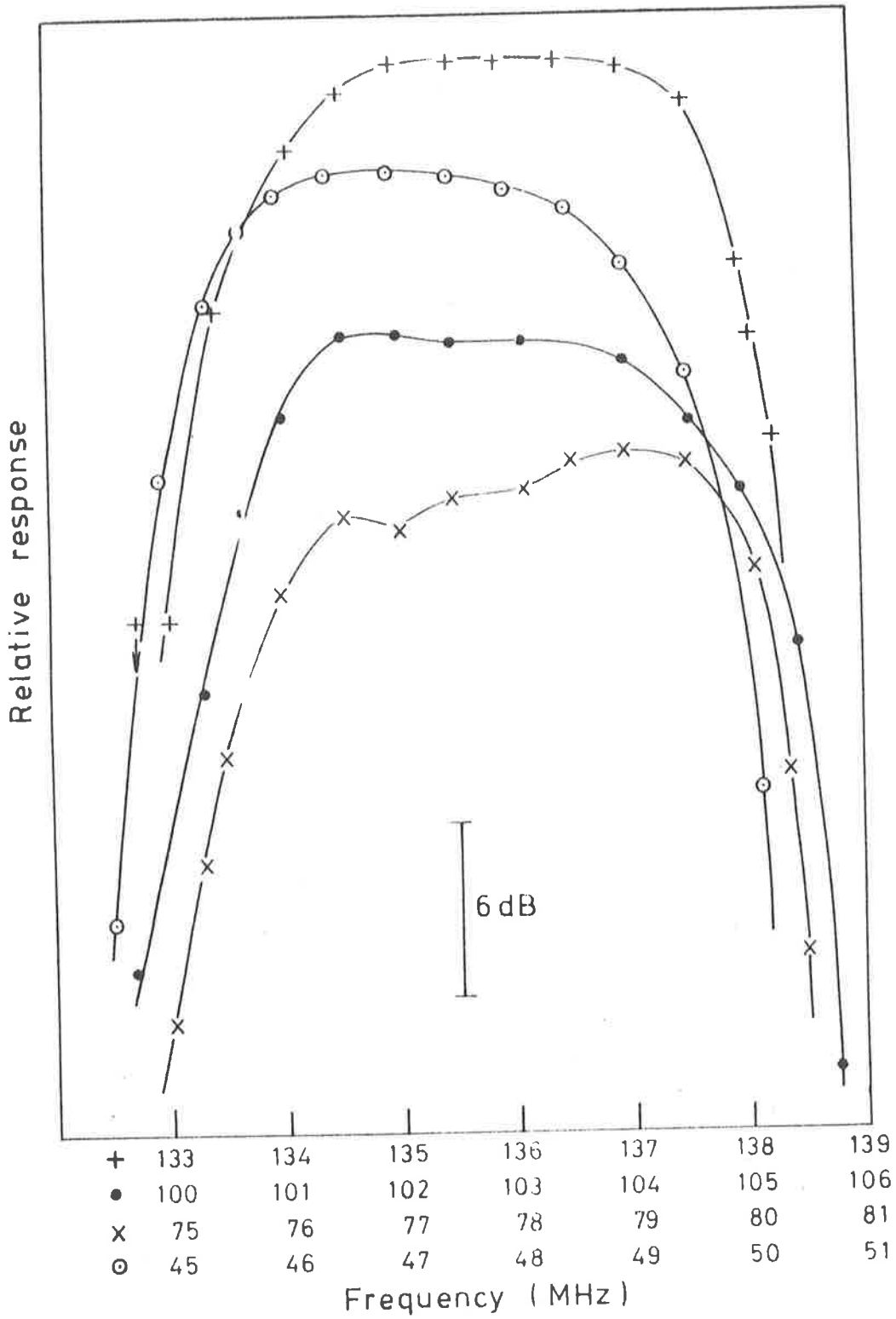

Fig 4.14 Frequency Response of Receivers (displaced vertically for clarity)

In general, given a radiation field E, then the power W passing through an area A is (e.g. (Kraus, 1950),

$$W = \frac{E^2 A}{120\pi}$$

where 120π is the impedance of free space. In terms of the radiation resistance of the antenna R , and the voltage induced on the antenna terminals, V_a,

$$W = \frac{E^2 A}{120\pi} = \frac{V_a{}^2}{R}$$

The effective aperture of an antenna is related to the maximum gain by

$$Gmax = 4\pi A/\lambda^2$$

In terms of the calibration procedure, if the impedances of the preamplifier, antenna and cable from the generator are Z_p, Z_a, Z_c, respectively, then the input to the terminals of the preamplifier in terms of the field strength per unit bandwidth (E_ν) and polar diagram F (θ,ϕ) is

$$V_i = \left(\frac{Z_p + Z_c}{Z_p + Z_a}\right) \frac{R^{\frac{1}{2}} A^{\frac{1}{2}} E_\nu \, d\nu}{f(\theta, \phi)(120\pi)^{\frac{1}{2}}}$$

For the impedances and bandwidth used, the conversion constant between V_i (μv) and $E\nu$ ($\mu Vm^{-1}MHz^{-1}$) for the four channels (for signals from the zenith), is (.14, .24, .33, .43) respectively.

The modulated signal from the generator (Wavetek model 1002 sweep generator) was measured, and fed through a step attenuator to the pre-amplifier. The characteristic proved to be linear from noise to close to saturation. Linearity was also checked for short pulses using the

'impulse' generator with the step attenuator.

4.5.3 Timing Measurements.

The jitter in the position of the radio pulse on the screen arising from the time taken for the shower front to move the distance between the antenna and C hut is expected to be less than 40 ns. The position of the pulse was checked by feeding an (attenuated) output from the C fast discriminator (appropriately delayed) into one channel of the signal multiplexing unit, and also with the impulse generator which supplied a trigger pulses to the inputs of the multiplex unit a fixed time before producing the impulse itself. A block diagram of the arrangement is shown in fig. 4.15.

Calculations indicate that the delay in the antenna for a 50-140 MHz range of frequencies is less than 10 ns, and thus can be neglected. By sending a short pulse down the cable and observing the reflection from the antenna, the time for low frequencies to travel down the antenna to the termination and back can be measured; the risetime of the reflected pulse is 20 ns, comparable with the figure expected for a 30MHz lower limit.

4.6.1 Extraction of Signals from noise.

The problem of extracting radio signals from noise has taxed all workers in the field. A number of techniques has been employed. Given a continuous signal in the presence of background noise with which it has a randomly varying phase, then the square of a 'noise' measurement may be subtracted from a 'signal plus noise' measurement to yield an estimate the square of the signal, averaged over a number of events, viz,

$$\Sigma\{(S+N)^2-N^2\} = \Sigma\{S^2+N^2 + 2SN\cos\phi - N^2\} = \Sigma S^2$$

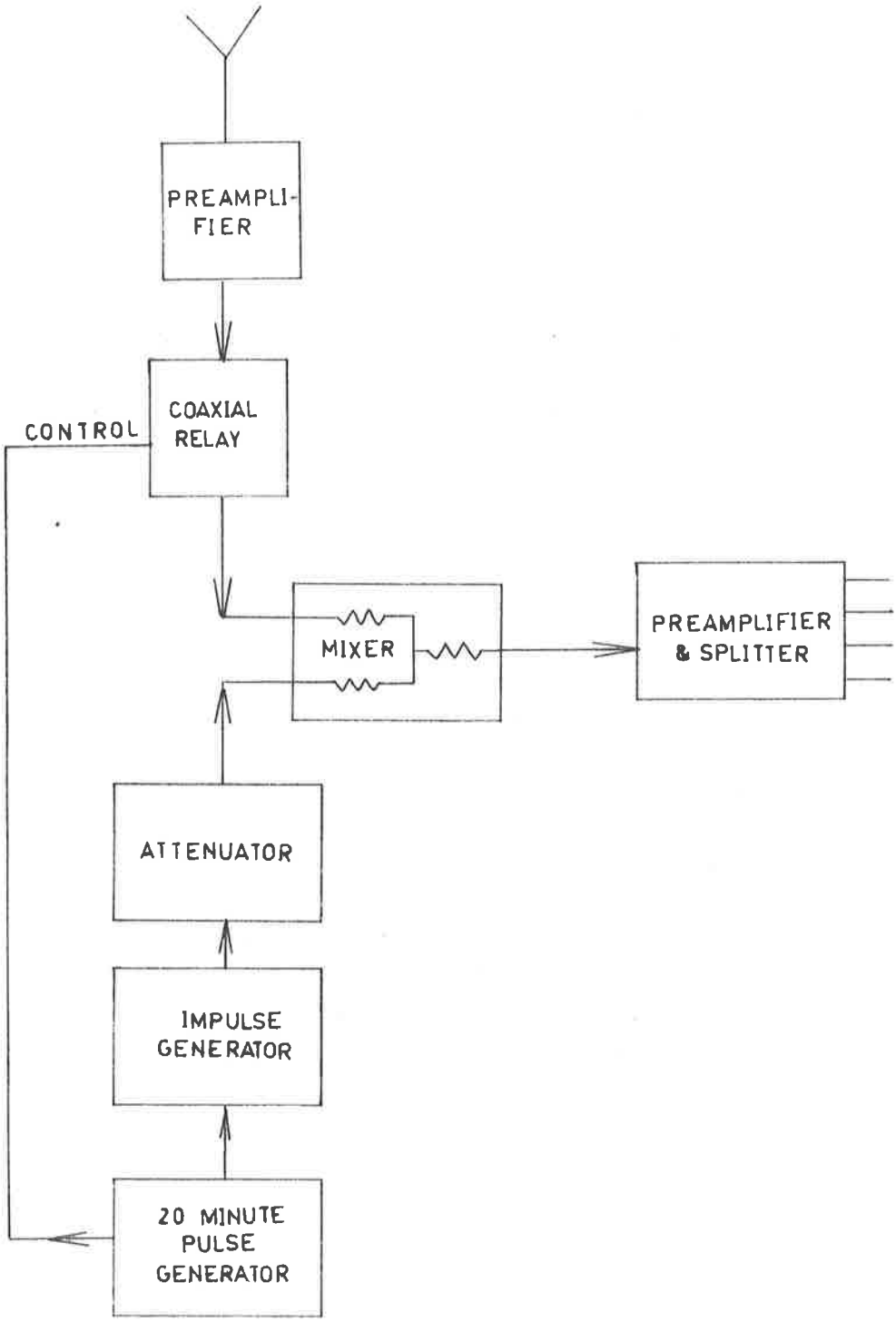

Fig 4.15 Block diagram of Calibration Procedure.

In the case of an impulse, the signal either adds to or subtracts from the noise waveform in the time domain. For an individual trace the best estimate of the signal was taken as the observed field strength at that time, with error bars determined by the level of noise on the rest of the trace.

Prewitt (1978) has considered the effect in the frequency domain of estimates of the most probable value of the signal for the case of an impulse and gaussian noise. For small signal to noise ratios, greater than one, the measured signal amplitude overestimates the true amplitude, by some 10% for a signal to noise (i.e. standard deviation) ratio of 2:1, increasing as the ratio falls. Thus the use of individual events as described above with poor signal to noise ratio will introduce a systematic overestimate of the field strength.

When many events are available for analysis, however, then the squaring followed by subtraction of 'noise' from 'signal plus noise' is applicable.

4.6.2 Factors Contributing to Measurement Errors.

1. Errors in individual events.

On a number of traces an absence of signal in one channel was observed. This was attributed to the presence of CW interference saturating the detector, which is capacitively coupled to the multiplexing stage.

2. Errors on averaging over events.

The estimate of the baseline is a possible source of error when only a limited sample of noise is available. If the 'true' baseline is lower than the 'recorded' baseline, the signal (as measured by averaging over a number of traces) will be reduced. Indeed, if the error is of broadly comparable magnitude to the signal, the effect may be

to mask the excess. If 'd' represents a baseline error, and S and N the signal and noise respectively, then the quantity computed will involve, in addition to the term S^2, a negative term

$$2 \Sigma d\{|\underset{\sim}{S}+\underset{\sim}{N}| - \underset{\sim}{N}\}$$

The exact behaviour of the term will depend on the distributions of the noise and signal components, especially for signals submerged in noise.

The distribution of values obtained by selecting the peak value in an interval will, in general, be different from that obtained by recording instantaneous values, and will depend on the width of the interval. This means that more events will be needed for a statistically significant result if an unnecessarily wide interval is chosen.

4.6.3 Background Noise and Interference.

The presence of manmade sources of interference has already been mentioned. The spectra of sources recorded some years apart are presented in fig 4.5.

In the absence of such sources, the main contribution to the noise is expected to be the galactic background in the range of frequencies used in the experiment, with receiver noise becoming more significant at the higher frequencies (e.g. David and Voge, 1969). The statistical properties of the background noise at Buckland Park have been investigated (Clay et al, 1973a). The amplitude probability distribution (APD) at 50MHz was studied with bandwidths up to 10MHz, and the noise pulse spacing distribution (PSD) studied with a 10MHz bandwidth for spacings between 200ns and 100s. It was found that the departure from a simple Rayleigh distribution for small pulses to the so-called "power Rayleigh" distribution

(see, for example, Spaulding et al, 1972) occurred at particularly low probability levels compared with those reported at typical localities (e.g. Spaulding et al, 1971).

Simple pulse counting techniques were applied to the low probability, high amplitude pulses. These pulses tended to occur in bursts, not obviously always correlated to human activities.

The onset of the 'power Rayleigh' section of the APD was highly variable and time dependent. The PSD confirmed, from its departure from a strictly exponential form, that such relatively wideband noise pulses are not randomly distributed.

These studies indicate that the background level at Buckland Park is comparatively low. However there are intermittent sources of interference (apart from transmissions), such as ignition noise and pumping equipment operated by nearby farmers.

CHAPTER 5

RESULTS

Large pulses, clearly standing out above noise were observed on all four channels during the time that the experiment was operational. The criteria used to select events for analysis will be discussed in the next section, followed by the particle array parameters of these radio showers. The next section deals with the distribution of normalised field strengths, including anomalously large (normalised) pulses. The frequency spectrum of the pulses is then considered. Finally, the implications regarding shower development are discussed.

5.1.1 Pulse Selection Criteria.

The information obtained for each event comprised the film frame containing one microsecond of output for each of the radio channels, with the time and (periodically) the "test" pulse. The array (usually) supplied timing and size and core location, together with an indication of goodness of fit for both the shower arrival direction and the fit to the standard lateral distribution curve used in the analysis.

The selection criteria used were briefly as follows: The requirement was that at least three of the four radio channels had pulses at the 'right' time, greater than any (noise) pulse on the trace by a factor of two. This, somewhat arbitrary requirement was arrived at by balancing, on the one hand, the errors in pulse height measurement for small pulses, with the rapidly decreasing number of pulses if the selection criteria were made too stringent. On checking the particle array output, a decision was made whether or not to include the pulses

in the analysis. Since it is only large showers which are expected to yield radio pulses observable above noise, it is not unexpected that many of these showers land near the edges of the array where the core location is poor and the fit to the assumed particle lateral distribution also poor. This must be taken into account when considering the acceptance of events for further analysis (fig. 5.1).

Event parameters on all showers retained in the analysis are shown in Appendix B.

5.2 Normalisation.

5.2.1 Field strengths.

The measured field strengths of the observed radio pulses are corrected for the antenna polar diagram, the mismatch between the antenna and preamplifier, as discussed previously, and the antenna polarisation, assuming a polarisation for the radio signal appropriate to that produced by a purely geomagnetic mechanism. In the set of radio showers, the arrival directions of the showers are such that this last correction factor is close to unity, the largest correction being less than 20%. The arrival directions of the radio showers are shown in fig. 5.2.

5.2.2 Zenith Angle.

Ideally, normalisation with respect to zenith angle could be done from the experimental distribution of field strengths as a function of zenith angle; however the relatively small number of events did not allow such a normalisation to be done with confidence. As a result, the results of the calculations of (in particular) Shutie (1973) (and others previously referenced) that the field strengths are largely independent of the depth of shower maximum, were applied. Namely, the field strengths should not depend on zenith angle (provided the zenith angle is not too large).

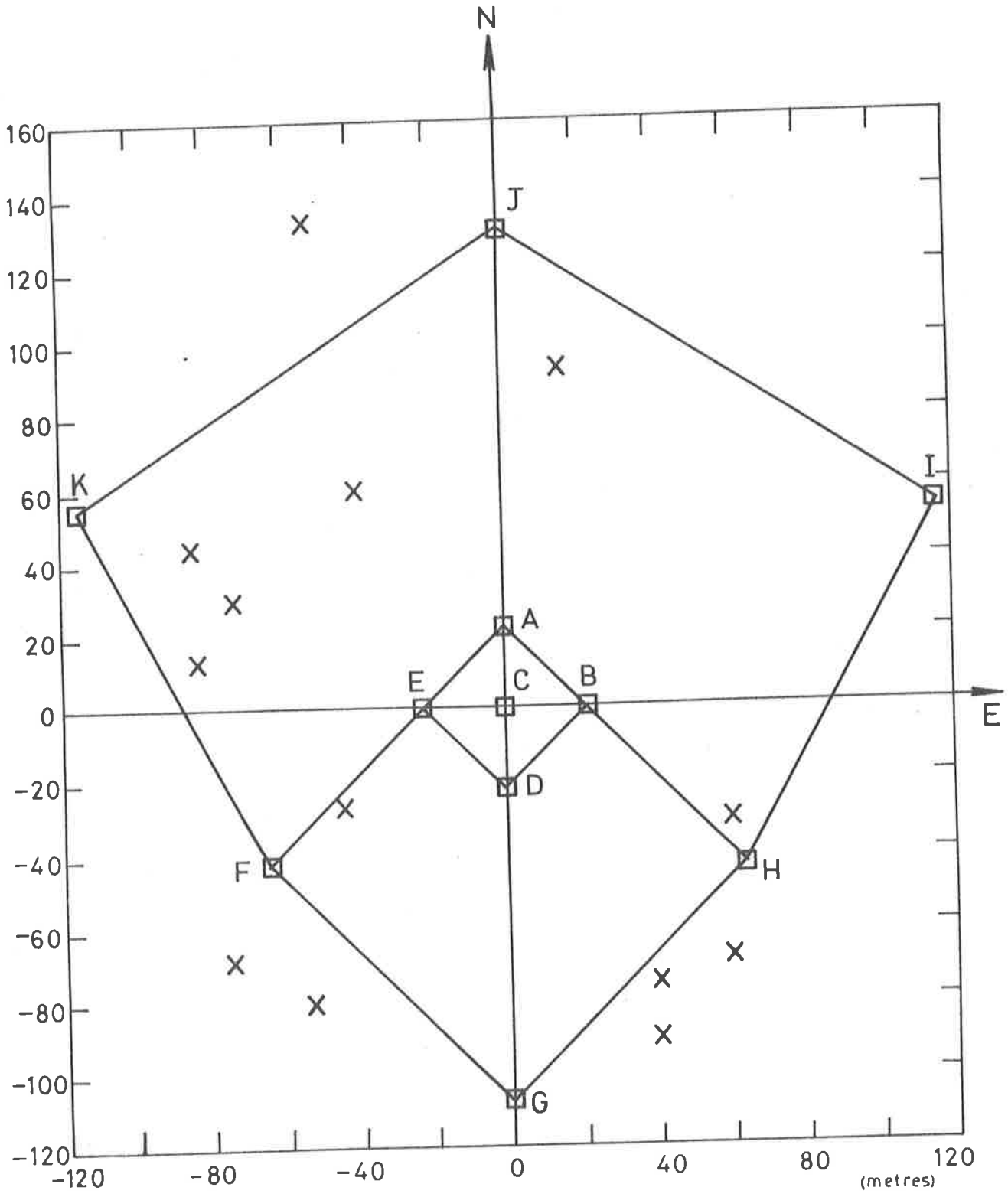

Fig 5.1 Core Locations of Radio Showers.

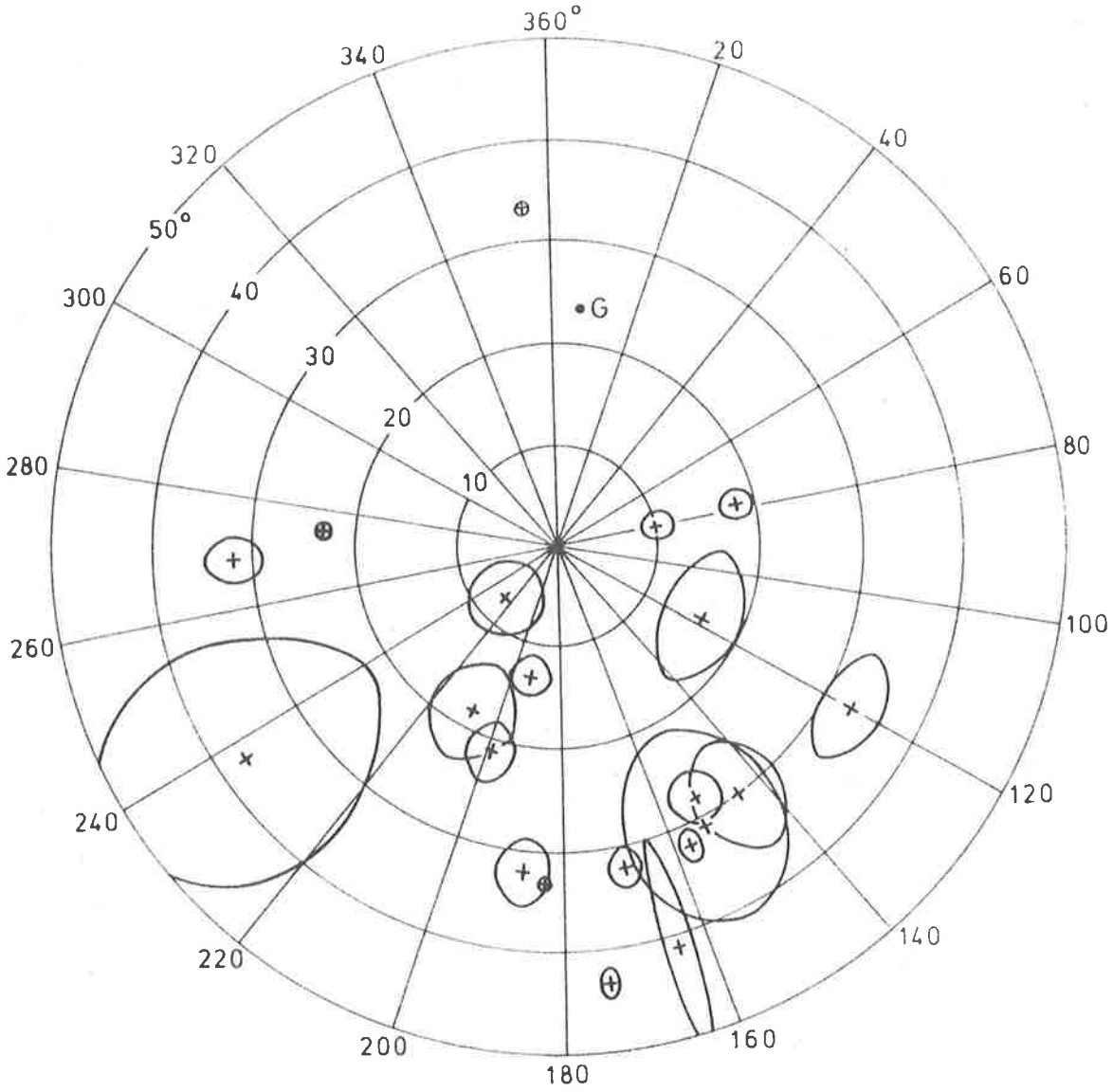

Fig 5.2 Arrival directions of Radio showers, in terms of zenith angle θ and azimuth ϕ. The uncertainties indicated in the arrival directions of individual showers are determined from the value of σ given by the array analysis program.

There is independent support for this from Haverah Park (Allan et al, 1973a).

5.2.3 Geomagnetic angle.

It is customary to normalise the radio field strengths with respect to the sine of the angle between the shower axis and the geomagnetic field. In the presence of other radiation mechanisms (see section 3.2.1), this procedure will tend to overestimate the normalised field strengths for showers arriving at small angles to the geomagnetic field. For a 10% in-phase contribution from another mechanism for example, this overestimate would exceed 10% for angles less than 30^{o}. The effective noise floor of the normalised pulses will vary inversely with the sine of the geomagnetic angle, introducing another possible source of systematic overestimation of field strengths at small geomagnetic angles.

The geomagnetic angle and the zenith angle are not independent; the correlation between them for the set of radio showers is clear from fig. 5.3, which indicates that for a given zenith angle, the direction tend to be that which maximises the geomagnetic angle. This tends to lend yet further support to a geomagnetic origin for the radiation.

5.2.4 Shower Size.

The normalisation of the measured sea level electron shower size was done using a simple model. As previously mentioned, showers detected by the Buckland Park array are expected to be well past maximum development. Fluctuations in the sea level size for a given primary energy mean that normalisation of field strengths with respect to a 10^{17}eV primary energy (for purposes of comparison) can only be done by averaging over a number of showers. The fluctuations in the "normalised" field strengths will

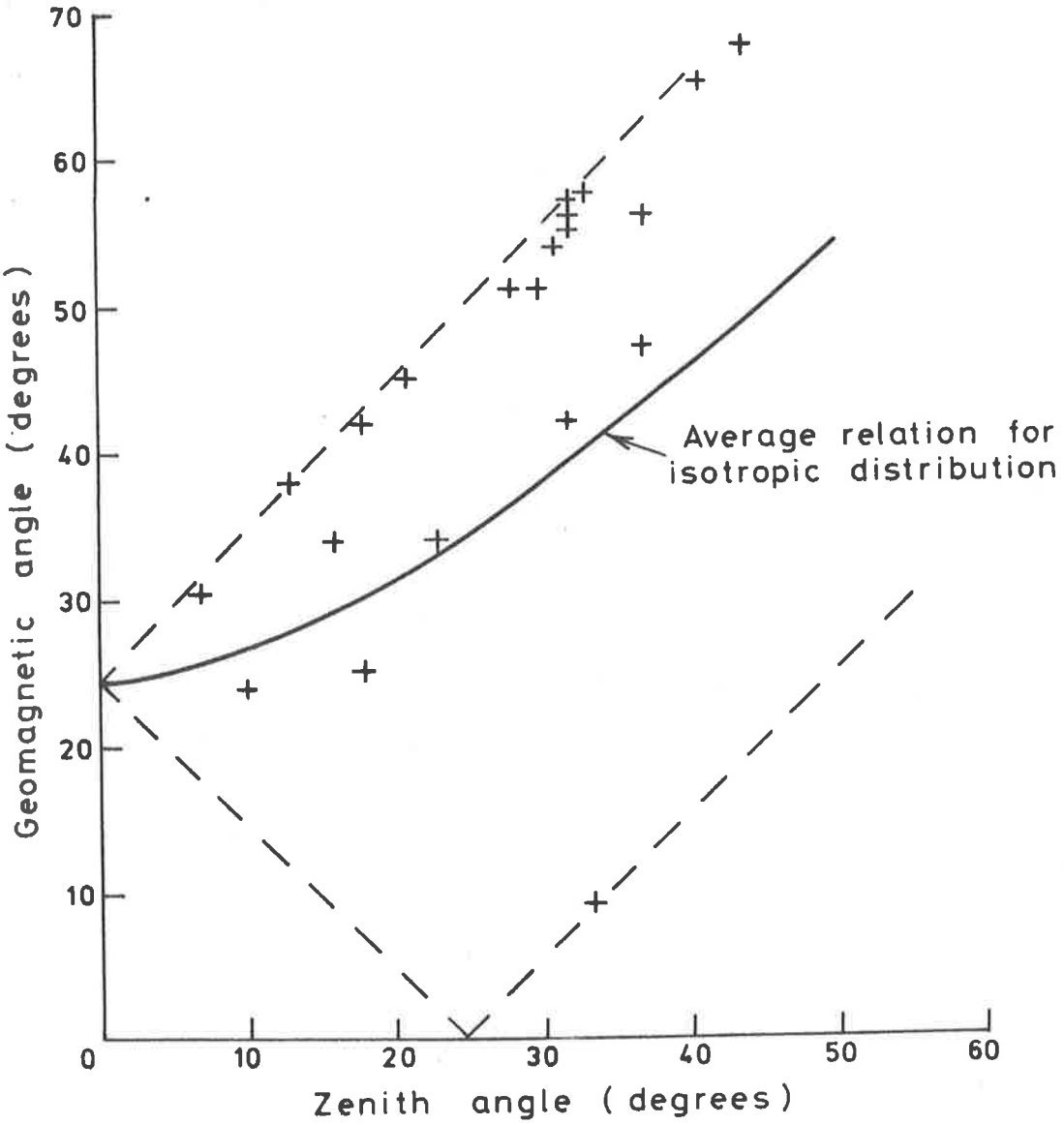

Fig 5.3 Geomagnetic angle (the angle between the shower axis and the geomagnetic field) versus zenith angle. The region enclosed by the dashed line represents the allowable combination of angles.

depend, 'inter-alia' on the electron size fluctuations. The elongation rate also needs to be considered in the normalisation. In consequence, on average, if the electron size at sea level depends on the primary energy as E^{α}, then α is expected to be greater than 1.

The exponent can be estimated, following Allan, by assuming that there is little change in the shape of the electron development curve, so the particle numbers depend both on the maximum size of the shower and also on the shift in its position, thus

$$\frac{dN}{N} = \frac{dN_{MAX}}{N_{MAX}} + \frac{d\,X_{MAX}}{\lambda}$$

(approximately), where λ is the shower attenuation length. Since the size at maximum is simply proportional to primary energy, and using recent values for the elongation rate of 70gmcm^{-2}, we obtain

$$E_p \propto N_{s\ell}^{.85}$$

A shower of 10^6 particles then corresponds to a maximum of 5-6x10^6 (Allan, 1971a, Gaisser et al, 1978) leading to

$$E_p = 10^{16} \left(\frac{N_{s\ell}}{10^6} \right)^{.85}$$

Allan (1971a) also obtains this result but using a different relation between Xmax and Ep.

This equation is an indication of what might be expected. For high values of elongation rate, approaching 90gmcm^{-2} (as discussed below), the exponent would be reduced further. While there is little direct experimental evidence for the behaviour of the attenuation length, it may in fact increase somewhat with shower energy. A change in shape of

the shower development curve (a broadening as energy increases) might be expected to lead to just such an increase, increasing the exponent. Calculations of Grieder (1979) indicated direct proportionality ($\alpha = 1$) over the range 10^{13}-10^{17}eV, while the estimates of Wdowczyk (1975) from the aeroplane data of Antonov and Ivanenko (1975), considered by Gaisser et al, (1978), is consistent with α=69. The relation between sea level size and primary energy, extracted from the above, is indicated in fig. 5.4.

The equation above applies to vertical showers. The extra thickness of atmosphere through which inclined showers have travelled results in a smaller shower electron size at sea level. Assuming that differences in shower development related to pressure may be neglected, so that the depth of atmosphere through which the shower develops to reach maximum is the same as for a vertical shower, then the only effect on sea level shower size is the extra thickness of atmosphere. If the attenuation length does not change significantly, then for the value of 200gcm^{-2} used above, and a total atmospheric depth of 1000gcm^{-2}, the appropriate correction factor is $e^{-5(1-\sec\theta)}$.

The distribution of shower sizes for the radio showers is shown in fig. 5.5.

5.3.1 Field strengths of the Observed Pulses.

The unequivocal radio pulses can be treated in several ways. In the first place, the normalised field strengths of the emission is itself of some interest, in view of the spread of values for normalised field strengths recorded at other arrays. These may be summarised as follows:

1. Haverah Park.

Field strengths of 10μVm^{-1} MHz^{-1} were reported in 1971 at 60 MHz. More

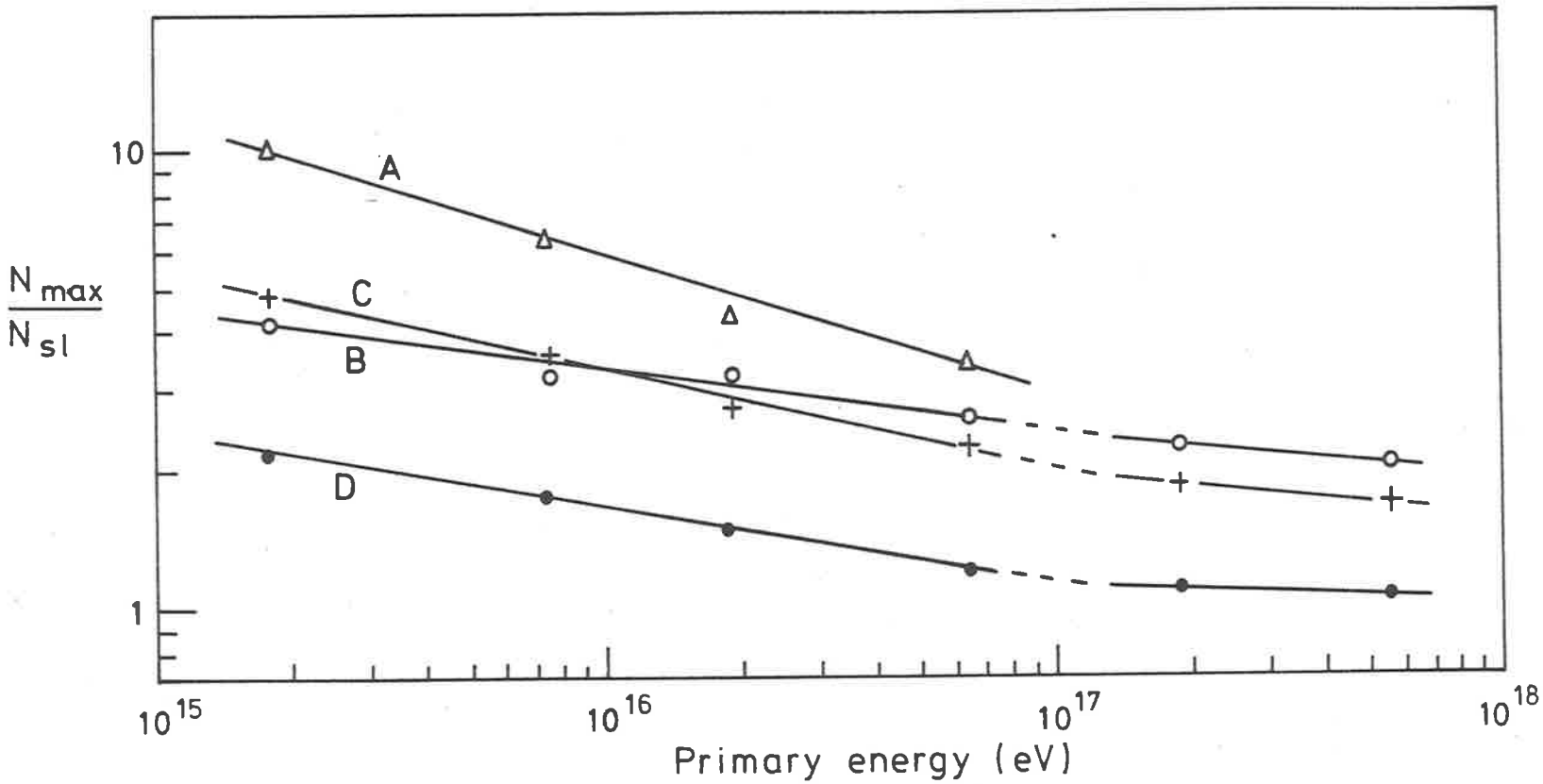

Fig 5.4 Relation between sea level size and primary energy.

A. Wdowczyk (1975) based on Antonov and Ivanenko (1975) reported in Gaisser et al. 1978.

B. Hillas, 1979 (calculations)

C, D. Gaisser et al, 1978 (calculations on Fe, p respectively)

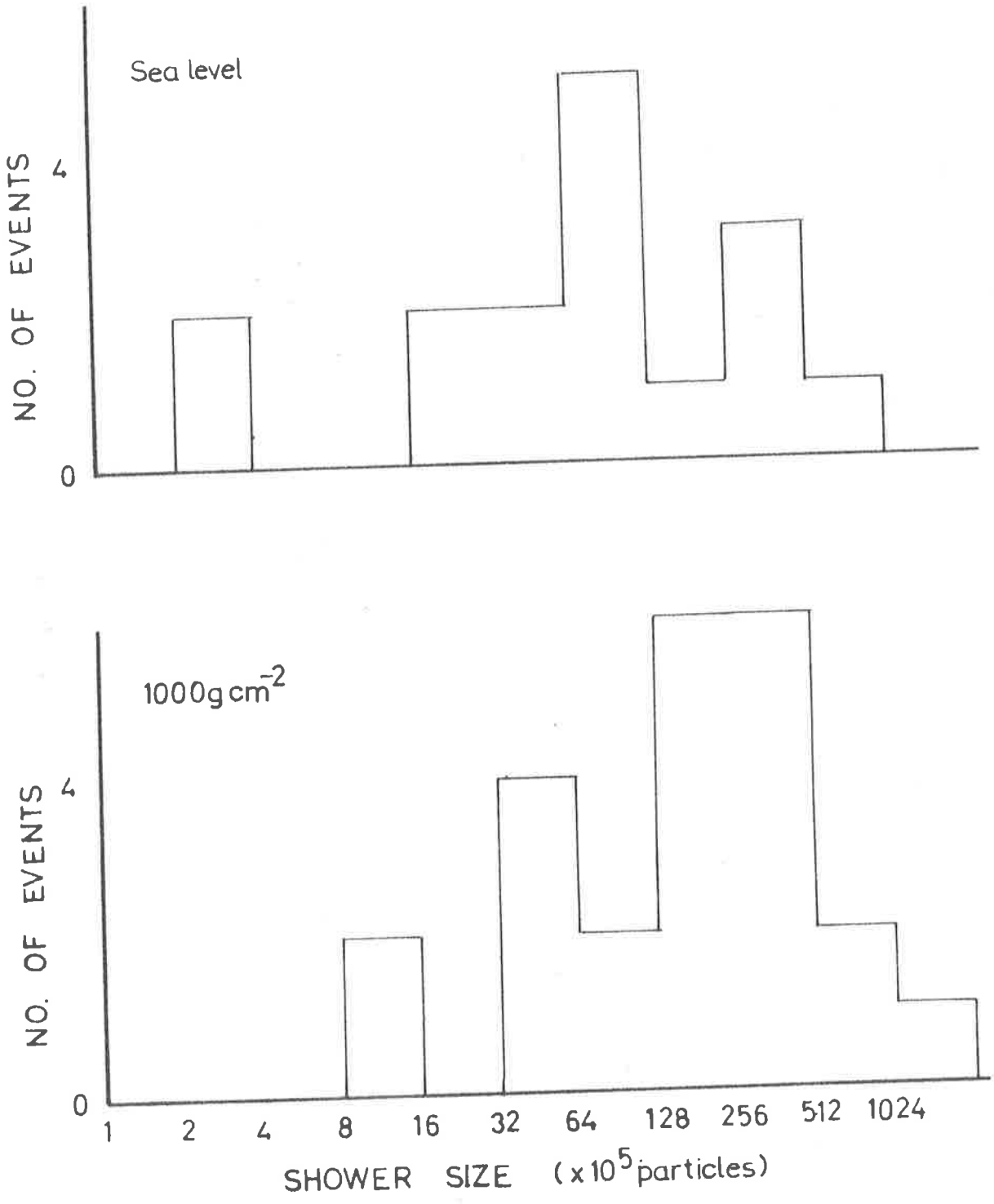

Fig 5.5 Distribution of shower sizes -

(a) sizes as measured at sea level

(b) sizes corrected to correspond to a depth of 1000 g.cm^{-2}, assuming a constant attenuation length of 200 g.cm^{-2}.

recently, lower values of $\sim 6 \mu Vm^{-1}\ MHz^{-1}$ have been reported, the decrease being attributed to better out-of-band rejection as a result of improvements in the band pass characteristics (Allan et al, 1971b, 1973a, 1975a).

2. M.S.U.

The most recent field strengths quoted are $\sim 2\ \mu Vm^{-1}\ MHz^{-1}$ at 58MHz (Atrashkevich et al, 1975), for a muon shower size of 10^5. (This corresponds to about $3.4\ \mu Vm^{-1} MHz^{-1}$ for a 10^{17}eV primary).

3. Bologna.

Much higher field strengths of some tens of $\mu Vm^{-1}\ MHz^{-1}$ (Mandolesi et al, 1976, Baggio et al, 1977), observed at 60 MHz.

Thus there are discrepancies between these three arrays all operating with radio receivers tuned to similar frequencies. At Haverah Park, particle densities are measured with water Cerenkov detectors, the parameter ρ_{600} being closely related to primary energy (Hillas et al, 1971). The MSU group uses muon detectors, which, as previously mentioned, also give an indication of primary energy. The ground indicators at both arrays are good indicators of primary energy.

At Bologna, the scintillation detectors estimate the electron shower size at sea level. For these old showers, the particle numbers are sensitive to the state of development as well as the initial primary energy. The Buckland Park detectors are also scintillators, with the same characteristics. In fact both groups share some design features common to the original Calgary array. It is perhaps useful to check whether the field strengths measured at Buckland Park are closer to those of Haverah Park and M.S.U. than to those at Bologna.

In fact, selecting only those events with clearly recognisable

pulses, and normalising as described above, including a correction for the zenith angle dependence of the measured shower size, the field strengths obtained fall between those reported at Haverah Park and M.S.U., and far below those from Bologna. The average of the field strengths for the four channels for the selected events are listed in table 5.1; the average field strength for the lowest three channels is 1.73 ± .13 μVm^{-1} MHz^{-1}, with the fourth channel marginally less at 1.40 ± .19μVm^{-1} MHz^{-1}; these values are about mid-way between those most recently reported at M.S.U. and Haverah Park. These may be compared with the field strengths calculated by various authors of $\sim 2\mu Vm^{-1}$ MHz^{-1}, both from relatively simple calculations (e.g. Allan, 1971a,b) and from the more extensive calculations of Hough (1973) and Shutie (1973). The error limits quoted do not take into account the uncertainties in the simplified model, which are not expected to change the conclusion drastically.

It thus appears that the measurements at Bologna are, for some reason, possibly spurious, contaminated or are systematically overestimated. However, published data from Bologna show no significant dependence of the normalised field strengths on geomagnetic angle, so the behaviour of the pulses is consistent with theoretical expectations, making a spurious origin or contamination unlikely (Baggio et al, 1977). The high value of the field strengths may perhaps be attributable to some feature of the calibration procedure. Such possibilities were considered at a meeting of the three groups, and the results of their discussions published (Atrashkevich et al, 1978).

Field strengths obtained at these arrays are compared in fig. 5.6. and Table 5.2.

5.4 Characteristics of the Radio Pulses.

The general characteristics of the radio pulse clearly observable above noise were examined both to confirm their behaviour with appropriate

TABLE 5.1 Average Field Strengths.

Frequency (MHz)	45	75	105	135
Field Strength ($E_\nu/\sin\alpha$)	3.25 ± .41	3.36 ±.52	3.93 ± .45	3.09 ± .55
Field Strength (normalized)	1.82 ± .16	1.65 ±.18	1.75 ± .16	1.40 ± .18

NOTE : the errors quoted for the normalized field strengths do not take into account the uncertainties in the model adopted for normalizing the pulses.

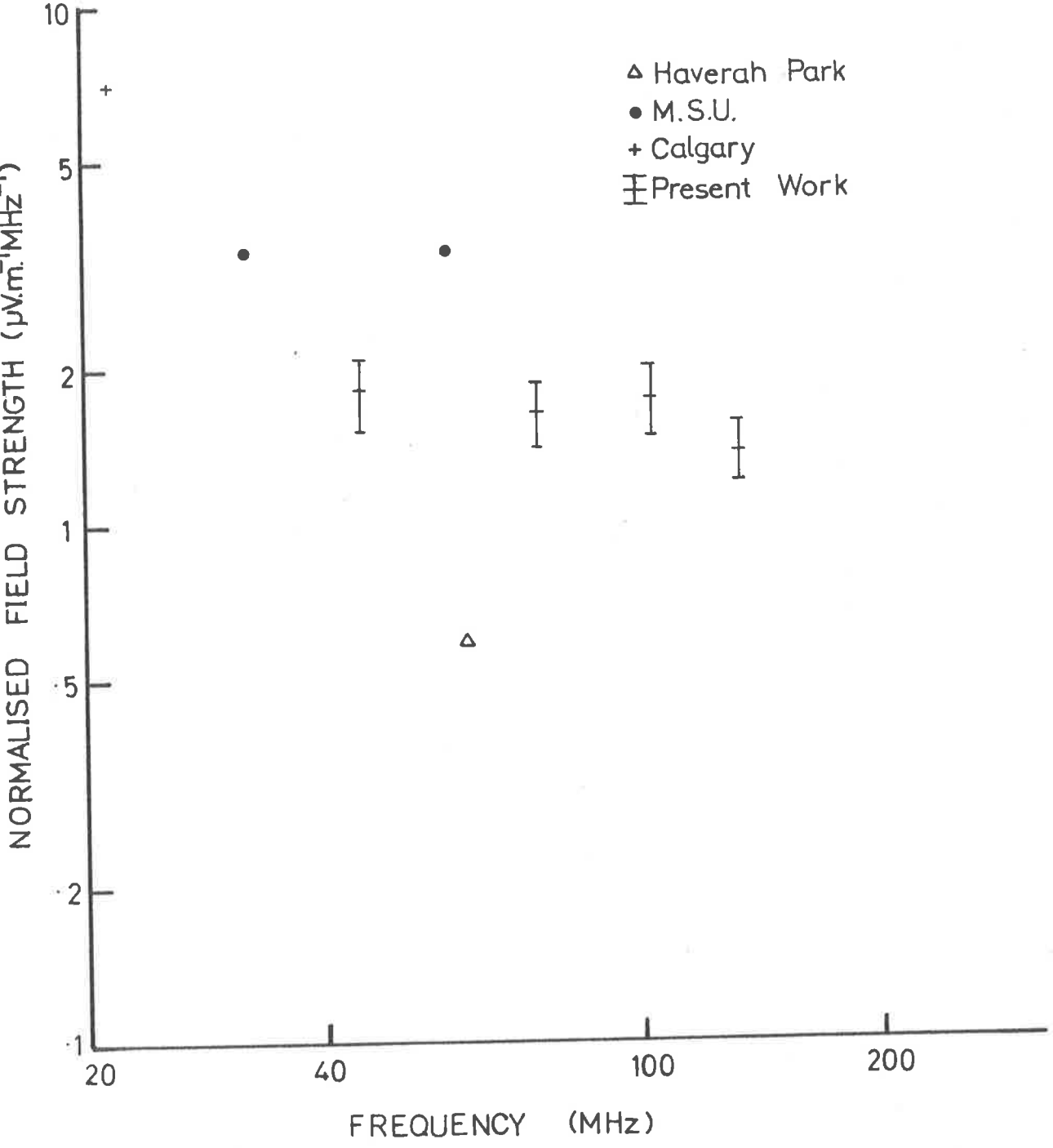

Fig 5.6 Field strengths measured at different arrays.

TABLE 5.2 COMPARISON OF FIELD STRENGTHS AND SPECTRA. (NORMALIZED WITH RESPECT TO SIN α WHERE α IS THE ANGLE BETWEEN THE SHOWER AXIS AND THE GEOMAGNETIC FIELD).

	FIELD STRENGTHS (Normalized) (in μVm^{-1} MHz^{-1})	NORMALIZATION
HAVERAH PARK		
Allan et al (1971b)	5, 10, 5 at 32, 60, 105 MHz resp.	Vertical 10^{17}eV shower
Allan et al (1973)	~ .9 at 60 MHz	Vertical 10^{17}eV shower
Allan et al (1975)	~ .6 at 60 MHz	Vertical 10^{17}eV shower
M.S.U.		
Atrashkevich et al (1975)	1.8 - 2.0 at 32, 58 MHz corresponds to ~ 3.4	$N_\mu = 10^5$ vert.10^{17}eV shower
ADELAIDE		
Present Work	~ 1.75 at 45 - 105 MHz	10^{17}eV shower (estimated with a simple model)
BOLOGNA		
Mandolesi et al (1976)	~ 15 for 46, 60, 65, 110 MHz corresponds to ~ 20	Average field strength of recorded pulses, Ne ~ 5×10^5 - 10^8 particles, average ~ 10^7. 10^{17}eV shower (estimated with a simple model).
CALGARY		
Prescott et al (1970)	.3 at 22 MHz (not corrected for no restriction on zenith angle or core distance) corresponds to ~ 7	Mean field over a decade of sizes, Ne ~ 10^6 particles, sin α ~ .4 on average. 10^{17}eV shower (estimated with a simple model).

parameters determined by the particle array, and to check on their consistency with a largely geomagnetic origin for the emission. The dependence of the field strengths (normalised according to the simple model previously described) on shower size and zenith angle was checked (figs. 5.7, 5.8). These dependences are not independent, since detected showers from larger zenith angles are, on average, produced by higher energy primaries. The average zenith angle of the set of radio showers is expected to be larger than that for the total number of showers detected by the array. The average angle for the array (without regard for size dependence) is about 21 degrees (basically consistent with a $\cos^{6or7}\theta$ dependence) compared with 24 ± 3 for the 'radio' showers. It may be seen in fig. 5.9 that small showers accompanied by radio pulses do tend to be more inclined than larger. (Events in the final restricted set less than, and greater than $2x10^7$ particles have average zenith angles of 29±3 and 18 ± 4 degrees respectively). Consequently, the use of a smaller attenuation length in the zenith angle correction would lead to a further reduction in the exponent relating electron size and primary energy.

5.4.1 Rate of occurrence of events.

On examining individual events, several points stand out. Firstly, a number of events yield normalised field strengths which are completely anomalous if a geomagnetic mechanism is assumed. Consequently, the possibility of an explanation for these events in terms of a geoelectric mechanism was considered. Two events occurred within eight minutes on Nov. 29, 1978, at a time when thunderstorms were reported in the area. The first yielded, on careful reanalysis of the array data, a field strength which was large, but not anomalously so, while the other, although a large shower, came from a highly unfavourable direction, yielding a flat spectrum with normalised field strengths approaching

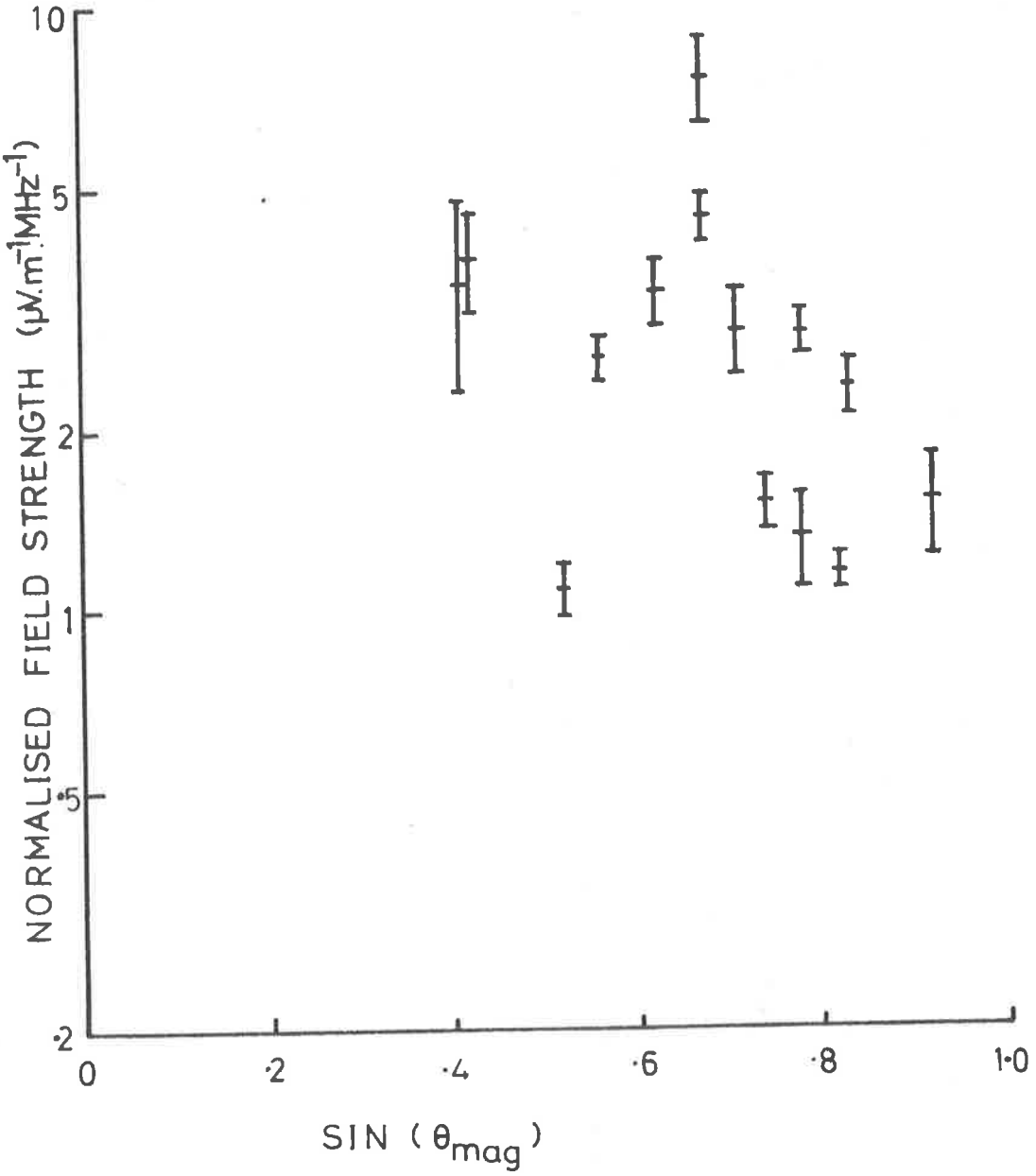

Fig 5.7 Normalised field strength versus the angle between the shower axis and the magnetic field.

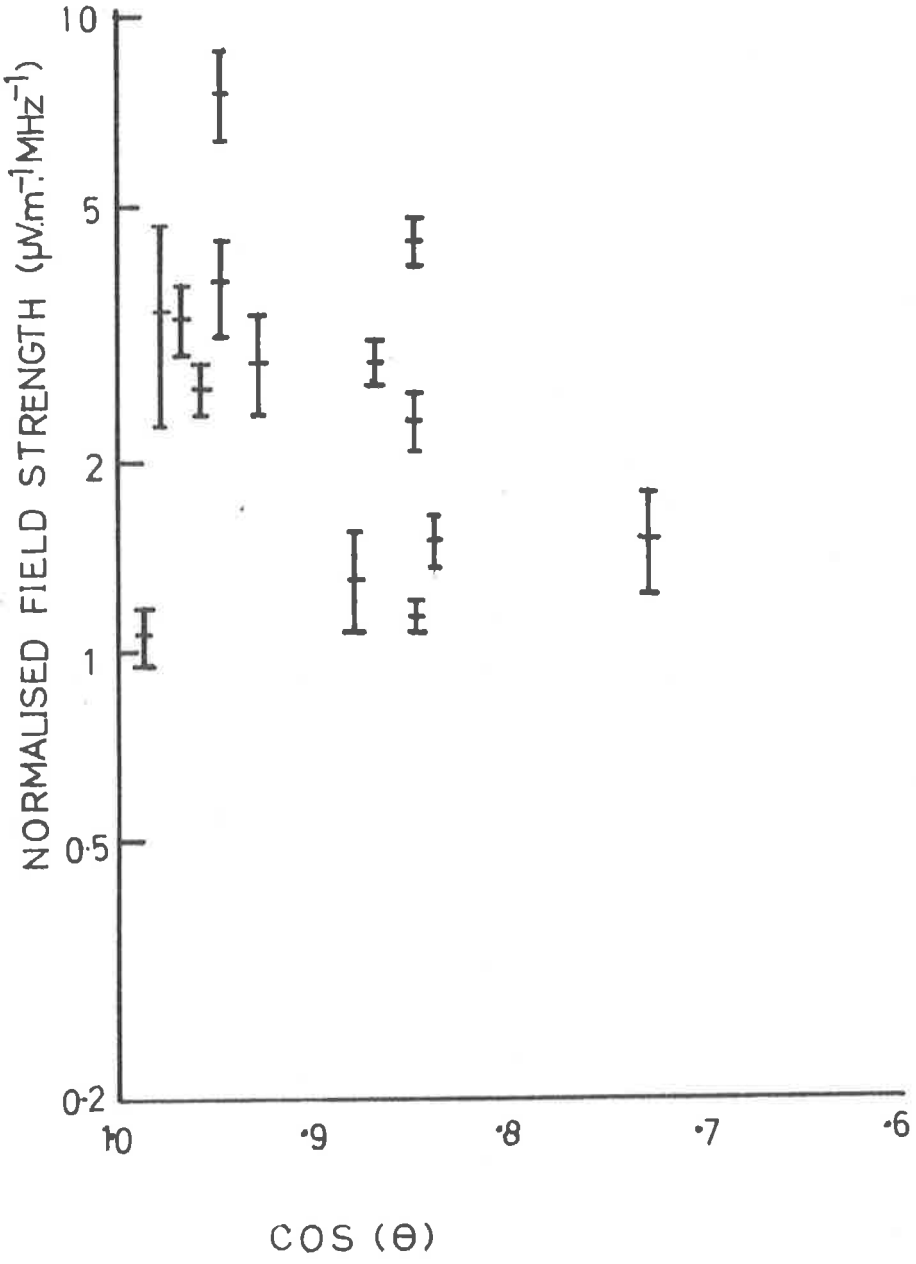

Fig 5.8 Normalised field strength versus the zenith angle.

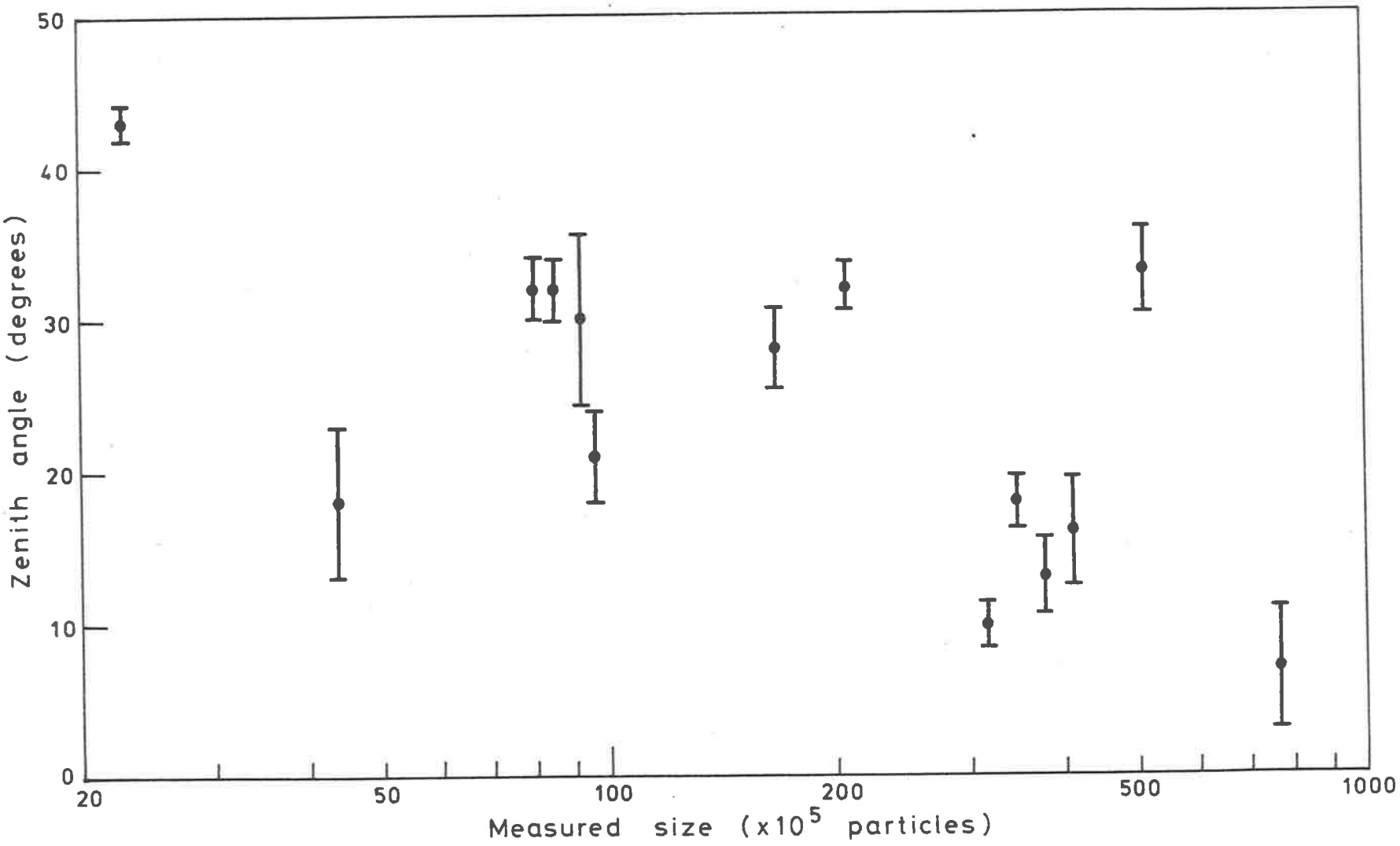

Fig 5.9 Zenith angle versus measured shower size.

$1mVm^{-1}\ MHz^{-1}$.

There were two other occasions when events occurred within a short time; on one occasion, three events within 2.5 hours, for one of which the normalised field strength was large, but the signal to noise ratio poor. The event was not included in the final set of data. No thunderstorm activity was reported at the time. On the third occasion, two events were recorded within half an hour, again without thunderstorm activity being reported. For one of these showers the normalised field strengths were high. However, the particle density distribution was unusually flat, being best fitted with the value of R_0=165.

5.4.2 High Field Strengths.

Several well-analysed showers were accompanied by anomalously large pulses. Two such events (recorded three months apart) were both small showers which fell near the antenna (approximately 20m and 10m away). The normalised field strengths were of the order of 20 and 200$\mu Vm^{-1}\ MHz^{-1}$. Neither event occurred at a time of thunderstorm activity; cloud conditions observed (during the days around the time of observation) were cumulus and altocumulus/altostratus respectively. Near the core one would not expect a significant signal from a mechanism (such as charge excess) producing radial polarisation. Two other events with high field strengths did not fit the "pattern" observed for the above events. Both fell more than 50m from the antenna and were more consistent with the geoelectric mechanism. Cumulus clouds and light showers were recorded for the period in which one of those showers fell; the other occurred during a thunderstorm.

In the light of such events, it is clear that although a certain proportion of events can be suspected of being at least in part due to a geoelectric mechanism, the number of thunderstorms experienced at the Buckland Park array is not in itself sufficient to prevent the collection

of data. There are, however, events which suggest the possibility of a geoelectric component at times when the prevailing weather conditions would appear not to be favourable to an enhanced field.

This is in agreement with the evidence attested by other groups, as previously described (in section 2.1.3). The variable nature of the contribution is a severe hindrance in radio emission studies. To minimize its effect would require not only monitoring variations in the geoelectric field but also, ideally, careful choice of geographical location of the array itself. Close study of individual events for consistency with any mechanism requires a careful re-examination of the particle array analysis, to ensure that the fitting was not unduly influenced by only one or two detectors and that the shower landed in a region where the array analysis is not influenced by shower fluctuations.

5.5.1 Radio Emission Spectrum.

The field strengths for the four frequencies were calculated on the assumption of constant antenna response over the band. Differences in the polar diagram of the antenna are not expected to be significant at small zenith angles, and the impedance correction is less than 10% for all channels. Because of the large errors on individual pulses, there is little information to be gained from inspecting individual events. For the selected pulses, the range of lateral distances is small, with only two radio showers falling further than 100m from the antenna. In the less restricted selection of showers there is a greater proportion of showers falling at such distances. For the purpose of displaying spectra details of the array analysis are not so important, so that these comparatively poorly analysed showers may be included.

The frequency spectra are presented in figures 5-10-5-12 for the events measured. Firstly, the spectra obtained by including all identifiable pulses, including those which occurred when either the array recording

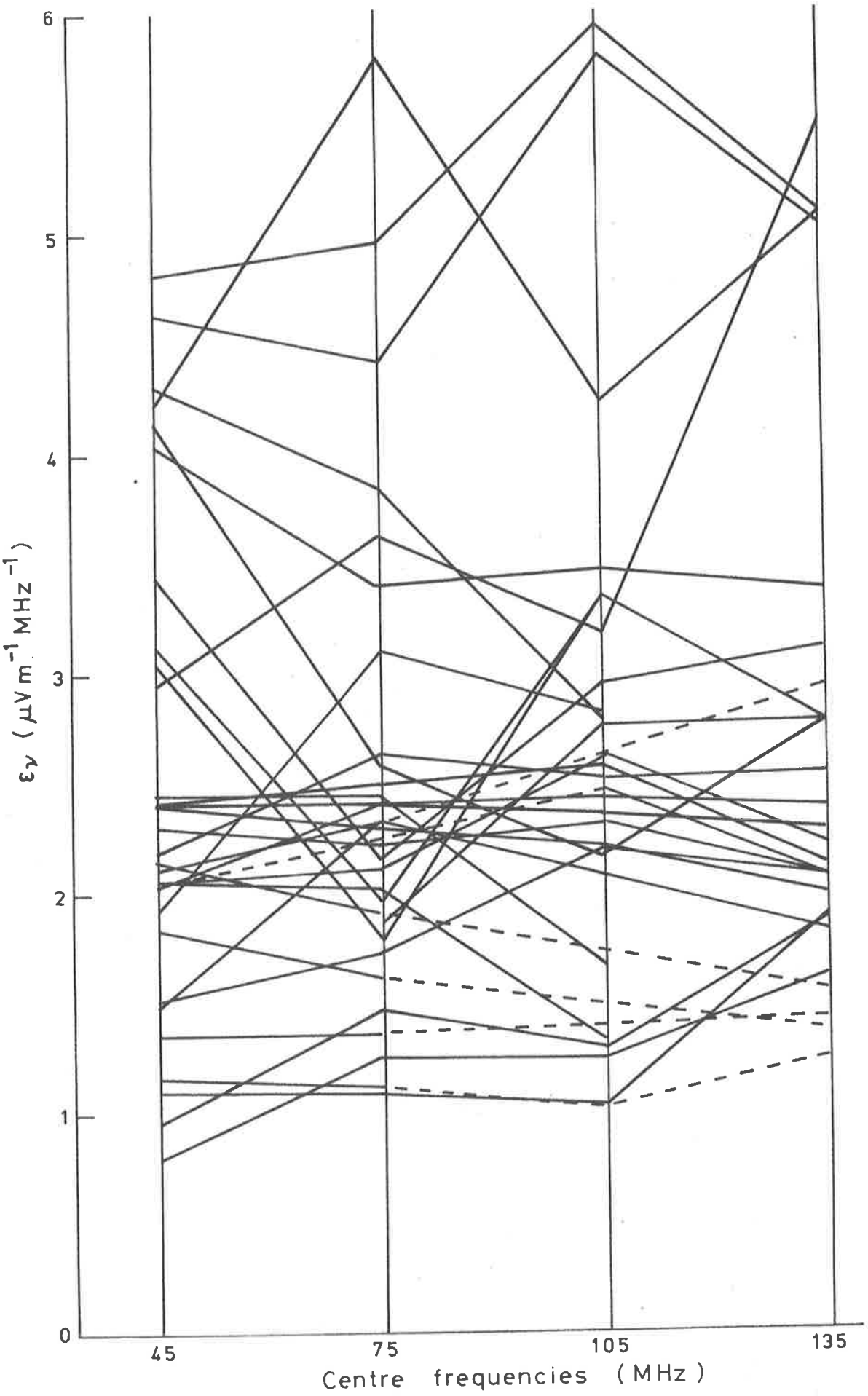

Fig 5.10 Unnormalized Frequency Spectra.

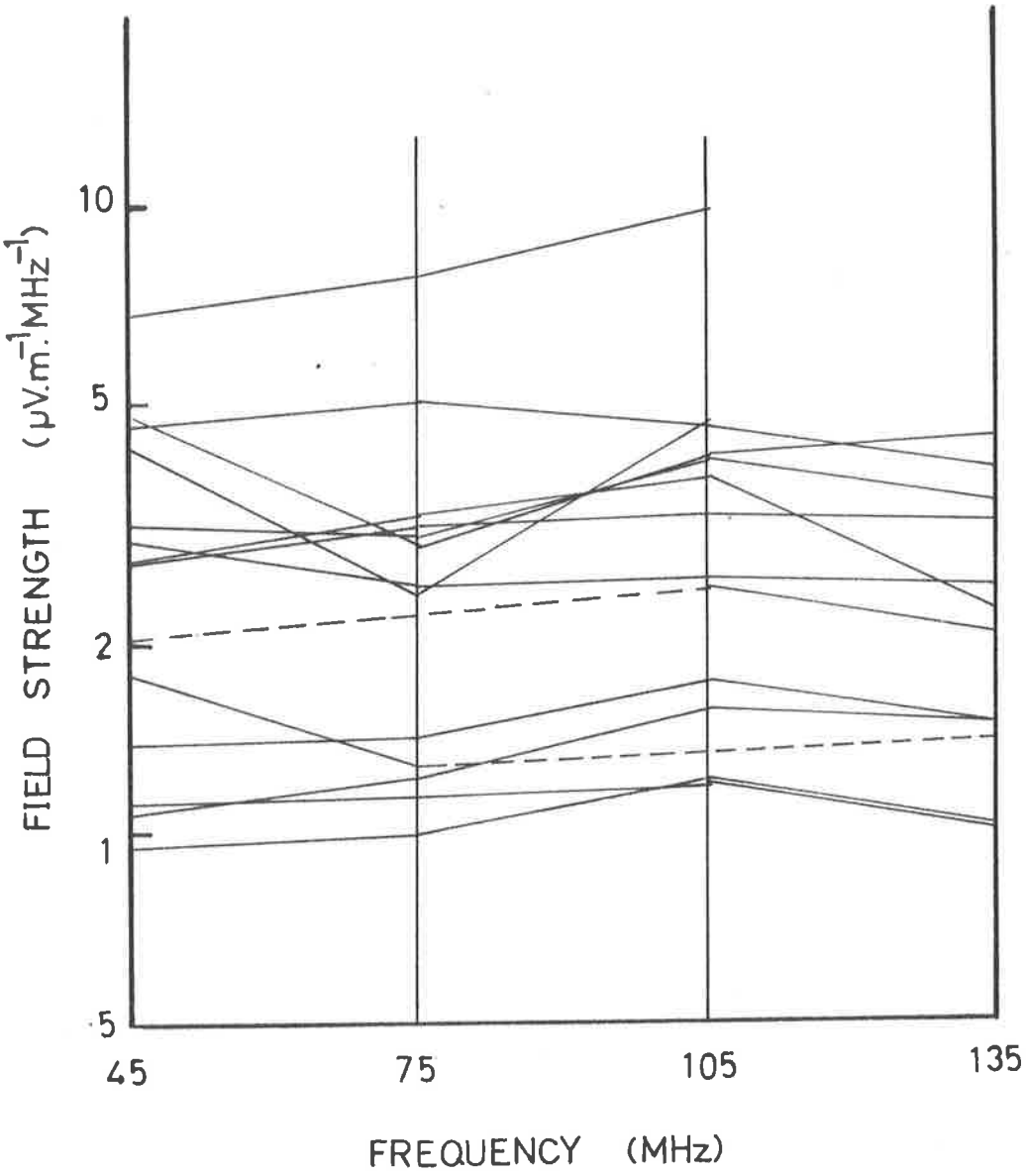

Fig 5.11 Normalised Frequency Spectra.

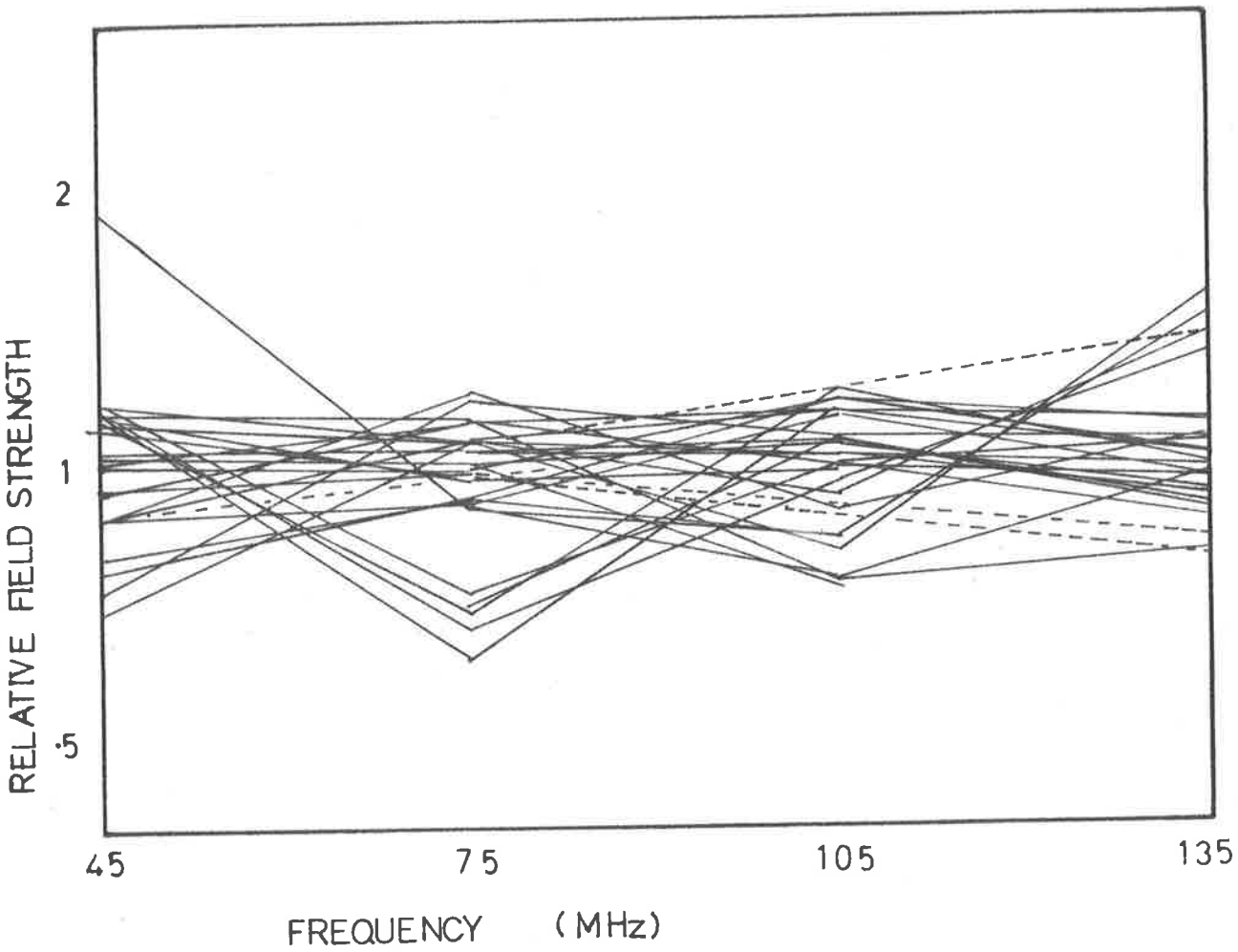

Fig 5.12 Frequency Spectra normalised to Unity.

electronics were not operational, or for which no convincing analysis was obtained. It may be seen that the conclusion drawn from considering the well analysed pulses is sustained. The results are consistent with a flat spectrum from 45-105MHz while the field strength at 135MHz, although reduced, has sufficient uncertainty to be consistent with a flat spectrum as well. Plots for events with core distances in the range 40-80m, and for those greater than 100m are also presented, together with plots for zenith angles less than and greater than 25 degrees. The plot for showers from larger zenith angles is essentially for showers developing on average further away from the antenna. The errors on individual pulses conceal any systematic differences for the various selections of data. Parameters which might be expected to influence the spectrum of an individual pulse thus cannot be examined closely. In summary:

1. Zenith Angle (fig. 5.14)

Showers from larger zenith angles have passed through a greater thickness of atmosphere and their spectra might be expected to be similar to those of vertical showers which have developed high in the atmosphere. However, for the range of core distances obtained in the present experiment, the spectral shape is expected to be insensitive to this height; e.g. Spectra extracted from the work of Shutie (1973) and Hough (1973) for different heights of maximum development for various core distances are shown in fig. 2.2.

2. Primary Energy (fig. 5.15)

Similarly, the change in the height of maximum development of showers as primary energy increases is not expected to lead to any significant change in spectral shape as a function of primary energy or

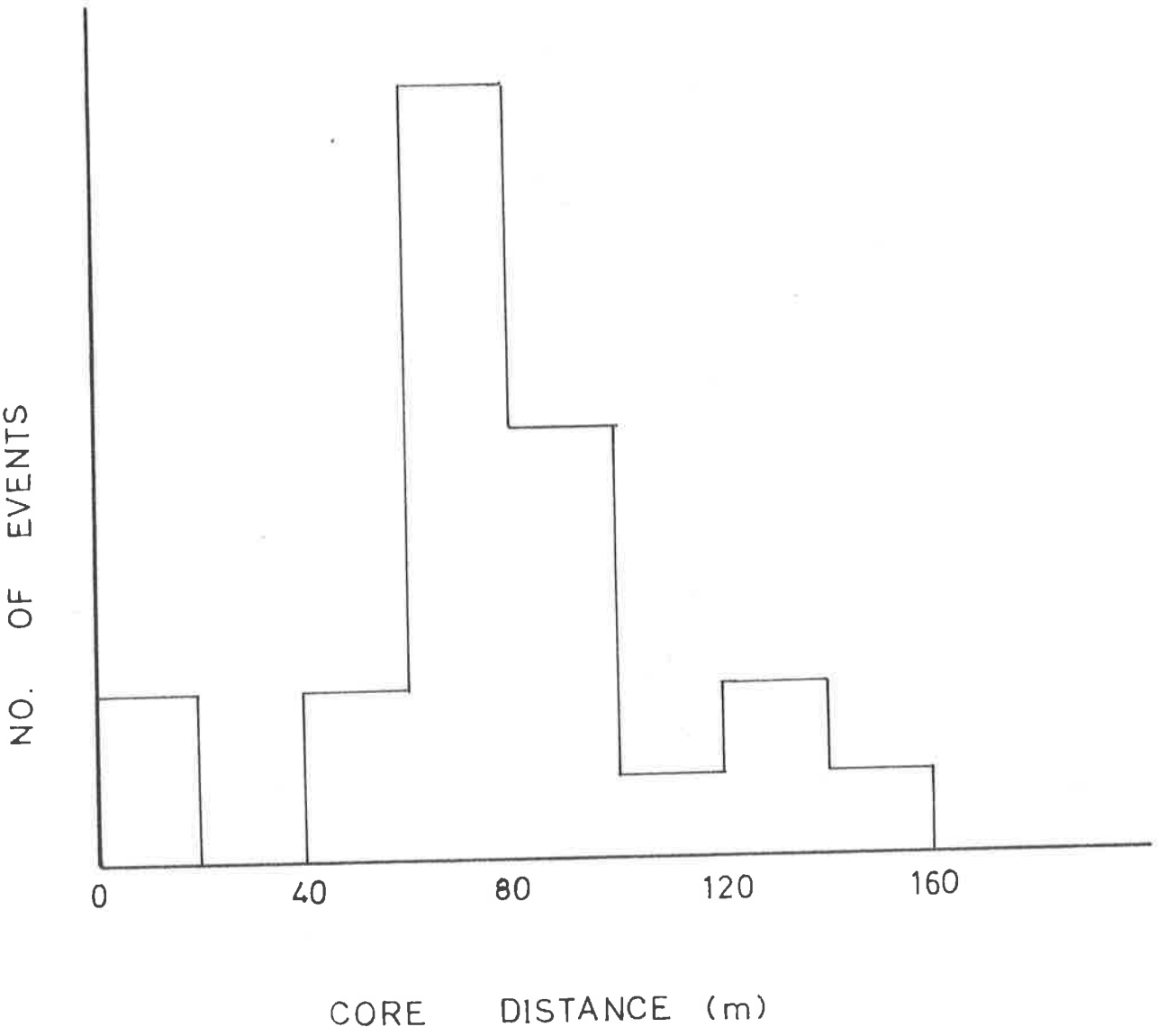

Fig 5.13a Distribution of core distances for radio showers.

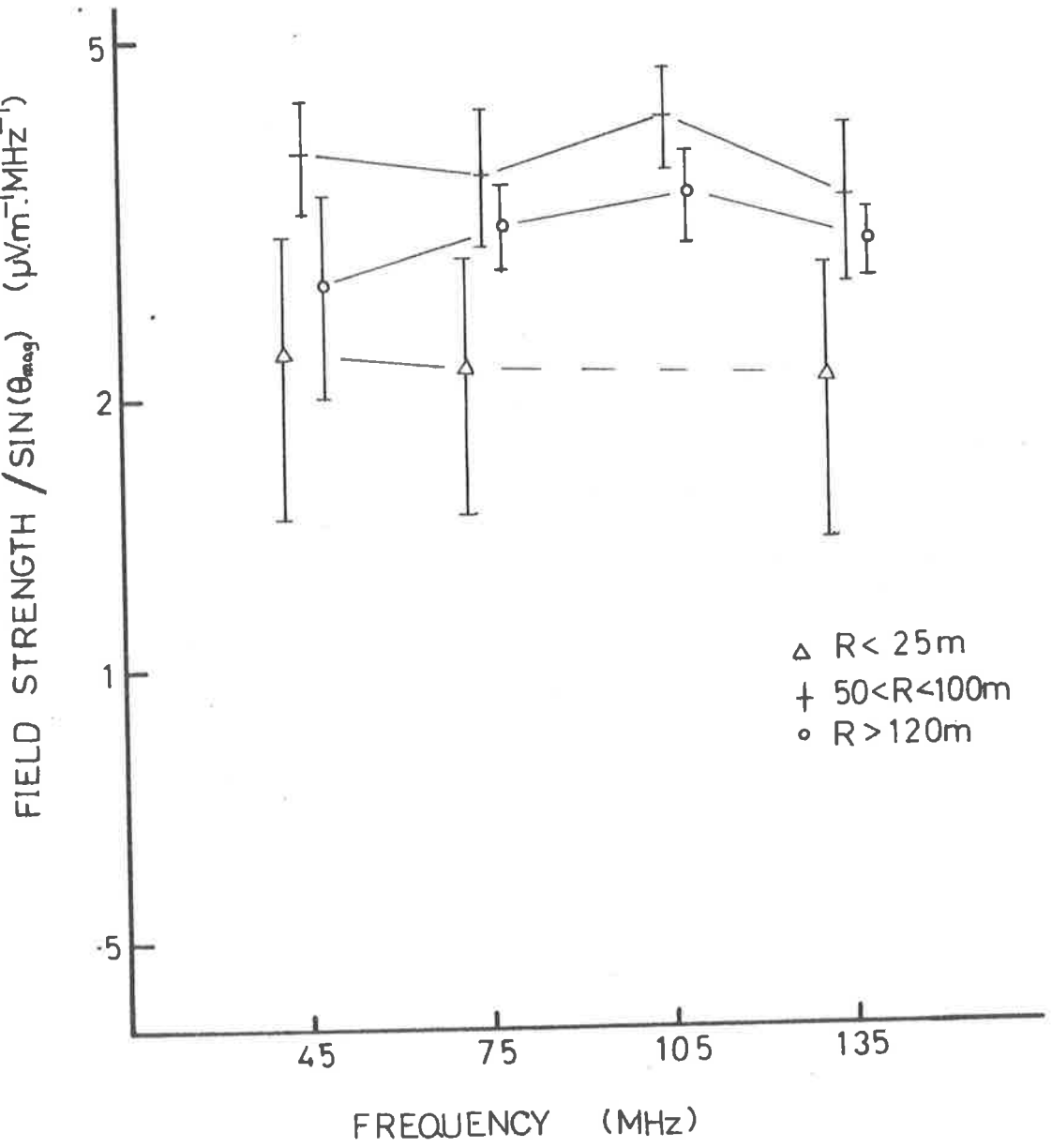

Fig 5.13b $E_\nu/\sin\theta_{mag}$ for three ranges of core distance.

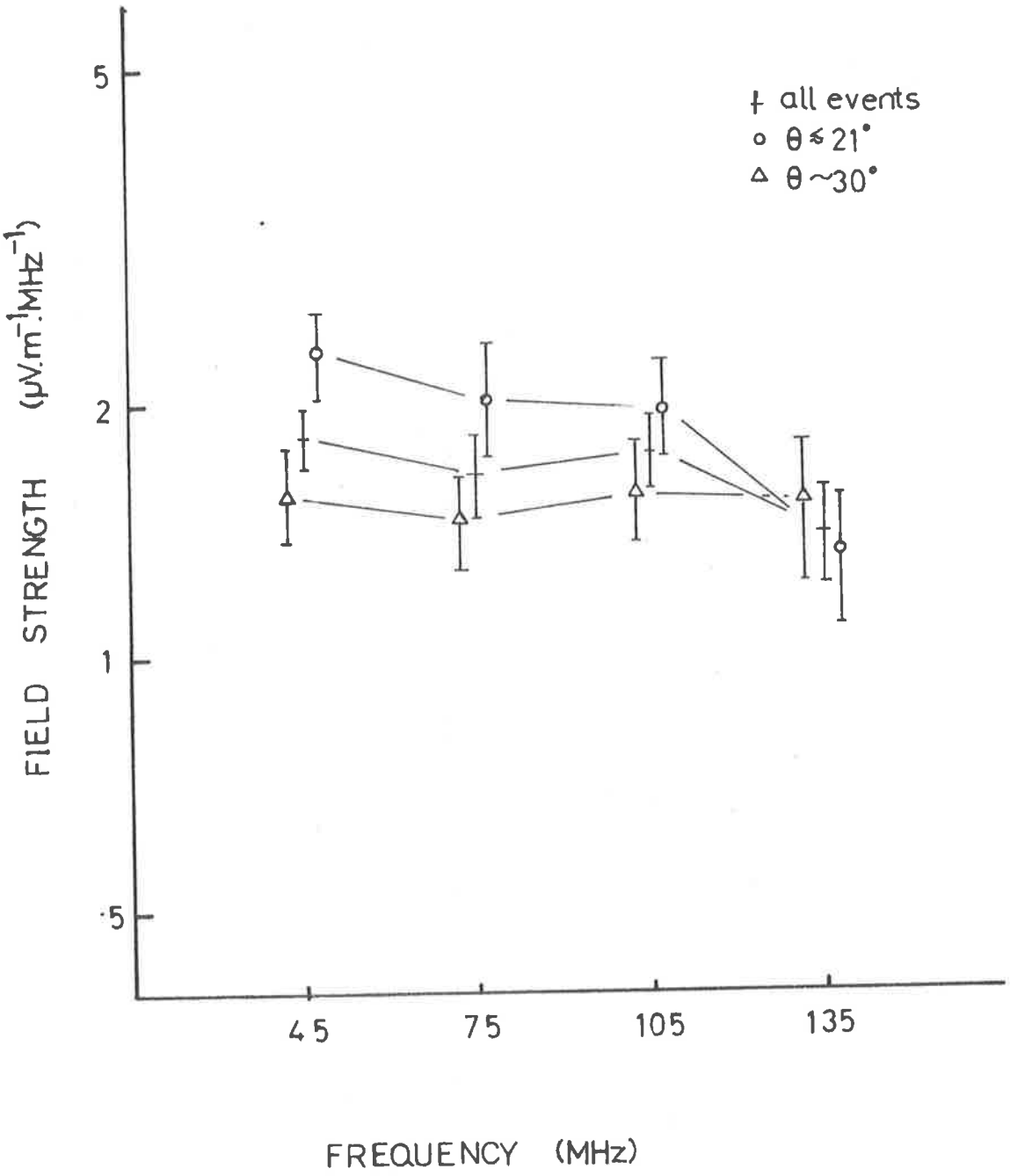

Fig 5.14 Frequency spectra for two ranges of zenith angle

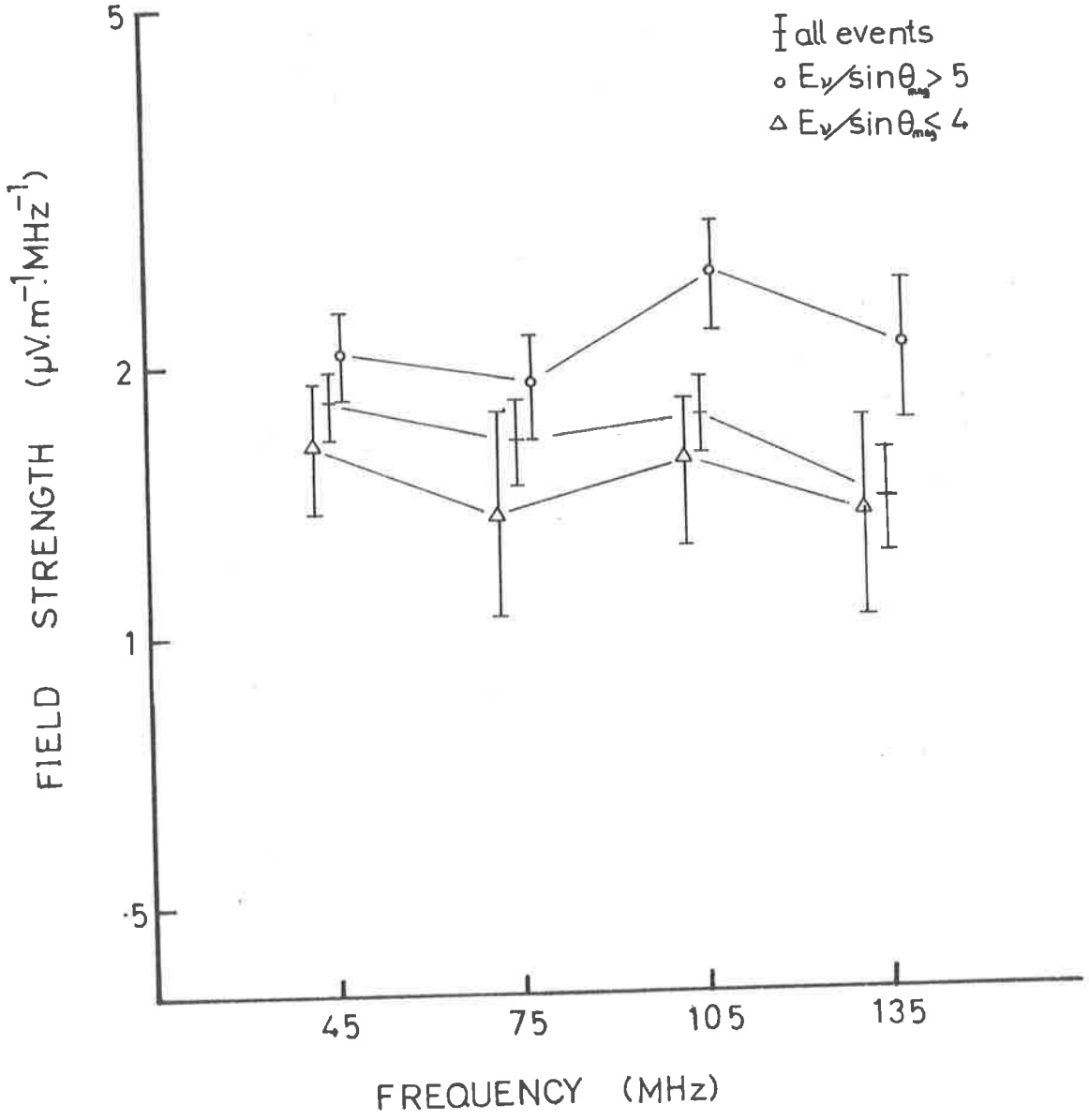

Fig 5.15 Frequency spectra for two ranges of $E\nu/\sin\alpha$

sea level size.

3. Radial distance (fig. 5.13)

In this limited range of radial distances no significant dependence is expected or observed.

5.5.2 Fluctuations.

Fluctuations in the spectra are comparable with the uncertainty in measuring the radio pulses in the presence of noise. The uncertainty in obtaining the spectrum for an individual shower might be affected by changes in the receiver characteristics; but, as previously mentioned, this was checked by sending a short pulse into the receiver at regular intervals. Drift in receiver characteristics, was, therefore, not a serious problem.

5.6.1 Depth of Maximum Shower Development.

As the electron size at sea level for a given primary energy is sensitive to the development of the shower, whereas the radio field strength is, within limits, sensitive to the size of the shower at maximum development, a simple model may be used to give an indication of the probable height of maximum development. The model used here is as follows:

The measured field strength (normalised for geomagnetic angle) is taken as being proportional to the shower size at maximum development. For the range of core distances 50-100m, and likely depths of maximum development, this is supported within about 20% by calculations (Shutie, 1973).

The shower size at sea level is taken to depend solely on the depth of atmosphere between maximum development and sea level. An assumption was made concerning the shape of the electron development curve, namely

that it did not depend strongly on primary energy. Published calculations for a scaling model by Hillas (1979), compared with experimental points obtained from a number of workers, mainly through the method of constant intensity cuts, support such an assumption. Other calculations, such as those of Gaisser et al (1978) are difficult to reconcile with the experimental data points.

It was assumed also, that the shower development curve does not change with zenith angle. The attenuation length was taken as 200g cm^{-2}, and was assumed to be constant. Experimental determinations of this are as yet lacking in precision (Ashton et al, 1979). In fact, all calculations would suggest a slowly decreasing attenuation length with zenith angle, and a more or less slowly increasing value with primary energy (as the shower maximum approaches the array). Thus, the equations used are

$$E_\nu = C_1 Ne_{MAX}$$

and $$Ne_{s\ell} = Ne_{MAX} \exp(-[\frac{x_0}{\cos\theta} - x_m + c_2]/\lambda)$$

with $x_o = 1000g\ cm^{-2}$, $\lambda = 200g\ cm^{-2}$

With $Ne_{s\ell}$ in terms of 10^5 particles, and E in $\mu Vm^{-1}\ MHz^{-1}$, this may be written as

$$x_m = x_0/\cos\theta + \lambda\ \ell n\ (\frac{Ne_{s\ell}}{E_\nu}) + C$$

Adjusting the constant C has the effect of moving the calculated heights of maximum development up or down in the atmosphere.

The constant depends both on the conversion factor from field strength to shower size at maximum development and the shape of the shower decay curve. Changes to either of these thus affect the calculated heights. Although the constant cannot be determined precisely, its value may be estimated. The best calculations yield a normalised field strength for

the emission produced by a vertical 10^{17}eV proton of $\sim 2\,\mu m^{-1}MHz^{-1}$. The depth of atmosphere over which the shower maximum changes only slightly is of the order of 150g cm^{-2} (see fig 5.20). The numerical value for the constant thus obtained is -1250g cm^{-2}. A decrease in the value taken for the normalised field strength by 50% would increase the calculated depths of shower maximum by 140g cm^{-2}, in this model.

The four channels can independently be used to estimate the height of maximum development, and an average obtained by weighting the individual estimates in accordance with errors in field strength. Uncertainties in field strength will lead to an uncertainty in the calculated height of maximum of $\lambda / E_\nu \, dE_\nu$ g cm^{-2}, thus being about 40g cm^{-2} for a 20% error in field strength.

For inclined showers, the error in the array parameter determination becomes significant. Since, as previously mentioned, the array has redundancy in the number of detectors used to measure the arrival direction, an estimate of the goodness of fit to a plane shower front may be made, and used to assign an error to the zenith angle. For average showers, the error of $2.5\sec\theta$ degrees would lead to an error in the calculated depth of maximum of 90g cm^{-2} for $\theta=45^o$. Events with a particularly poor fit to the times were rejected, the criterion used was that the value of σ (as previously described) be less than 8.

5.6.2 Results.

The height of maximum development calculated as above was plotted against the measured sea level shower size for all events with core distances in the range 50-110m. There was no significant difference between the linear regression lines for the different channels, as can be seen from fig 5.16. Since the average measured spectrum was flat (within experimental uncertainties), and independent of shower

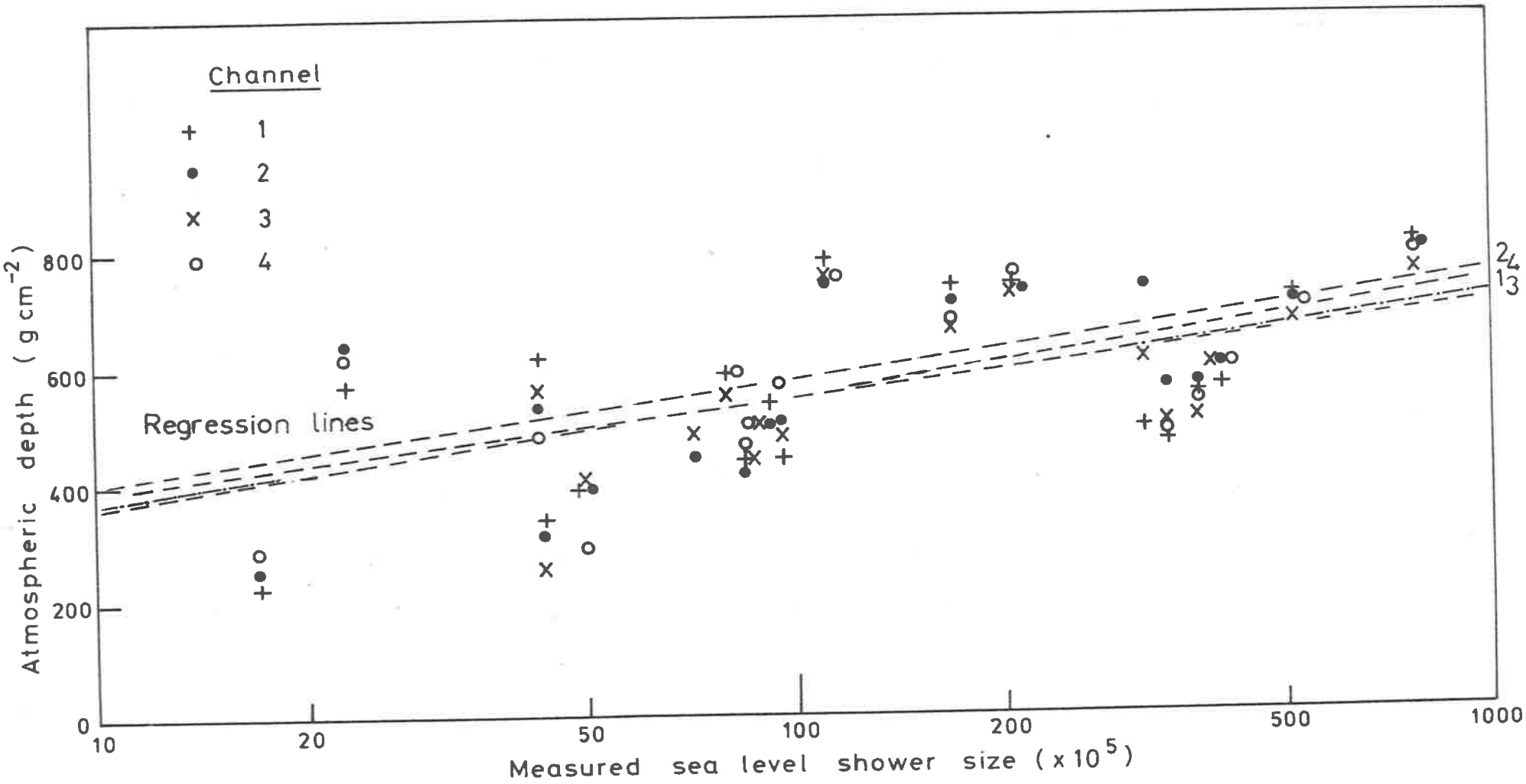

Fig 5.16 Depth of shower maximum for all channels versus measured sea level shower size.

parameters, the calculated heights of maximum were averaged over the number of channels exhibiting a pulse for that event, weighted in accordance with the measurement uncertainties for the individual channels. The data were replotted in fig. 5.17. Several marginal events were not replotted; these included three with marginally high χ^2 and one with no estimate of the error in direction owing to anomalous timing data.

With this more restricted set of events, the main contributions to the uncertainty came from the uncertainty in field strengths and in determining shower directions for inclined showers. The (weighted) errors due to the field strengths were added in quadrature to those in shower directions. Errors in the average field strength measurements average $40 gcm^{-2}$ and those produced by direction uncertainties also $40g\ cm^{-2}$ for the selected events.

The linear regression fit to the plot of depth of maximum development versus (the logarithm of) the measured sea level size yields a value of $95 \pm 32\ gcm^{-2}\ decade^{-1}$.

The elongation rate (in terms of sea level shower size) cannot be estimated from this plot however, as there is a systematic trend of decreasing zenith angle as the shower size increases (fig 5.9). The average zenith angle of the showers in the sample smaller than $2x10^7$ electrons as measured by the array is 29 ± 3 degrees, whereas for those showers greater than $2x10^7$ particles, the average is 18 ± 4 degrees. As previously mentioned, one would expect that small (measured) showers would be more likely to yield pulses above noise if they arrive at larger zenith angles, since it is their size at maximum development which has mainly determined the field strength of the radio pulse.

In principle the plot of calculated height of maximum development against the logarithm of the field strength (normalised for the sine of the angle between the shower axis and the geomagnetic field) should yield

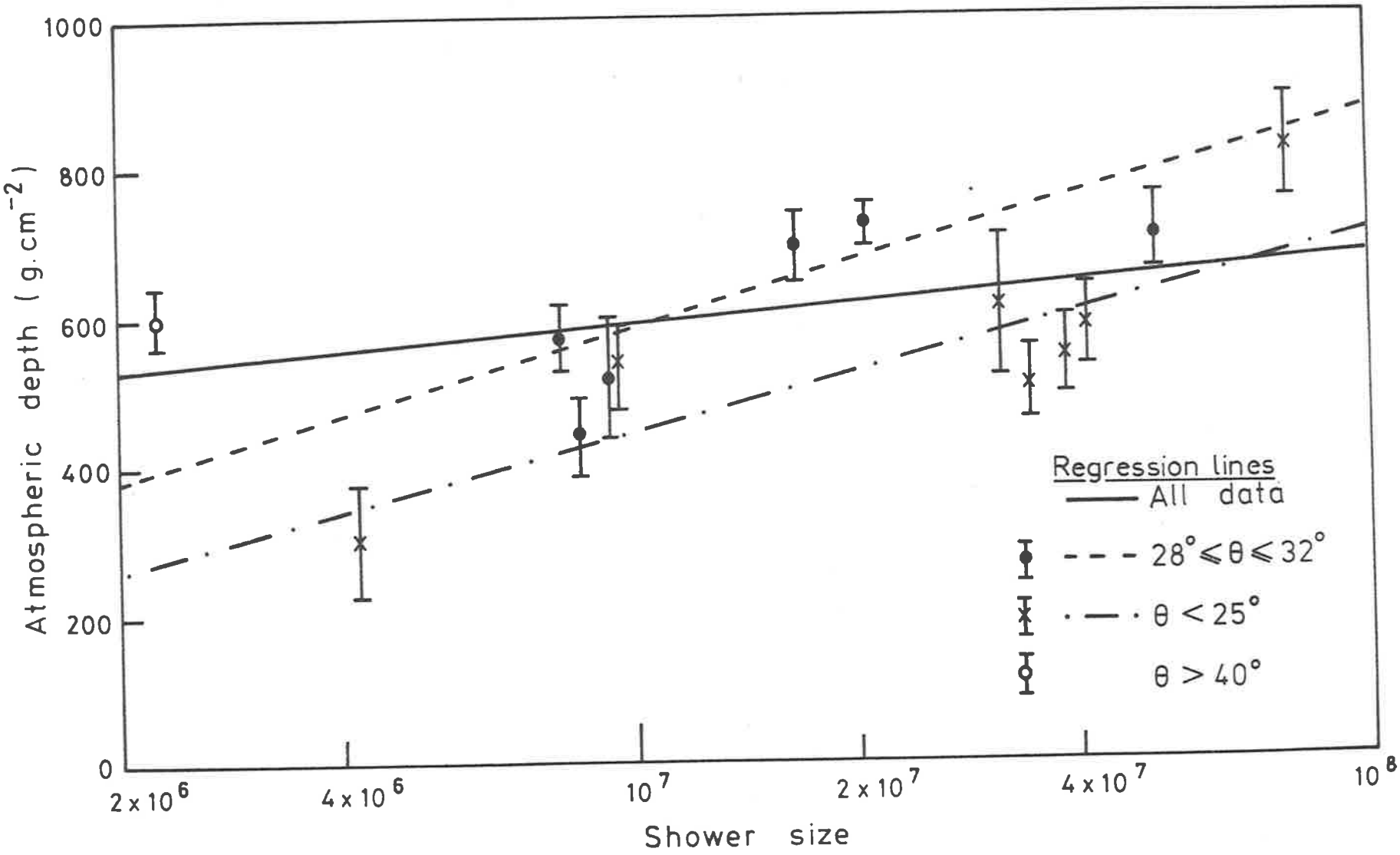

Fig 5.17 Depth of shower maximum for selected events, all four channels averaged, versus sea level shower size.

an estimate of the elongation rate. Referring to fig. 5.18, it may be seen that the scatter effectively conceals any non-zero rate. This may be attributed, in part, to the presence of significant measurement errors in the field strengths taken as the independent parameter in the above calculation. (An overestimate of field strength tends to produce an underestimate in depth of shower maximum.)

In order to obtain a better estimate of elongation rate, the data were replotted as a function of the shower (electron) size at a fixed depth in the atmosphere, taken as 1000g cm^{-2}. The shower attenuation length was taken as constant, as above, (200g cm^{-2}). Owing to the systematic trend of zenith angle with shower size, this plot has a reduced range of shower sizes (fig 5.19). The scatter of the data points about the regression line is reduced compared with fig 5.17, although the slope of the regression line is markedly steeper, namely $250\pm40 gcm^{-2}$ $decade^{-1}$. A check was made on the consistency of this plot with the previous one. Taking the block of events in a five degree interval around 30 degrees, the regression line was recalculated, and found to be $290\pm70 gcm^{-2}$ $decade^{-1}$. The events falling within 23^{o} of the zenith were also used in this way and the value obtained was $260\pm70 gcm^{-2}$ $decade^{-1}$. The average zenith angles for these two blocks of data were 30^{o} and 15^{o}, consistent within errors with the value previously mentioned. (The difference (at 10^{7} particles) between the calculated depths of maximum development for the two groups is approximately $110 gcm^{-2}$, which compares well with the $130 gcm^{-2}$ expected for these angles). This would indicate that the adopted model for correction is not grossly unreasonable. Smaller values of attenuation length (i.e. more rapidly decaying showers) lead to enhanced values of the slope.

In order to estimate the effect on the data of an attenuation length depending on the thickness of atmosphere between the depth of maximum development and the depth of the array, an alternative model

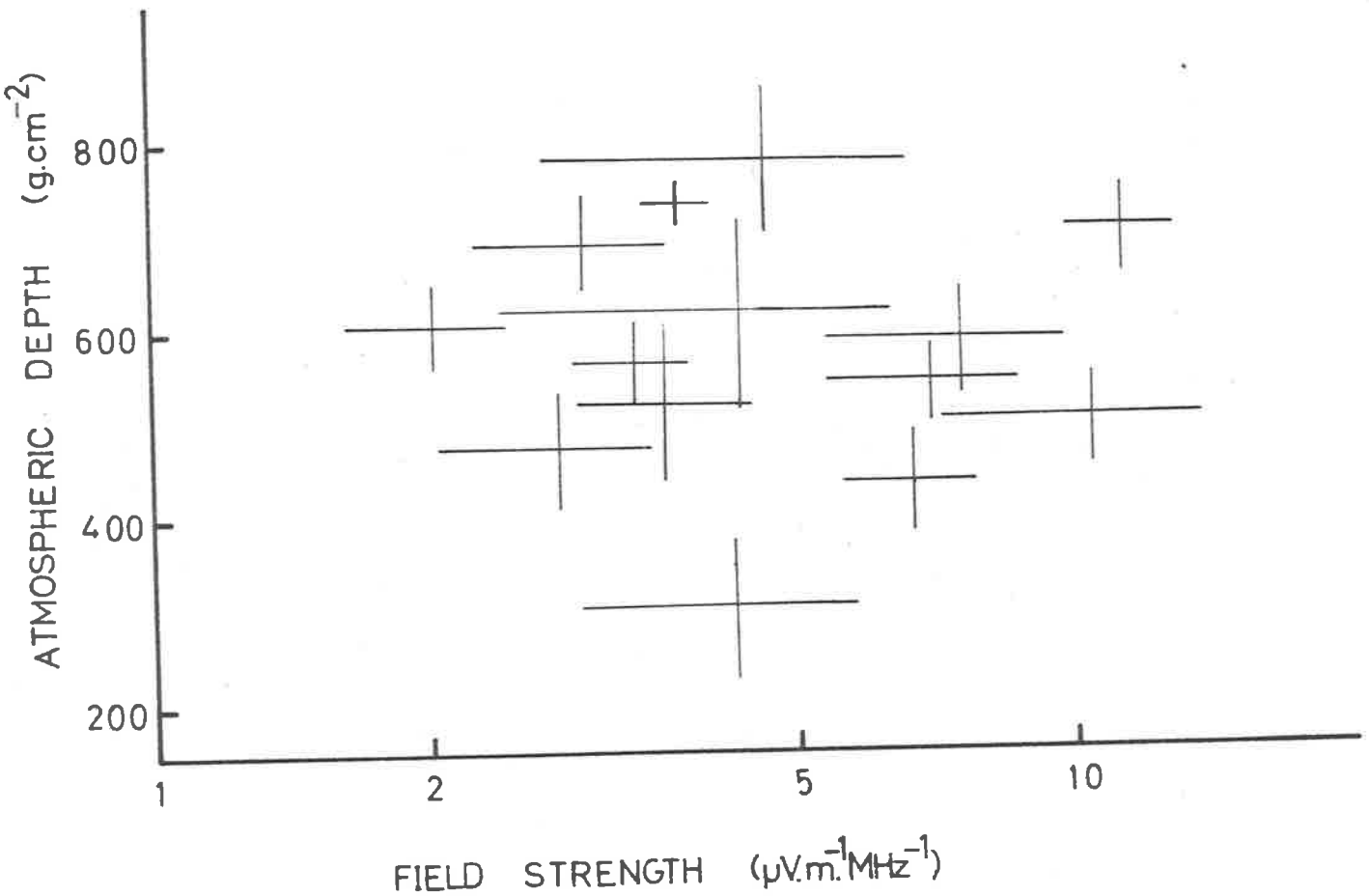

Fig 5.18 Depth of shower maximum versus field strength.

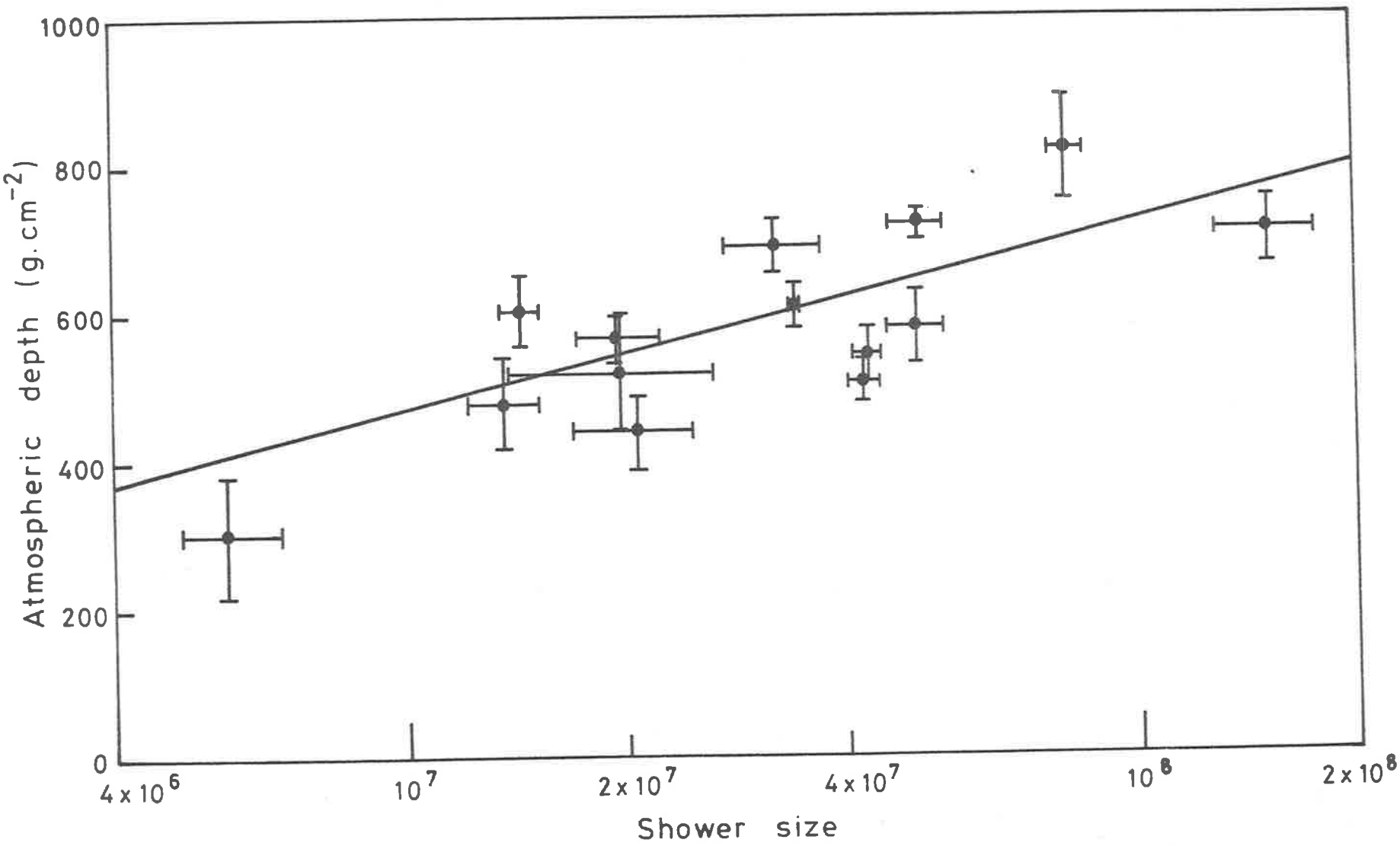

Fig 5.19 Depth of shower maximum versus shower size at 1000 g.cm^{-2} depth.

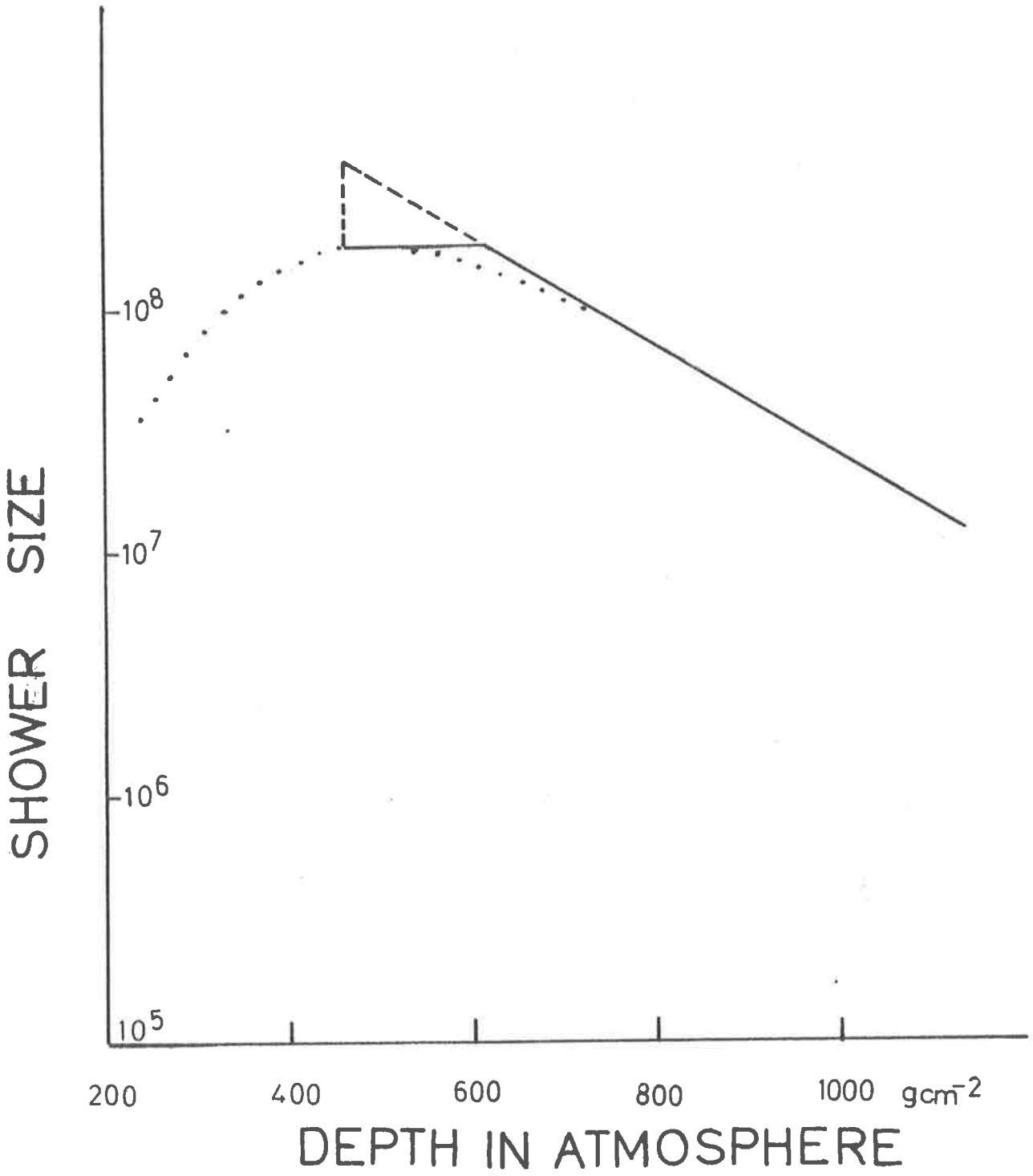

Fig 5.20 Model of Development Curve.

was applied. Showers just past maximum development should have a much larger attenuation length than those which have decayed further. The model chosen took the attenuation length to vary as a power of the thickness of atmosphere between shower maximum and the detector. From the published curves calculated by Hillas (1979), the attenuation length at depth X varies approximately as $\lambda = \lambda_0 (X - Xmax)^{-.55}$, with $\lambda_0 \sim 670$ g cm^{-2}. This attenuation length approaches the value of 200g cm^{-2} some 600g cm^{-2} past shower maximum. The form is convenient for algebraic manipulation, modifying the formula for the depth of shower maximum as follows:

$$X_{MAX} = X_0/\cos\theta + 380(\ell n \ Ne_{s\ell}/E_\nu)^{1.55} + \text{constant}$$

The constant depends as before, on the radio emission normalisation, and the average height of maximum. As might be expected, such an approach led to a greatly enhanced rate, which was even more incompatible with the range of acceptable results.

The elongation rate itself is expressed in terms of the logarithm of the primary energy so the values above for the slope of the plots against electron number will be reduced. For a power law dependence of $N_e \pm \alpha E^{.85}$ the elongation rate estimate becomes 212±35gcm^{-2} decade^{-1}. At the highest energies, where the detected showers are closer to maximum development and the particle numbers changing more slowly with depth, the exponent is closer to unity, and the elongation rate higher.

A similar technique, but relating the height of maximum development to the width of the Cerenkov pulse produced by the shower particles has been applied at Adelaide with significant results by Thornton and Clay (1979). The data suggest a change in the elongation rate at sea level sizes corresponding to the well-established break in the cosmic ray

spectrum at about 10^{15}eV. The sea-level sizes at which this occurs are less than those for which the radio pulses are observable above noise. Consequently the present data cannot be used as a direct comparison in this size region, and the fact that both experiments indicate very high elongation rates is coincidental. Although the Adelaide Cerenkov experiment and the present experiment were running side by side for some time, there are in fact, no events in common which exhibit both radio and Cerenkov pulses.

5.6.3 Comparison of Elongation Rates.

The value of the elongation rate with the reservations expressed above, may be compared with values obtained through other techniques. In table 5.2 are values collated by Suga (1979) and Gaisser et al, (1979) of measurements of the elongation rate. These values were extracted from experiments employing a variety of independent techniques. These include the risetimes and lateral distributions of the deep water Cerenkov signals at Haverah Park, (Lapikens et al, 1979, Craig et al, 1979) the pulse widths and lateral distributions of the atmospheric Cerenkov pulses, (Kalmykov et al, 1979, Hammond et al, 1979), and equi-intensity cuts of the longitudinal development (Aguirre et al, 1979a). The experimental data summarised by Suga (1979) and Gaisser et al (1979) are seen to have a large spread - however the value obtained in the present experiment significantly exceeds the average calculated from the above.

The significance of comparatively high elongation rates has been discussed at length by Gaisser et al (1979) and others. For a fixed composition, the elongation rate is independent of the primary mass. The relation between depth of maximum development and primary energy E_o (effective mass N), and for constant pion and nucleon interaction lengths, is

$$X_{max} = 85(1 - \alpha) \log_{10} E_o/N + \text{constant}.$$

TABLE 5.3

RECENT ESTIMATES OF ELONGATION RATE

(extracted from Gaisser et al, 1979, Suga, 1979).

Reference	Method	Energy Range	Value (gcm^{-2} $decade^{-1}$)
Aguirre et al, 1979a	Shower development curves from constant intensity cuts (Mt. Chacaltaya).	10^{15}-10^{18}	100± 50
Barrett et al, 1977	Risetimes in water Cerenkov detectors (Haverah Park).	$2x10^{17}$-$5x10^{18}$	90±10
Craig et al, 1979	Lateral distribution of deep water Cerenkov emission (Haverah Park).	10^{18}	70±25 (corrected)
Dyakonov et al, 1979	Cerenkov lateral distribution (Yakutsk)	$3x10^{17}$-$3x10^{18}$	120±75
Glushkov et al, 1979	Cerenkov lateral distribution (Yakutsk), and total flux v. electron density at 600m.	10^{17}-$3x10^{18}$	60±30
Hammond et al, 1978	Shower development curves mapped by Cerenkov array at ground level (Haverah Park.)	$2x10^{17}$-$2x10^{18}$	85±37
Kalmykov et al, 1979	FWHM of Cerenkov pulse at 300m (Yakutsk)	10^{16}-10^{18}	33±18
Lapikens et al, 1979b	Risetimes of deep water Cerenkov signals (Haverah Park).	$2x10^{17}$-10^{19}	105±7
Linsley, 1977	Shower lateral structure (Volcano Ranch).	10^{18}	85±39

where E_o is the energy of the primary referred to the critical energy. The term $(1-\alpha)$ is related to the multiplicity in the fragmentation region, being limited to values between 0 (for scaling) and 0.5 (the energy conservation limit). For the Landau model (with $E^{\frac{1}{4}}$ multiplicity) α is about 0.1 (Gaisser et al, 1978).

High elongation rates $\frac{dX_{max}}{d\log_{10}E_p}$ can thus be produced by two factors; one is a change in composition from a heavy to a light primary, and the other is a change in the nature of the high energy interactions. Values of 85-90g cm^{-2} per decade are difficult to reconcile with $E^{\frac{1}{2}}$ multiplicity ($\sim$ 43g cm^{-2}) are somewhat higher than $E^{\frac{1}{4}}$ multiplicity models ($\sim$ 70g cm^{-2}), but are not inconsistent with models which have scaling in the fragmentation region ($\sim$ 87g cm^{-2} decade $^{-1}$) (Gaisser et al, 1978, 1979). There is evidence for a change in the elongation rate at lower energies which may be suggestive of a change in composition from heavy to light primary nuclei (Thornton and Clay, 1979), (possibly as a result of an energy region in which heavy primaries are present in addition to the otherwise predominantly light nuclei in the primary beam). This focusses attention on details of the nuclear interactions involved. Model calculations suggest that a rising p-p cross-section (as might be extrapolated from measurements below 50TeV) would have the effect of reducing the elongation rate by $\sim 20 \pm 10$g cm^{-2} and shifting the shower maxima further up in the atmosphere. Refinements in model calculations (including the consideration of selection effects resulting from fluctuations arising from a mixed composition), and the resolution of contradictions between different experimental observations may allow the field of possible interpretations to be narrowed down.

5.6.4 Systematic effects.

According to our present understanding of the production of radio emission, the field strength observed on the ground over a range of lateral distances is largely independent of shower development details. The observed electron size at sea level, however, does depend on shower development. Selection of events on the basis of the observed size at sea level would systematically favour late-developing showers. Selection of events on the basis of their radio pulses, however, would show little such bias, except that for showers reaching maximum development very close to the array, the field strengths cannot be taken as being independent of shower development, and are smaller than for showers developing higher in the atmosphere. In terms of the model used in calculating depths of maximum, the effect is in the direction of increasing the elongation rate.

The relatively poor signal to noise ratio for the radio pulses does mean that sampling problems are significant. The consequent overestimation of field strengths is expected to be greater for smaller signals than larger; this also tends to produce an increase in the estimated elongation rate. Thus, since there are systematic effects which would tend to bias the results in the direction of enhanced rates, it is suggested that the high value of elongation rate estimated in this section does not necessarily represent a basic inconsistency between interpretations of air shower phenomena.

This question is discussed further in Appendix B

5.6.5 Fluctuations in the height of maximum development.

There remain fluctuations in the height of maximum development when experimental uncertainties are accounted for, of the order of $100 gcm^{-2}$.

Such an estimate represents an upper limit, since a highly simplified model was adopted for shower development and the (calculated) independence of radio pulse field strengths on fluctuations in shower development has limited experimental support. In addition the varying contribution to the emission of a geoelectric mechanism lends doubt that the observed fluctuation is a significant indicator of the primary composition. Indeed, uncertainties in the technique would appear to make it unlikely that fluctuation details are derivable from radio emission studies.

CHAPTER 6

CONCLUSIONS AND SUGGESTIONS FOR FURTHER WORK

The present status of radio investigations into extensive air showers does not hold out much hope for future revelations about air showers from this technique. There is a consensus of opinion about the main characteristics of the emission: A generally rather flat spectrum in the range of some tens of MHz, with a falling spectrum on either side, but with the possibility of a time varying contribution particularly at low frequencies, possibly related to geoelectric effects (Crouch, 1979). The magnitudes of the field strengths measured are comparable with calculations based on the geomagnetic mechanism, and a proportion of pulses consistent with the high electric fields associated with conditions for thunderstorm activity has been recorded by most of the groups working in the field.

Although these general characteristics are not in dispute, and the dependence of the behaviour of the emission on various models of shower development is believed to be understood, the application to the problem of identifying the primary particles has failed to live up to its initial promise. Apart from the presence of 'contamination' from the geoelectric mechanism, and the low collecting rate of detectable pulses with suitable signal to noise ratios, there remains a considerable scatter in the normalised field strengths in addition to that produced in normalisation by the uncertainties in relating the particle information to primary energy.

The use of simple models allows estimates of the height at which maximum shower particle numbers occurs, and permits an estimate of the shower elongation rate for purposes of comparison with other work. The hope of checking on the height of shower maximum by investigating the frequency spectrum of the radio emission has not been realised.

In the present experiments, placing the antenna near the centre of the array to measure the emission for small radial distances proved unsuccessful, since the smallest radial distance for a 'radio' shower was still some 50 metres. Siting the antenna at 200-300m from the array would allow measurements of the spectrum which would be expected to have scatter attributable in part, to fluctuations in shower development. However, the rapidly falling lateral distribution, leading to poorer signal to noise ratios, make it unlikely that such fluctuations would be detectable in the presence of this experimental scatter.

Thus, work on determining details of the primary composition by looking for fluctuations in the height of maximum development from the characteristics of the radio emission does not appear likely to yield unambiguous results. In common with other groups, our work in this area has now come to an end.

However, work using optical Cerenkov emission does appear likely to provide a satisfactory approach to the problem. Work is in progress at the Buckland Park array on both the lateral distribution of Cerenkov pulses and the pulse shapes themselves, the latter in particular offering hope for a solution to the problem. The fact that pulses with good signal to noise ratios are obtainable over a much wider range of shower sizes means that the collecting rate of useful events (at times of clear atmospheric conditions) is far greater, and more stringent acceptance criteria on the array analysis may realistically be used. Clearly, the application of several techniques to the same showers would lend more weight to the conclusions reached, Cerenkov techniques being the cornerstone of this approach.

In the appendix, a discussion is presented of a pilot experiment designed to develop techniques for recording very fast pulses and their application to the study of time profiles of particle energy flow. The apparatus is now being used in the Cerenkov programme.

APPENDIX A

ENERGY DEPOSITION

In this appendix will be described a preliminary experiment set up to investigate particle profiles. A brief resume of previous work in the field will precede the detailed description of the Buckland Park system.

A.1. Air Shower Studies.

The electron distribution in the shower front is clearly of relevance to model calculations and to studies of the radio and Cerenkov emission. One would expect the distribution both in space and energy of the electrons responsible for the emission to depend on the stage of development of the shower and on atmospheric depth.

The lag of electrons behind the shower front is caused by several factors. In addition to the lag produced by the angle at which the production particle is travelling, multiple scattering is a dominant process. This scattering is highly dependent on energy, and increases very rapidly as the electron energy falls below about 100 MeV. As the core distance increases, the softening of the energy spectrum of highly scattered electrons is of necessity accompanied by an increasing lag of the particles with respect to undeflected particles at the leading edge of the shower front. Thus the thickness of the shower front is expected to increase with core distance.

The early experimental work on the longitudinal structure of the shower front studied the relative time delays between detectors, and was largely inspired by the need to consider the accuracy of arrival direction determinations of air shower arrays. Bassi et al (1953) measured the relative delays between three liquid scintillator counters. They found

the electron disc thickness to be 1-2 metres, with a radius of curvature of more than 1300m. The penetrating particles were found in a less curved disc of 2-3 metres thickness, lagging the electron disc by not more than 3 metres.

The lateral dependence of the disc thickness was first measured by Linsley and Scarsi (1962), at Volcano Ranch. They found that the electron distribution broadens at large core distances, (200-1500m) and the radius of curvature increases. Thielert and Wiedecke (1964) found an expression for the dependence of the standard deviation ($\sigma(r)$) of the instantaneous electron distribution, of the form;

$$\sigma(r) = \tfrac{1}{2}\ (1+{}^{r}/_{62})^{2\cdot5}$$

in good agreement with the values of Linsley and Scarsi.

Near the shower core, work has been done at Kiel, again measuring relative arrival times between detectors, both shielded and unshielded. (Woidneck et al, 1971, Woidneck and Bohm, 1975). This group, in fact, investigated the average shape of the shower front for both muons and electrons, with a resolution of 1.3ns for the electron front and 2.7ns for the muon front. The data were fitted to a distribution of the form $d(t) = t^a \exp(-bt)$. At distances 4-10m, the parameters have values $a=0.9\pm0.3$ and $b=0.6\pm 0.1ns^{-1}$ up to 12ns. At greater core distances (25-63m), values are $a=0.3\pm0.3$ and $b = 0.4\pm0.1ns^{-1}$. The corresponding FWHM (rather than standard deviation, σ) are about 3.6ns. The broadening is in part due to an increasing contribution from the muon front, which slightly precedes the electron component.

The work described above produced average shower front structures. The electron distributions obtained by the workers at Kiel were found by triggering off a large area scintillator, and measuring the delay for particles travelling through a second scintillator of area small enough that the probability of more than one particle passing through

it was negligible. Building up a distribution is a cumulative process which can give no indication of the inherent fluctuations between showers. It might be expected that fluctuations in shower development should be revealed in variations in the particle front structure.

At large core distances, the time at which an individual particle is detected should be determined, amongst other things, by the height of origin of the particle. Thus the shape of the particle front should be related to details of the shower development. When viewed off axis, late developing showers might be expected to have a broader shower front than earlier developing showers. Close to the axis, where the electron component is most numerous, multiple scattering masks such an effect (Woidneck and Bohm, 1975).

Work has been done at Haverah Park for core distances greater than 200m. The Leeds group has studied pulse profiles from the deep water Cerenkov tanks. Early work concentrated on establishing the broad features of the pulse profiles as functions of core distance and zenith angle, together with a comparison with calculations (Baxter et al, 1965, 1968, Hillas 1965). Later work has concentrated on the consideration of fluctuations in longitudinal development (Marsden et al 1971, Lapikens et al 1973, Waltson and Wilson 1974). The measurement paramenter chosen was '$t_{\frac{1}{2}}$', the time in which the recorded signal rose from 10% to 50% of the final amplitude. Calculations indicate that this parameter should be sensitive to the depth of first interaction for a proton primary (Hillas et al, 1970, Dixon and Turver, 1974). Considering the residual fluctuations when the dependence on core distance, zenith angle and energy, and the effects of measurement sampling are considered, the presence of a proton component in the primary flux was indicated (Watson and Wilson, 1974). Further refinements in calcuations and analysis have produced quantitative measurements of the fluctuations in the depth of maximum development and

the elongation rate (Barrett et al, 1977). Protons remain the favoured primary particles at 10^{18}eV.

The Nottingham group at Haverah Park have studied muon arrival times with shielded scintillators (Blake et al, 1978a, 1979). They have found the average muon time-spread to be significantly faster than that expected from standard model cascade calculations. Their work is complementary to that of the Leeds group, and has potential for the study of shower development. (Dixon and Turver, 1974).

The group operating at Mt. Chacaltaya (5,200 m.a.s.l.) has studied both electron and muon arrival time structures in order to investigate the early stages of shower development. Although the risetime of the muon component is shorter, and the tail longer, than calculations for various multiplicities suggest, the shapes of the electron and muon components are similar for very large showers (above 10^{18}eV) (Aguirre et al, 1979b).

A. 2. Pulse Profiles near the core.

The structure of the air shower front has been investigated near the core by groups at Adelaide (at Buckland Park) and Tokyo, the latter with better resolution (Sakuyama and Suzuki, 1979). Theoretical calculations bearing on the work will be discussed in connection with the preliminary experiment conducted at Adelaide. (McDonald et al, 1977).

A. 2.1 Pulse Profiles near the core.

The model of the air shower front is that of a distribution of particles of steadily decreasing average energy as the shower plane passes an observer. The absorption of low energy electrons by ionisation loss puts an ultimate limit on the thickness of the shower front. The shape of the arrival time distribution for the electromagnetic component has been calculated by

several authors. Locci et al (1967) have performed a Monte Carlo calculation of the density distribution as a function of core distance (1-35 metres), shower height and time, for approximation B. Bosia and Navarra (1969) used the Landau diffusion equations (in approximation A) to derive certain features of the distribution; namely the mean delay and standard deviation relative to the mean as a function of shower age, of electrons of different energies. These two calculations considered electrons of energy greater than 10MeV and the critical energy (86MeV) respectively. Although not directly comparable, the standard deviations are in numerically good agreement.

These calculations suggest that there is only a small change in this standard deviation with shower development, once the shower has travelled several radiation lengths in the atmosphere. This suggests that measurements of this parameter (near the core) are not sensitive to details of shower development.

An analytical solution for the development of a shower in an isothermal atmosphere has been developed by Green (1978). The solution is currently the subject of the development of a computer calculation (Rawinsky, private communication).

A.3.1. The Buckland Park System.

The preliminary experiment at Buckland Park comprised a fast scintillator detector situated in B hut (see fig. 4.1). The detector consisted of a 300mm diameter disc of NE104 scintillation, 25mm thick, painted with NE560 white paint on the back, and enclosed in a black housing. (see fig. A1). This scintillator was chosen for its fast decay time of 2ns. The scintillator was viewed by an EMI 1820B fast photomultiplier of diameter 50mm, from a distance of 520mm. This is a low noise tube with a bialkali photocathode and a linearly focussed 12-dynode multiplier system. The

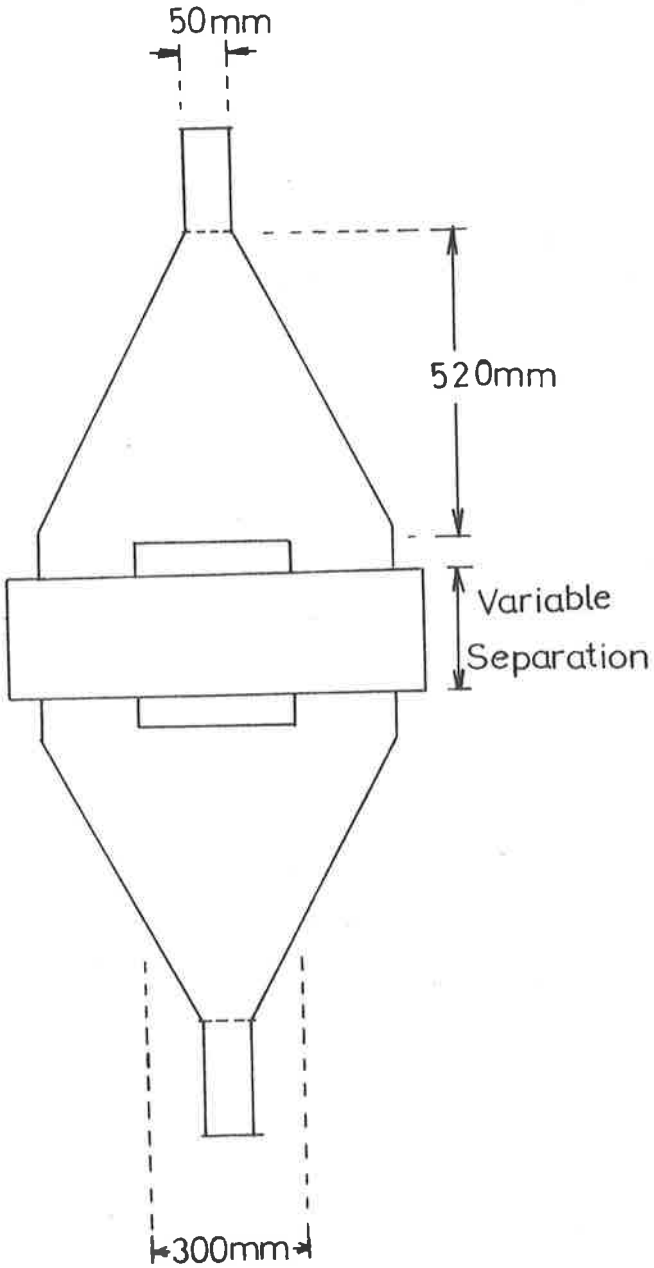

Fig A.1 Detector housing

output of the tube was connected via a suitable length of cable to a Tektronix 7912 transient recorder with 500MHz bandwidth. This recorder essentially comprises a cathode ray storage tube which is read using a TV type raster to produce an analogue output which may be displayed on a TV monitor and photographed. It is functionally equivalent to a long-persistence phosphor.

The recorder was triggered by the fast array scintillator at site B, thus reducing trace jitter problems. The monitor was photographed only when the particle array provided a trigger. The internal delay in the recorder plus the persistence of the monitor was sufficiently long to allow the use of a mechanical shutter action. A block diagram of the recording system appears in fig. A2.

The apparatus was later extended by the addition of a further detector mounted below the first. A resistive circuit mixed the output signals from the two photomultipliers to enable a single-trace display. This system was run with varying thickness of lead between the two detectors, although results obtained with this arrangement will not be discussed further.

A. 3.2 Response of Detector to Particles.

The response of plastic scintillator detectors to particles has been studied by a number of authors, both in terms of a comparison with other detectors, and also in terms of detector geometry. Comparisons have shown that there are more "scintillator particles" than ionizing particles observed by Cloud Chambers and ionisation chambers; there the ratio of the two depends on the thickness of scintillators, the energy of the incident particles; and hence on the density of charged particles, the radial distance from the shower core, and shower size. This increase is largely due to nuclear interactions produced in the scintillator by

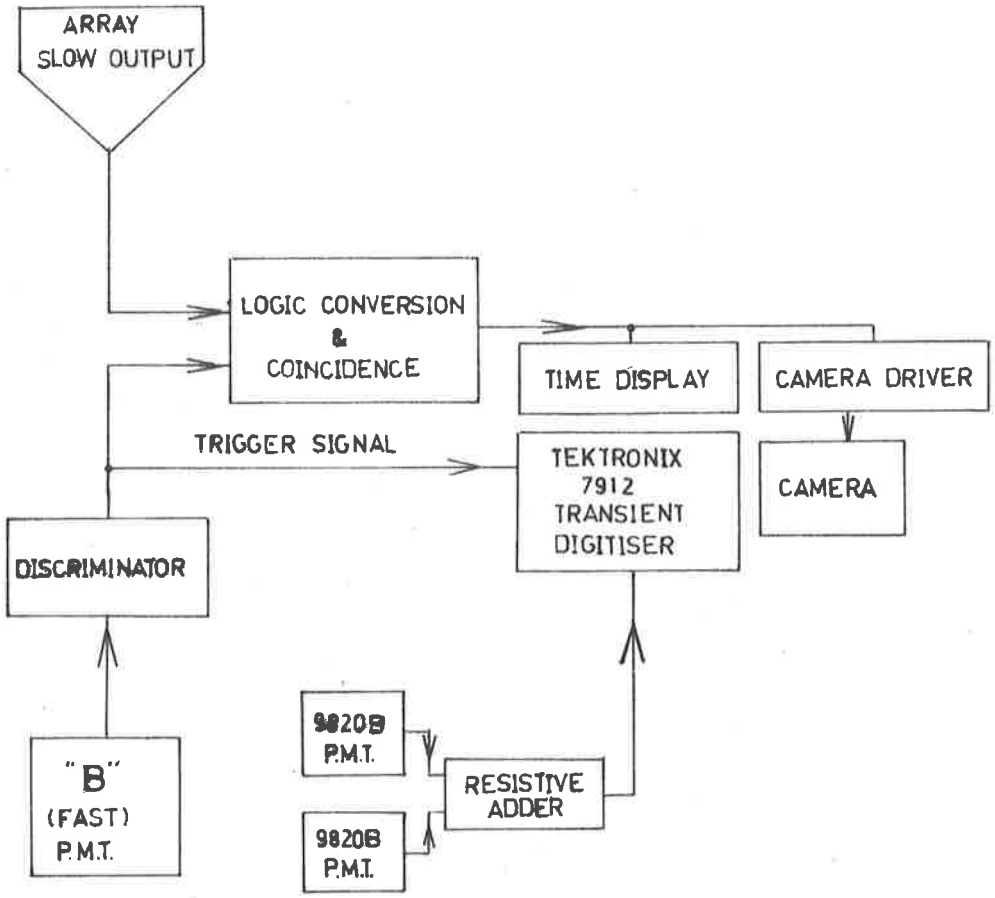

Fig A.2 Recording system

strongly interacting particles, together with some cascading of the electromagnetic component within the scintillator itself (Chatterjee et al, 1962, Bray et al, 1965, White and Prescott, 1968, Blake et al, 1978). A scintillation detector is usually calibrated in terms of its response to a single vertical muon; the number of particles being given by the ratio of pulse height to the average response to a single particle (in the Gaussian limit), the average (for a Landau distribution) being greater than the mode. The energy deposited by an electron above the minimum ionising energy is about $2 MeV gm^{-1} cm^{2}$, and changes little with energy; there is a further (relatively small) contribution from the photon component, although at large core distances the photons far outnumber electrons and their contribution becomes significant (Kellerman and Towers, 1970). For electrons of low energy, below about 5 MeV for this thickness of scintillator, the detector becomes energy sensitive. Thus a scintillator is, in a sense, sensitive to both energy and particle number.

The thickness of the scintillator is also significant. For a thicker slab of scintillator, the minimum ionising energy will be greater so that the number of particles recorded(when the pulse heights are calibrated in terms of equivalent single vertical muons) will be less.

A.3.3. Efficiency of the system.

The light output of NE104 scintillator, with an efficiency of 68% that of anthracene, will be about 10^{4} photons for excitation by a 1 MeV electron (Birks, 1964). The distribution of light emission will be uniform. The fraction of the light striking the photomultiplier is expected to be that which travels directly to the tube, either with or without a reflection off the bottom white painted surface. Emission at angles greater than 39 degrees to the vertical will suffer total internal reflection;

light at other angles will be rapidly absorbed in successive reflections off the matt black interior walls of the detector housing. Calculating the solid angle for emission, with the dimensions for the detector known, the fraction of the beam froma point htanθ from the centre of the scintillator, which strikes the tube directly, is given by:-

$$\frac{r^2}{4h^2} \qquad \left(\frac{\cos^5\theta}{\eta^2-\sin^2\theta}\right)$$

where r is the radius of the photomultiplier tube, h its height above the scintillator, and η the refractive index of the scintillator (1.58). Doubling this for the cone reflected from the bottom surface of the scintillator, suggests that the fraction of the light striking the detector is about 5×10^{-4} decreasing by up to 20% near the edge of the scintillator. With NE104 scintillator, the effective efficiency of the bialkali photocathode is about 25%, so a minimum ionising particle (~5MeV) will thus result in the production of about 6 photoelectrons on average in the photocathode.

Statistical fluctuations in the fraction of photons producing photoelectrons in the cathode, the effect of the Landau distribution of the energy loss of fast charged particles, variations in the path length of inclined particles, variations in the amount of light collected from different regions of the scintillator and phosphor, and the statistics of secondary multiplication all contribute to variations in the signal observed at the anode of the photomultiplier.

The efficiency of plastic scintillator may be compared with that of a glass Cerenkov detector. The photon yield per unit length will be close to the asymptotic value, given by

$$\frac{2\pi}{137}\int_{\lambda_1}^{\lambda_2}\frac{d\lambda}{\lambda^2}$$

(Jelley, 1958a). This yields about 2500 photons per 5cm. in the wavelength range in which the bialkali photocathode is sensitive. The sensitivity of this detector will extend to lower energies than the scintillator. However, the angle of production of these photons, at the Cerenkov angle θ_c given by

$$\sin \theta_c = \frac{c}{\eta v}$$

imposes stringent limitations on the geometry and area of such a detector. The production of such signals in the glass envelopes of photomultiplier tubes has been discussed by Clay and Gregory, 1976.

A.3.4 Results.

Pulse widths

In the initial run, the distribution of observed pulse widths was studied. The probability of a full width at half maximum is plotted for measured pulses of an amplitude greater than that corresponding to about 4 particles. This distribution peaks at 11ns. Allowing for the system instrumental time resolution, this leads to a value of about 6ns for the FWHM of a typical shower. The distribution of FWHM itself has a FWHM of 4ns. A selected group of events (more than 10 particles) had a similar distribution with average FWHM of 12ns and similar width (fig. A3). This width may be due to fluctuations in the 'true' pulse as well as fluctuations in the single particle response.

These values may be compared with those obtained more recently by the Japanese group (Sakuyama and Suzuki, 1979). Their average FWHM are smaller, in good agreement with the results from Kiel, and are thus compatible with the distributions calculated for electromagnetic cascades (section A.2.1.) The distributions of FWHM recorded by the two groups are of similar width.

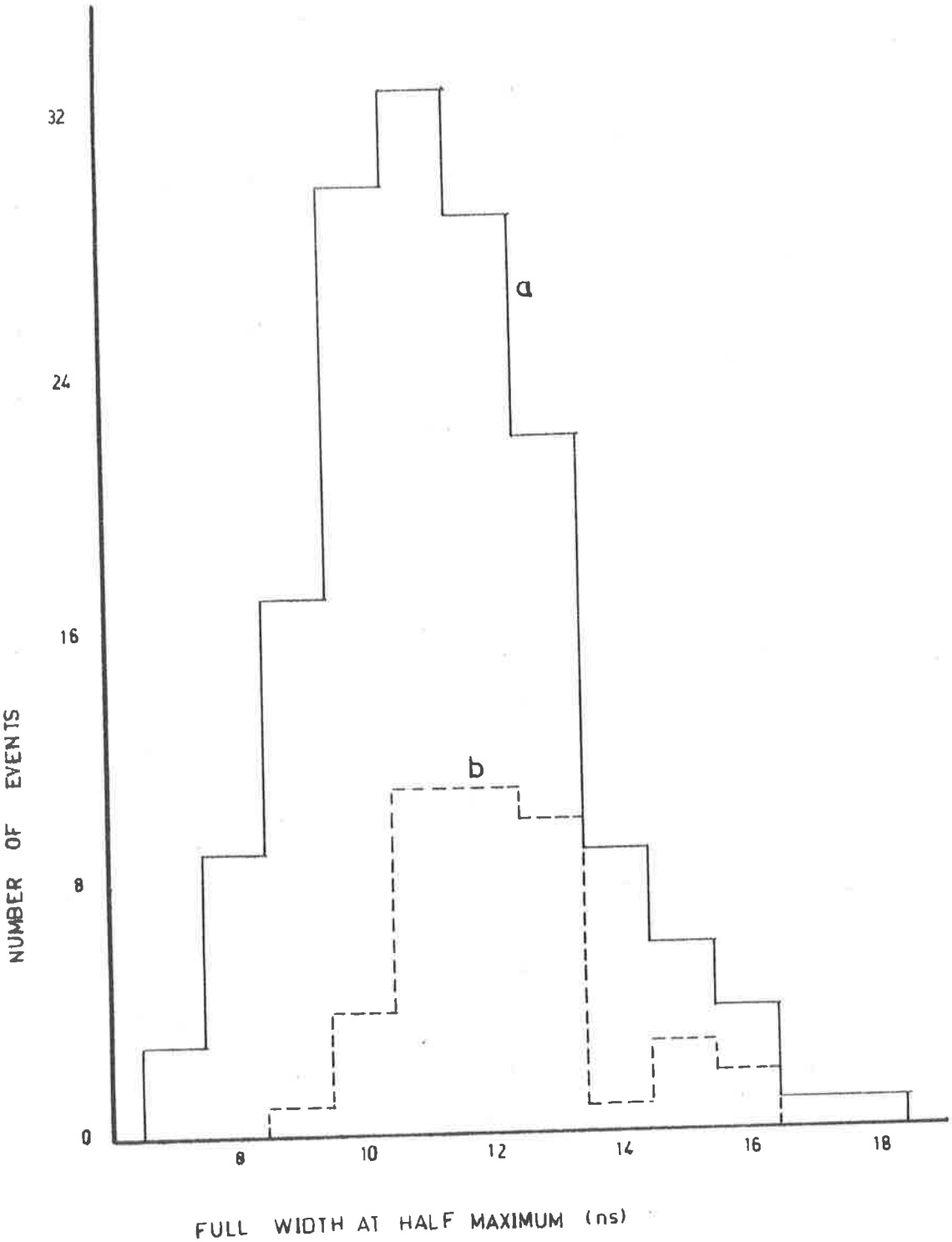

Fig A.3 (a) Distribution of FWHM

(b) as above, more than 10 particles in detector

Dependence of FWHM on Shower Parameters.

An attempt was made to resolve the dependence of the FWHM on air shower parameters, in particular, shower size and density, zenith angle, and radial distance. These parameters are not independent, since showers falling further away tend to produce lower densities near the detector. Thus there is a tendency, for the pulses falling within the dynamic range of the recording system, for large densities to be associated with larger values of core distance.

The result of this investigation was as follows: Within the resolution of the system no significant dependence of FWHM on core distance up to 50m or zenith angle was established. There was, however, a systematic dependence on the particle density. This is, in large part, attributable to the experimental arrangement: a low particle densities, the detector acts more like a sampling detector (after the fashion of the Kiel group), with a greater proportion of very few particle traversals through the detector than at higher densities. Establishing the shape of the energy deposition in the scintillator requires a high density of particles. In the present (pilot) experiment, the photomultiplier set up limited the dynamic range of the detector, and the position of the pulse on the trace was not independent of the amplitude of the scintillator signal used as a trigger. The observed dependence of FWHM on particle density is shown in figure A4.

A.3.5 Shape of the Energy Deposition Curve.

In the pilot experiment, details of the shape of the shower front structure were not investigated in any great detail. Pulse shapes range from smooth pulses which are candidates for fitting by Pearson Type III distributions, to pulses exhibiting a series of peaks extended over,

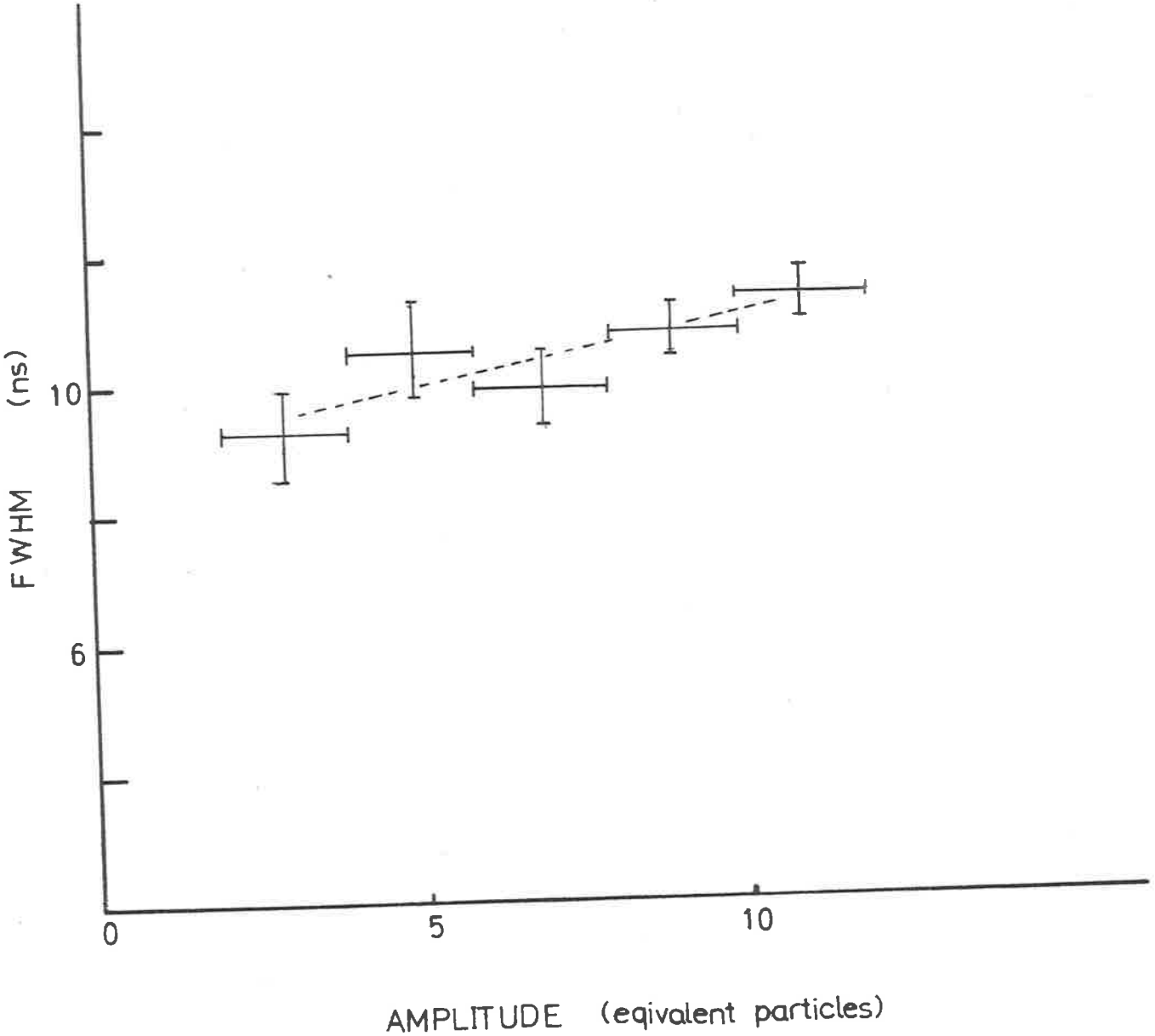

Fig A.4 FWHM v. detector signal amplitude

in some cases, tens of nanoseconds. The observed structure for individual showers is a combination of the shower characteristics and statistical effects both from the number of particles triggering the detector and the response of the detector to these particles. Examples of representative and extreme shapes are shown in fig. A5.

The detector was calibrated in two ways, one by comparison with the densities recorded by the adjacent B detector, and also by the recording of pulses coincident with a trigger from a (small) detector immediately below the scintillator. The shape of the single particle response is of course required for deconvolving the pulse produced by the passage of an air shower through the detector. Subtracting the FWHM of the single-particle-response from the FWHM of the recorded pulse in quadrature yields the true FWHM only if these FWHM are related in the same way to the variance of the energy distributions observed (as would be the case for Gaussian distributions). In fact, for non-symmetric distributions, with extended tails, the true FWHM can be obtained only by a deconvolution program, or by approximating the distributions by analytical functions and calculating the resulting FWHM.

In the pilot experiment, extensive deconvolutions were not performed; a typical shower-accompanied pulse was, however, deconvolved and the resulting FWHM of the smoothed deconvolved pulse compared with that obtained by subtraction in quadrature of the FWHM. The result is shown in fig. A6. It must be noted that the FWHM of the signal produced by a single particle itself fluctuates.

A.4 Suggestions for further work.

Clearly investigations into the detailed shape of the energy deposition of air shower particles require a system with improved resolution. The limitations on the resolution of the present system

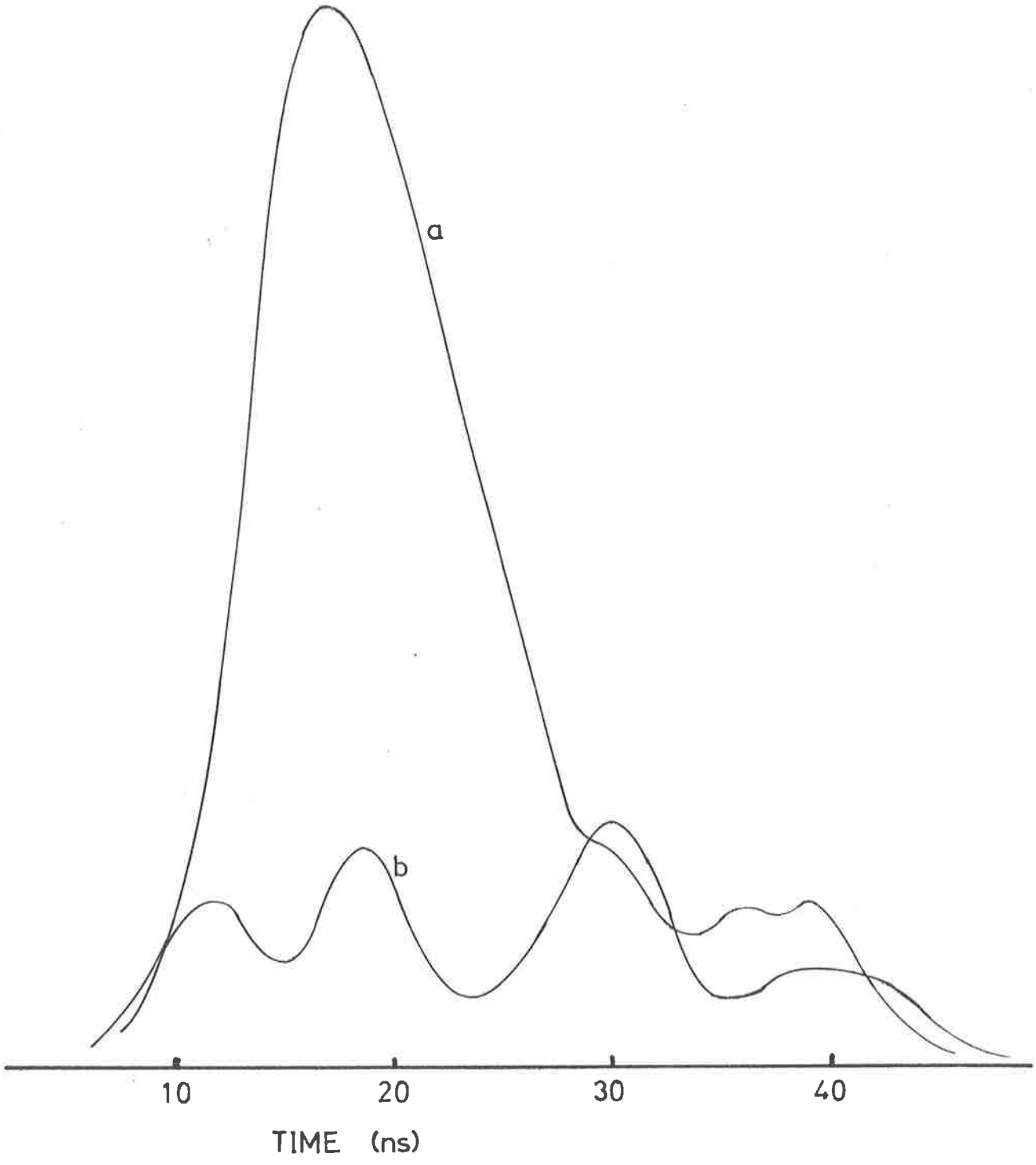

Fig A.5 Examples of pulse shape

(a) relatively smooth pulse

(b) extended structure

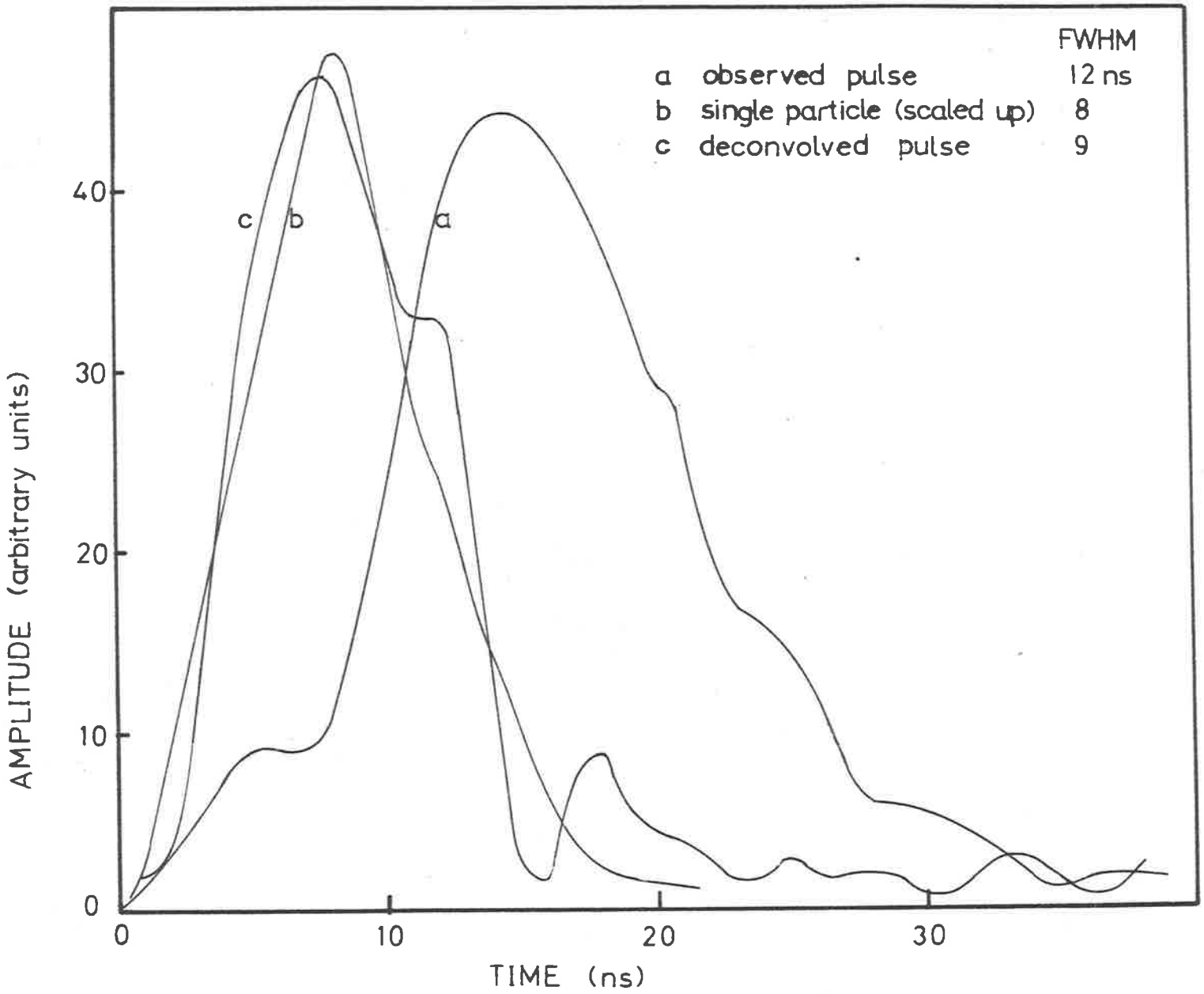

Fig A.6 Example of deconvolved pulse.

arise from several factors; the risetimes of the scintillator and photomultiplier, and also the geometry of the system and cabling.

The response of scintillators has been studied, and measured by a number of authors, using single-photon sampling techniques. This approach enables the average pulse shape to be obtained. A sample of NE104 scintillator has been found to produce a pulse with FWHM of 2.2ns, and scintillation decay time of 2.0ns (Birks and Pringle 1971). The lateral dimension of the detector should not affect the time resolutions; even for a horizontal particle, for example, the transit time is only 1ns. Similarly the orientation of the detector with respect to the scintillator will not result in significant scatter.

The most inconvenient limitation in the pilot experiment was the performance of the photomultiplier; the tube used suffered from a relatively sudden onset of saturation at about the 30 particle level, although linearity was well maintained up to this point. The investigation of high densities to allow examination of the details of the energy deposition in the scintillator would thus require the use of alternative photomultipliers.

Studies of the muon component are of relevance to model calculations, but of less direct relevance to studies of the radio and Cerenkov emission. Indeed the measurement of the shape of the muon front with heavily shielded scintillators would appear to be feasible only near the core with a relative low data collection rate.

REFERENCES

NOTE: The abbreviation PICCR stands for the Conference Papers of the series of International Cosmic Ray Conferences.

ABROSIMOV, A.T., Allan, H.R., Clay, R.W., Jones, J.K., Neat, K.P.
Acta. Phys. Hung. 29, Suppl B, 705, 1970.

AGUIRRE, C., Anda, R., Trepp, A., Kaneko, T., Yoshii, H., Nishi, K., Yamada, Y., Tajima, N., Nakatani, H., Gotoh, E., Kakimoto, F., Mizumoto, Y., Suga, K., Izu, N., Kamouchi, Y., Inoue, N., Kawai, M., Mackeown, P.K., Toyoda, Y., Murakami, K.
PICCR (Kyoto) 8, 107, 1979a.

AGUIRRE, C., Anda, R., Trepp, A., Kakimoto, F., Mizumoto, Y., Suga, K., Inoue, N., Kawai, M., Izu, N., Kamouchi, Y., Yuguchi, Y., Tachi, K., Kaneko, T., Yoshii, H., Nishi, K., Yamada, Y., Tajima, N., Nakatani, H., Gotoh, E., Mackeown, P.K., Murakami, K., Toyoda, Y.
PICCR (Kyoto), 8, 112, 1979.

ALLAN, H.R., JATP 29, 1103, 1967.

ALLAN, H.R., Clay, R.W., Jones, J.K., Abrosimov, A.T., Neat, K.P., Nature 222, 635, 1969.

ALLAN, H.R., Clay, R.W., Jones, J.K.
Acta Phys. Hung. 29, Suppl 3, 725, 1970.

ALLAN, H.R., Prog. in Elt. Part. and Cos. Ray. Phys. Vol. X, 169, 1971a.

ALLAN, H.R., PICCR (Hobart) 3, 1108, 1971b.

ALLAN, H.R., PICCR (Hobart) 3, 1113, 1971c.

ALLAN, H.R., Jones, J.K., Mandolesi, N., Prah, J.H., Shutie, P.
PICCR (Hobart) 3, 1097, 1971a.

ALLAN, H.R., Jones, J.K., Mandolesi, N., Prah, J.H., Shutie, P.
PICCR (Hobart) 3, 1102, 1971b.

ALLAN, H.R., Nature 237, 384, 1972.

ALLAN, H.R., Shutie, P.F., Sun, M.P., Jones, J.K.,
PICCR (Denver) 4, 2407, 1973.

ALLAN, H.R., Sun, M.P., Jones, J.K.,
PICCR (Munich) 8, 3082, 1975.

ALLAN, H.R., Crannell, C.J., Hough, J.H., Shutie, P.F., Sun, M.P.,
PICCR (Munich) 8, 3077, 1975b.

ANTONOV, R.A., Ivanenko, I.P.,
PICCR (Munich) 8, 2708, 1975.

ASHTON, F., Parvaresh, A., Saleh, A.J.,
PICCR (Munich) 8, 2831, 1975.

ASKARYAN, G.A., Soviet Phys. JETP 14, 441, 1962.

ASKARYAN, G.A., Soviet Phys. JETP 21, 658, 1965.

ATRASHKEVICH, V.B., Vedeneev, O.V., Khristiansen, G.B.,
JETP lett. 13, 76, 1971.

ATRASHKEVICH, V.B., Vedeneev, O.V., Prosin, V.V., Khristiansen, G.B.,
PICCR (Denver) 4, 2399, 1973.

ATRASHKEVICH, V.B., Vedeneev, O.V., Khristiansen, G.B.
PICCR (Munich 8, 3086, 1975.

ATRASHKEVICH, V.B., Vedeneev, O.V., Allan, H.R., Jones, J.K., Mandolesi, N., Morigi, G., Palumbo, G.G.C.
Yadernaya, Fizika, 28, 712, 1978.

BAGGIO, R., Mandolesi, N., Morigi, G., Palumbo, G.G.C.
Nuovo Cimento, 40B, 289, 1977.

BARRETT, M.L., Walker, R., Watson, A.A., Wild, P.
PICCR (Plovdiv) 8, 172, 1977.

BASSI, P., Clark, G., Rossi, B.,
Phys. Rev. 92, 441, 1953.

BAXTER, A.J., Watson, A.A., Wilson, J.G.
PICCR (London) 2, 724, 1965.

BAXTER, A.J., Watson, A.A., Wilson, J.G.,
Can. J. Phys. 46, S9, 1968.

BERGESON, H.E., Boone, J.C., Cassiday, G.L.,
PICCR (Munich), 8, 3059, 1975a.

BERGESON, H.E., Boone, J.C., Cassiday, G.L.,
PICCR (Munich) 8, 3064, 1975b.

BIRKS, J.B., 'The Theory and Practice of Scintillation Counting'.
Pergamon, 1964.

BIRKS, J.B., Pringle, R.W.,
Proc. R.S.E. (A), 70, 22, 1971/2.

BLAKE, P.R., Nash, W.F., Prescott, I.C.,
11 Nuovo Cimento 1, 360, 1978a.

BLAKE, P.R., Nash, W.F., Strutt, R.B.,
J. Phys. G 4, 617, 1978b.

BLAKE, P.R., Connor, P.J., Nash, W.F., Mann, D.M., O'Connell, B.
PICCR (Kyoto) 8, 82, 1979.

BOSIA, G., Navarra, G.,
11 Nuovo Cimento 62B, 301, 1969.

BRAY, A.D., Crawford, D.F., Jauncey, D.L., McCusker, C.B.A.,
Melley, D., Nelson, D., Poole, P.G., Rathgeber, M.H.,
Seet, S.H., Ulrichs, J., Wand, R.H., Winn, M.M.
Rev. Sci. Instr. 36, 587, 1965.

BRAY, A.D., Nature 223, 723, 1969.

CARRELL, R.L., IRE Int, Conv. Rec. 1, 61, 1961.

CASSIDAY, G.L., Bergeson, H.E., Chiu, T.W., Cooper, D.A., Elbert, J.W.,
Loh, E.C., Steck, D., West, W.J., Mason, G.W., Boone,J.,
Linsley, J.
PICCR (Plovdiv) 8, 258, 1977.

CASTAGNOLI, C., Silvestro, G., Picchi, P., Verri, G.,
Nuovo Cimento, 63B, 373, 1969.

CHALMERS, J.A., 'Atmospheric Electricity', Pergamon, 1957.

CHARMAN, W.N., Nature 215, 497, 1967.

CHARMAN, W.N., Fruin, J.H., Jelley, J.V., Porter, R.A., Smith, F.G.
Soviet Phys. JETP 53, 88, 1967.

CHARMAN, W.N., JATP 30, 195, 1968.

CHARMAN, W.N., Jelley, J.V., Can. J. Phys. 46, S216, 1968.

CHATTERJEE, B.K., Murthy, G.T., Naranan, S., Ranga Swami, T.N., Sreekantan,
B.V., Srinivasa Rao, M.V.,
J. Phys. Soc. Japan 17, Supp. A-3, 254, 1962.

CLAY, R.W., Hough, J.H., Prescott, J.R.,
PICCR (Hobart) 3, 1132, 1971.

CLAY, R.W., JATP, 34, 1129, 1972.

CLAY, R.W., McDonald, D.M., Prescott, J.R.,
Aust. J. Phys. 26 551, 1973a

CLAY, R.W., Crouch, P.C., Gregory, A.G., Prescott, J.R.
PICCR (Denver) 4, 2420, 1973b.

CLAY, R.W., Crouch, P.C., Gregory, A.G., Hough, J.H., Prescott, J.R.,
PICCR (Munich) 8, 3093, 1975.

CLAY, R.W., Gregory, A.G.,
J. Phys. A 10, 135, 1977

COLGATE, S.A., J. Geophys. Res. 72 4869, 1967.

COLGATE, S.A., O'Donnell, B.D.,
PICCR (Hobart) 3, 947, 1971.

CRAIG, M.A.B., McComb, T.S.L., Turver , K.E.,
PICCR (Kyoto) 8, 180, 1979.

CROMPTON, R.W., unpublished, 1974.

CROUCH, P.C., Kuhlmann,J.D., Clay, R.W., Gregory, A.G., Patterson, J.R., Thornton, G.J.
PICCR (Plovdiv) 11, 166, 1977.

CROUCH, P.C., Ph. D. Thesis, University of Adelaide, 1979.

DAVID, P., Voge, J., Propagation of Waves, Pergamon, 1969.

DIXON, H.E., Earnshaw, J.C., Hook, J.R., Smith, G.J., Turver, K.E.,
PICCR (Denver) 4, 2475, 1973.

DIXON, H.E., Turver, K.E., Waddington, C.J.
Proc. Roy. Soc. A 339, 157, 1974.

DIXON, H.E., Turver, K.E. Proc. Roy. Soc. A339, 171, 1974.

DYAKONOV, M.N., Knurenko, S.P., Kozlov, V.I., Kolosov, V.A., Krasilnikov, A.D., Krasilnikov, D.D., Lischenyuk, F.F., Orlov, V.A., Pavlov, V.N., Sidorov, R.G., Sleptsov, I.E.
PICCR (Kyoto) 8, 174, 1979.

DZIBOWSKI, T., Gawin, J., Grochalska, B., Pachala, S., Wdowczyk, J.,
PICCR (Plovdiv) 8, 46, 1977.

ELBERT, J.W., Boone, J.C., Bergeson, H.L., Cady, R., Cassiday, G.L., Loh, L.C., Steck, D.
PICCR (Kyoto) 8, 166, 1979.

FEGAN, D.J., McBreen, B., O'Mongain, E.P., Porter, N.A., Slevin, P.J., Can. J. Phys. 46, S250, 1968.

FEGAN, D.J., Lettere al Nuovo Cimento, 3, 715, 1972.

FELGATE, D.G., Stubbs, T.J., Nature 239, 151, 1972.

FEYNMAN, R.P., Leighton, R.B., Sands, M.,
The Feynman Lectures in Physics. Vol. I, Addison-Wesley, 1963.

FUJII, M., Nishimura, J., Acta Phys. Hung. 29, Suppl. 3, 709, 1970.

FUJII, M., Nishimura, J. PICCR (Hobart) 7, 2753, 1971.

GAISSER, T.K., Protheroe, R.J., Turver, K.E., McComb, T.J.L.,
Rev. Mod. Phys. 50, 859, 1978.

GAISSER, T.K., McComb, T.J.L., Turver, K.E.,
PICCR (Kyoto) 9, 275, 1979.

GALBRAITH, W., Jelley, J.V., Nature 171, 349, 1953.

GLUSHKOV, A.V., Grigorev, V.M., Efimov, N.N., Pravdin, M.I., Dimenstein, O.S., Sokurov, V.F.
PICCR (Kyoto) 8, 158, 1979.

GREEN, H.S., Advances in App. Prob. 10, 4, 73, 1978.

GREGORY, A.G., Clay, R.W., Prescott, J.R.,
Nature 245, 86, 1973.

GREISEN, K., Phys. Rev. Lett. 16, 748, 1966.

GRIEDER, P.K.F., Rev. Nuovo Cimento, 7, 1, 1977.

HAMMOND, R.T., Orford, K.J., Protheroe, R.J., Shearer, J.A.L., Turver, K.B., Waddoup, W.P., Wellby, D.W.,
Nuovo Cimento 1C, 315, 1978.

HAZEN, W.E., Hendel, A.Z., Smith, H., Shah, N.J.,
Phys. Rev. Lett. 24, 476, 1970.

HAZEN, W.E., Hendel, A.Z., Smith, H., Castle, R.J.,
PICCR (Hobart) 3, 1125, 1971.

HAZEN, W.E., Hendel, A.Z., PICCR (Hobart) 3, 1127, 1971.

HILLAS, A.M., PICCR (London) 2, 758, 1965.

HILLAS, A.M., Hollows, J.D., Hunter, H.W., Marsden, D.J.,
Acta Phys. Hung. 29, Suppl 3, 533, 1970.

HILLAS, A.M., Marsden, D.J., Hollows, J.D., Hunter, H.W., PICCR (Hobart) 3, 1001, 1971.
HILLAS, A.M., Phys. Rep. 20C, 61, 1975.
HILLAS, A.M., PICCR (Kyoto) 9, 13, 1979.
HOUGH, J.H., Prescott, J.R., Proc. 6th Interam. Seminar on Cos. Rays, La Paz 2, 527 1970.
HOUGH, J.H., Prescott, J.R., Clay, R.W., Nature Phys. Sci. 232, 14, 1971.
HOUGH, J.H., J. Phys A 6, 892, 1973.
ISBELL, D.E., I.R.E. Trans. AP 8, 260, 1960.
JELLEY, J.V., Cerenkov Radiation and its Applications, Pergamon, 1958a.
JELLEY, J.V., Suppl. Nuovo Cimento 8, 578, 1958b.
JELLEY, J.V., PICCR (London) 2, 698, 1965.
JELLEY, J.V., Fruin, J.H., Porter, N.A., Weekes, T.C., Smith, F.G., Porter, R.A., Nature 205, 327, 1965.
KAHN, F.D., Lerche, I. Proc. Roy. Soc. A, 289, 206, 1966.
KALMYKOV, N.N., Nechin Yu.A., Prosin, V.V., Fomin, Yu.A., Khristiansen, G.B., Berezhko, I.A., Grigoriev, V.M., Efimov, N.N., PICCR (Kyoto) 9, 73, 1979.
KAMINSKY, A.T., Shmatko, E.S., PICCR (Plovdiv) 8, 490, 1977.
KELLERMAN, E.W., Towers, L., J. Phys. A, 3, 284, 1970.
KHRISTIANSEN, G.B., Atrashkevich, V.B., Vedeneev, O.V., Kulikov, G.B., Prosin, V.V., Solov'eva, V.I., Chukanov, V.A., Iz. Akad. Nauk SSSR. Ser. Fiz. 35, 2102, 1971a.
KHRISTIANSEN, G.B., Atrashkevich, V.B., Vedeneev, O.V., Prosin, V.V., PICCR (Hobart) 6, 2181, 1971b
KHRISTIANSEN, G.B., Atrashkevich, V.B., Vedeneev, O.V., Paper delivered at the European Symposium on Cosmic Rays (unpublished), 1972.
KNOP, C.M. IEEE Trans. AP-18, 807, 1970.
KRASILNIKOV, D.D., PICCR (Kyoto) 8, 26, 1979.
KRAUS, J.D. Antennas, McGraw-Hill, 1950.
LANGENBERG, K.J., App. Phys. 20(2), 101, 1979.
LAPIKENS, J., Watson A.A., Wild, P., Wilson, J.G., PICCR (Denver) 4, 2582, 1973.
LAPIKENS, J., PICCR (Plovdiv) 8, 178, 1977.
LAPIKENS, J., Lloyd-Evans, J., Pollock, A.M.T., Reid, R.J.O., Watson, A.A. PICCR (Kyoto) 8, 19, 1979a.
LAPIKENS, J., Walker, R., Watson, A.A., PICCR (Kyoto) 8, 95, 1979b.
LERCHE, I., Nature 215, 268, 1967.
LEIBING, D.F., Internal Report, Cosmic Ray Group, University of Adelaide, 1978.
LINSLEY, J., Scarsi, L., Phys. Rev. 128, 2384, 1962.
LINSLEY, J., PICCR (Plovdiv) 8, 207, 1977.
LOCCI, M.A., Picchi, P. Verri, G., Nuovo Cimento 50B, 384, 1967.
MANDOLESI, N., Morigi, G., Palumbo, G.G.C. JATP 36, 1431, 1974.
MANDOLESI, N., Morigi, G., Palumbo, G.G.C., J. Phys. A, 9, 815, 1976.
MARSDEN, D.J., Hillas, A.M., Hollows, J.D., Hunter, H.W. PICCR (Hobart) 3, 1013, 1971.

MASON, B.J., The Physics of Clouds 2nd edn. Clarendon Press, 1971.

McCUSKER, C.B.A., Peak, L.S., Rathgeber, M.H., Phys. Rev. 177, 1902, 1969.

McDONALD, D.M., Clay, R.W., Prescott, J.R. PICCR (Plovdiv) 8, 228, 1977.

ORFORD, K.J., Turver, K.E., Nature 219, 706, 1968.

ORFORD, K.J., Turver, K.E., Nature 264, 727, 1976.

PRESCOTT, J.R., Palumbo, G.G.C., Galt, J.A., Costain, C.H., Can. J. Phys. 46, S246, 1968,

PRESCOTT, J.R., Hough, J.H., Pidcock, J.K. Acta Phys. Hung. 29, Suppl. 3, 717, 1970.

PRESCOTT, J.R., Hough, J.H., Pidcock, J.K. Nature Phys. Sci, 233, 109 , 1971.

PREWITT, J.F., IEEE Trans. AP26, 730, 1979.

PULFER, J.K., Proc. I.R.E. 49, 644, 1961.

SAKUYAMA, H., Suzuki, N., PICCR (Kyoto) 13, 282, 1979.

SAMORSKI, M., Staubert, R., Trumper, J., Bohm, E., PICCR (Hobart) 3, 959, 1971.

SHUTIE, P.F., Ph. D. Thesis, University of London, 1973.

SIVAPRASAD, K. Aust. J. Phys. 31, 439, 1978.

SMITH, G.J., Turver, K.E. PICCR (Denver) 4, 2369, 1973.

SPAULDING, A.D., Rebique, C.J., Crichlow, W.Q. J. Res. Natn. Bur. Stand. D66, 713, 1962.

SPAULDING, A.D., Ahlbeck, W.A., Espeland, L.R., U.S. Dept. Commerce Telecommun. Res and Engng-Rep No OT/TRER 14.

SPENCER, R.E., Nature 222, 460, 1969.

STUBBS, T.J., Nature Phys. Sci. 230, 172, 1971.

SUGA, K., PICCR (Kyoto) 14, 325, 1979.

THIELERT, R., Wiedecke, L., Zeitschrift fur Physik 179, 199, 1964.

THORNTON, G.J., Clay, R.W. Phys. Rev. Lett. 43, 1622, 1979.

VERNOV, S.N., Khristiansen, G.B., Abrosimov, A.T., Atrashkevich, V.B., Vedeneev, O.V., Neat, K.P. Acta Phys. Hung. 29, Suppl 3, 731, 1970.

VERNOV, S.N., Khristiansen, G.B., Abrosimov, A.T., Atrashkevich, V.B., Vedeneev, O.V., Neat, K.P. Iz. Akad. Nauk SSSR 34, 1995, 1970.

VOLOVIK, V.D., Zalyubovsky, I.I., Levchenko, V.N., Samburova, S.I., Sogokon, A.B., Khirnuy, A.I., Shmatko, E.S., PICCR (Denver) 4, 2427, 1973.

VOLOVIK, V.D., Zalyubovsky, I.I., Levchenko, V.N., Sogokin, S.I., Khirny, A.I., Shmatko, E.S., Iz. Akad. Nauk. SSSR Ser. Fiz. 38, 1013, 1974.

VOLOVIK, V.D., Zalyubovskiy, I.I., Shmatko, E.S., Iz. Akad. Nauk Ser. Fiz. 40, 1026, 1976.

WATSON, A.A., Wilson, J.G. J. Phys. A 7, 1199, 1974.

WDOWCZYK, J., PICCR (Munich) 11, 4002, 1975.

WDOWCZYK, J., Wolfendale, A.W., Nature 281, 356, 1979.

WHITE, G.M., Prescott, J.R., Can. J. Phys. 46, S287, 1968.

WILSON, R.R., Phys. Rev. 108, 155, 1957.

WOIDNECK, C.P., Bohm, E., Trumper, J., deVilliers, E.J. PICCR (Hobart) 3, 1038, 1971.

WOIDNECK, C.P., Bohm, E., J. Phys. A. 8, 997, 1975.

APPENDIX B

This appendix provides further details relating to the statistics of the radio experiment.

1. Parameters of Individual Events

A list of the events in the restricted set referred to in Chapter 5 is given below, together with the basic array parameters (direction information, core location and size), and the radio pulse field strengths (unnormalised) for the four channels. The diagrams associated with this set are Figures 5.1, 5.6 to 5.9, 5.14, 5.15, 5.17 to 5.19 and Tables 5.1 and 5.2. Additional events were used in Figures 5.2, 5.3, 5.5, 5.10 to 5.13 and 5.16

2. Efficiency of Radio Detection

A total of approximately 6,000 showers were recorded while the radio experiment was operational. The number of these events larger than the tabulated sea level sizes is listed below for size thresholds of 5×10^6, 1×10^7, 2×10^7 and 4×10^7 particles. These estimates are derived from a sample of some 3,000

TABLE B-1

EVENT CHARACTERISTICS

EVENT IDENTIFICATION	ZENITH ANGLE (DEGREES)	AZIMUTH ANGLE (DEGREES)	CORE LOCATION (RELATIVE TO C HUT)		SIZE ($\times 10^5$ PARTICLES)	UNNORMALISED RADIO PULSES (μVm^{-1} MHz^{-1})			
			EAST (M)	NORTH (M)		1	2	3	4
50356	43	174	40	- 77	23	1.6	1.1	-	1.2
50246	18	208	- 53	- 80	45	1.9	2.2	2.8	-
90251	30	145	40	- 90	78	2.0	2.4	2.4	2.4
40750	32	169	60	- 31	80	2.0	-	2.5	2.1
80814	32	269	- 85	46	85	2.1	2.3	2.1	1.8
130203	21	199	- 53	133	96	1.7	2.0	2.3	1.4
70342	28	151	-120	10	167	1.5	1.7	2.2	2.1
10166	32	157	- 73	32	206	2.4	2.5	2.6	2.1
120173	10	80	- 44	- 27	317	3.0	1.8	3.3	-
130174	18	78	- 83	12	347	3.4	2.1	2.9	3.1
130105	13	192	- 40	62	378	4.6	4.4	5.8	5.0
80105	16	118	18	94	410	4.0	3.3	3.5	3.4
80110	33	120	63	- 69	517	4.8	5.0	5.9	5.1
30350	7	226	- 75	- 67	780	2.1	2.1	2.6	2.2

TABLE B-2

INTEGRAL NUMBER SPECTRUM

SHOWER SIZE (PARTICLES)	EXPECTED NUMBER OF SHOWERS	OBSERVED NUMBER OF RADIO SHOWERS
10^6	1,300	-
2×10^6	-	14
5×10^6	144	12
10^7	34	8
2×10^7	8	7
4×10^7	2	3

showers recorded while the radio array was running in a period of four months in 1979. The figures are supported, within statistical limits, by a much larger sample, supplied by P. Gerhardy, of all events (43,666) recorded by the Buckland Park array during 1980, when the radio system was no longer operational. However, the array operating conditions are believed not to have been significantly different while the radio system was operational.

Figure B-1 shows the integral size spectrum for the fourteen events in the restricted set, compared with that derived from the sample of 3,000 events, referred to above, corrected for 6,000 events.

It will be observed that the proportion of array events also detected by the radio system increases with detected shower size. A strict qualitative comparison between the two plots is not feasible. Firstly, the two plots relate to different sets of showers. Secondly, there are differences in the details of shower selection, both owing to the definition of array area used in selecting events, and also in the re-analysis of very large events which tend to be accompanied by saturation in one or more individual detectors. These

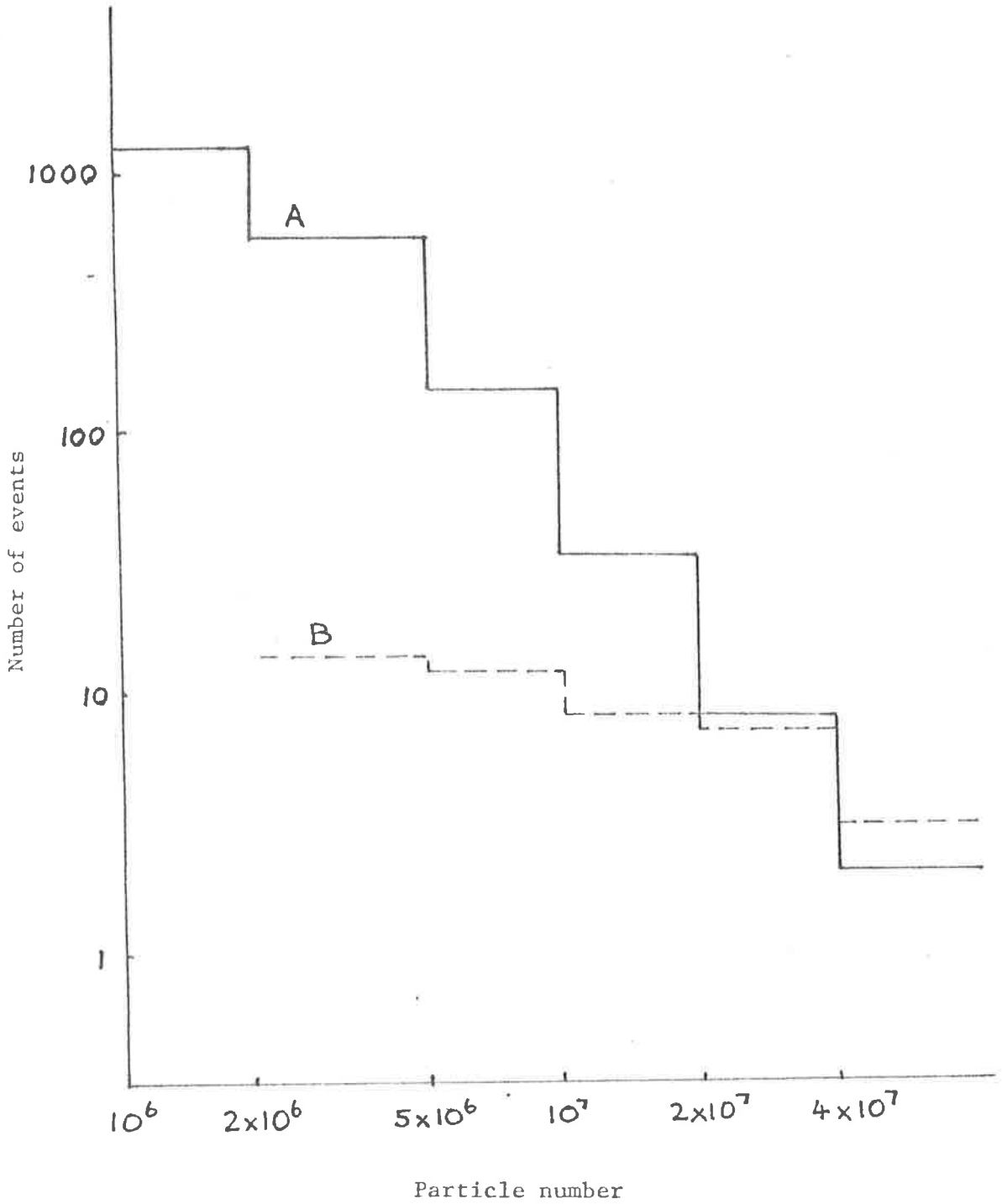

Fig. B — 1 Integral number spectrum

A Estimated number of showers in sample

B Number of radio showers in sample (see text)

factors will tend to depress the spectrum of "expected" events relative to "observed" radio events at the highest energies. Thus, any estimates of radio system efficiency will be upper limits. In addition, the statistics at the highest energies are extremely poor. Thus, only the general trend of the graph should be considered.

The plot serves to confirm and reinforce the conclusions reached in Chapter 5. It shows that the present radio system is a particularly inefficient detector of showers. Even at a threshold of 10^7 particles the percentage of showers detected by the radio system is of the order of 30%. As mentioned above, this is likely to be an upper limit.

It follows that any attempt to measure general shower properties on the basis of so small a sample, especially as shower size decreases, must be examined for possible biases. As discussed in Section 5.6.4, there are, indeed, biases in the present experiment which operate to increase the elongation rate as derived in this thesis. In addition to those factors, there is a further effect, particularly significant for smaller showers: for a given primary energy, there will be some

distribution in the height of maximum development. Showers developing earlier will be smaller at sea level than those developing later, although their measured radio field strengths may be essentially the same. Thus, in terms of the model adopted here, these smaller measured showers almost certainly represent highly fluctuated, more energetic showers which suffered early development. Thus, the apparent elongation rate as derived here will be too large and cannot be interpreted as a general air shower characteristic; indeed, it would appear unlikely that the radio approach will produce a good estimate of such a parameter.